Experiments Towards the Development of a Laser Suitable for an Interferometric Gravitational Wave Detector

by

Allan Carmichael

Department of Physics and Astronomy
University of Glasgow.

Presented as a thesis for the degree of
Ph.D. in the University of Glasgow.
February 1992.

Contents

List of Figures

Acknowledgements

I would like to thank Jim Hough and Gavin Newton for encouragement, help and advice during the period of this work.

Thanks are also due to the other members of the gravitational waves group, past and present, for encouragement and advice; Harry Ward, Brian Meers, Norna Robertson, Graham Kerr, Norman Mackenzie, David Robertson, Peter Veitch, Anne Campbell, Kenneth Strain, Caroline Cantley, Euan Morrison, Jennifer Logan, Sheila Rowan and Kenneth Skeldon.

I am grateful to M. Hamilton, A. Brillet, I. Frietag and G. Labeyrie for valuable contributions during the period of this work.

I would like to thank Norman Mackenzie for allowing me to use his TEX thesis style and for access to numerous other applications installed on the computers.

I am grateful to Alistair Grant and Anne Campbell for their work in proof reading this thesis.

Jim Pittillo, Allan Latta, David Edwards and Angus McKellar and the workshop deserve thanks for technical assistance during the experimental work.

I am grateful to Prof R. Ferrier and to the University for financial support during this work; I was in reciept of a University post graduate scholarship during this work.

The final word of thanks goes to my family and friends for their good influence and support.

Preface

The research group at Glasgow has been at the forefront of interferometric gravitational wave detector development since 1978. This thesis describes work carried out by the author in the period October 1988 to September 1991, towards the development of a laser suitable for the present and future generation of gravitational wave detectors.

Chapter 1 is an introduction to gravitational waves. This includes a review of sources and the most likely methods of detecting gravitational waves. This is based on the work of many people.

Chapter 2 describes a diode pumped Nd:YAG laser. This was designed and built by the author in collaboration with J. Hough, and the author developed it further to run polarised and at a single frequency.

Chapter 3 describes the measurement of the frequency noise of the laser developed in Chapter 2. The author designed and built the feedback system and carried out the measurements. The servo technique described in Chapter 3 to remove intensity oscillations of a diode pumped Nd:YAG was developed and applied during a stay of two weeks in Orsay, France; this work was done in collaboration with A. Brillet and G. Labeyrie, who were responsible for much of the circuit design.

Chapter 4 describes the development of a flashlamp pumped single frequency ring Nd:YAG laser. The author was responsible for the design and building of the laser, following discussions with M. Hamilton, J. Hough and G. Newton.

Chapter 5 describes injection locking experiments using the flashlamp pumped YAG of Chapter 4, and this was carried out with the help of H. Ward and J. Hough. Some later work on this was carried out in collaboration with I. Freitag from Hanover, Germany, who visited the Glasgow lab for two weeks.

Chapter 6 contains a review of second harmonic generation and gives the results of several experiments towards the development of a second harmonic version of the laser in Chapter 4. The author was responsible for carrying out the experiments in collaboration with G. Newton.

The author carried out the work described in Chapter 7, following a suggestion from J. Hough. This chapter covers the examination of the correlation of frequency fluctuations of the fundamental and second harmonic light of the laser developed in Chapter 6.

Summary

Gravitational waves are distortions in the curvature of space-time. They were predicted by Einstein in 1916 but it is only since the early 1960's that experimental progress has been made towards the detection of gravitational waves. The most probable sources are astrophysical in nature; the detection of gravitational radiation will open up a new field of observational astronomy.

The research group at Glasgow has been developing a technique to detect gravitational waves using optical interferometry. The technique is based on a Michelson interferometer. The gravitational waves cause a differential displacement of the interferometer arms and the subsequent phase change of the laser light in the orthogonal arms is detected as an intensity change. In order to have a good chance of detecting some astrophysical sources an interferometer arm length of around 1 km is required. Such long base line detectors need to be operated with a laser source of around 100 W of frequency and intensity stabilised light.

Chapter 1 is a general introduction to gravitational waves. A review of sources is given and this is followed by descriptions of the two main terrestrial detection techniques; bar detectors and interferometric detectors. Chapters 2 to 7 describe experiments towards the development of a laser capable of supplying around 100 W of frequency and intensity stabilised light.

Chapters 2 and 4 describe a diode pumped Nd:YAG laser and a flashlamp pumped Nd:YAG laser respectively. An interferometer can be operated with infrared light and so both of these lasers are potential sources as they stand (if developed further). However, engineering problems can be avoided if visible light is used: the diffraction is less and so the vacuum pipes are smaller. Chapter 6 describes the conversion of the flashlamp pumped laser to operate at the second harmonic. The nonlinear susceptibility of KTP is used to generate the second

harmonic. Chapters 3,5 and 7 describe techniques that can be applied to improve the characteristics of frequency and intensity stability of a laser or describe the experimental measurements of the laser characteristics (frequency stability and intensity) that are particularly important to interferometric detectors. These include injection locking, servo control to remove intensity noise, frequency noise measurement and the generation of a second harmonic error signal for frequency stabilisation.

Chapter 1

Introduction to Gravitational waves

1.1 Introduction

The theory of General Relativity [Einstein 1916] predicts that a wave like distortion of the curvature of space-time will be propagated through space at the speed of light. Despite it being almost 80 years after the initial prediction the direct observation of gravitational waves has still to be achieved. The observation of gravitational waves is important because it will not only confirm relativistic theory but will open up a new form of astronomy. This Chapter begins with a description of the nature of Gravitational waves, some possible astrophysical sources, how the waves interact with matter and the most likely method of sensing them. A more detailed analysis can be found in *300 years of Gravitation* [Thorne 1987]. This is followed by a review of current detectors, mainly interferometric detectors and the operating requirements that led to the motivation of the work in this thesis.

1.2 Introduction to Relativity

The curvature of space-time is described by the Einstein curvature tensor E; the magnitude of the components of E gives the magnitude of the curvature. The source of the curvature is the stress-energy tensor T, which describes the mass, energy and momentum of a system, all of which contribute to the curvature of

space-time. The field equations can be expressed as

$$T = \frac{c^4}{8\pi E} G$$

where c is the speed of light and G the gravitational constant; the Einstein tensor is a contraction of the Reimann curvature tensor. The nonlinear nature of the field equations leads to the possibility that waves will be scattered by strong background curvature or that in the region of intensely curved space, for example, near a black hole, nonlinear harmonic generation may occur. The nonlinearity creates mathematical problems and for a simple solution the field equations must be approximated as linear. A weak field approximation is used in which space-time is almost flat. The metric tensor (which describes the distance between events) is separated into two terms, one of which is a perturbation term h_{ij}. The wave equation of the linear field equations, in flat space time is given by [Blair 1991]

$$(\frac{-1}{c^2}\frac{d^2}{dt^2} + \Delta^2)h_{ij} = 0$$

where t denotes time. This has a sinusoidal plane wave solution

$$h_{ij} = A_{ij} \exp(i\omega(t - z/c))$$

for a wave travelling with frequency ω in the z direction, where A is the amplitude tensor. In a transverse, traceless gauge this has 4 components. Due to symmetry there are only two independent components and these correspond to two polarisations of the wave.

1.3 Interaction with matter

The separation of test masses in free fall varies under the influence of a gravitational wave. For a two particle system, one at $x = 0$, $y = z = 0$, and one at $x = e$, $y = z = 0$, the proper distance between them changes by $\frac{1}{2}he$ for a wave amplitude of $h_{xx} = h$ and $h_{xy} = o$. For the transverse system of two particles, one at the origin and one at x=z=0, y=e the length change is $-\frac{1}{2}he$ [Mackenzie 1989]. The

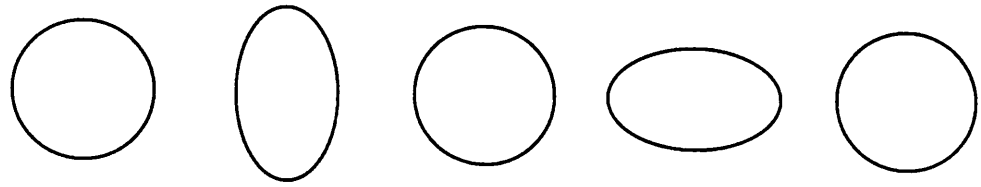

Figure 1.1: Deformation of a ring of particles when a gravitational wave propagating perpendicular to the page with $h_{xy} = 0$ passes through.

effect a wave has can clearly be seen by considering a circle of particles in the x,y-plane. The observer at the centre of the circle will see the proper distances vary in time such that the pattern of particles alternates between an ellipse and a circle. Figure 1.1 shows the effect on such a ring of particles when a gravitational wave with $h_{xy} = 0$ and propagating perpendicular to the page passes . The deformation is invariant under a rotation of π, unlike an electromagnetic wave that is invarient under a rotation of 2π, and is consequently a spin 2 transverse wave.

1.4 Production of Gravitational waves

Gravitational waves are produced by the acceleration of matter. Electromagnetic radiation is most efficiently produced from a dipole, but unlike charge, mass is not available in a plus and minus form. General relativity predicts that gravitational waves are produced from a changing quadrupole moment. Thus any symmetric acceleration of mass is eliminated as a source. The amplitude of a gravitational wave is [Kafka 1988]

$$h_{ik} = \frac{2G\ddot{Q}_{ik}}{c^4 r}$$

where Q is the quadrupole moment of the mass system. The quadrupole nature of gravitational waves leads to very weak production and very weak interaction. The rate of energy lost by a source is [Kafka 1988]

$$-\dot{E} = \frac{G}{5c^5}\dddot{Q}^2$$

In comparison, the rate of energy loss by an electromagnetic source is

$$-\dot{E} = \frac{2}{3c}\ddot{d}^2$$

where d is the electric dipole moment and the source velocities are $\ll c$.

1.5 Sources of Gravitational Waves

The production of gravitational waves at some level in the laboratory is possible, as any system of masses with a changing quadrupole moment acts as a source. However, the technological and physical limits to the magnitude and rate of change of a laboratory quadrupole moment mean that the energy radiated as gravitational waves would be too small for detection. For example, consider a bar of mass 10^5kg, 10m long and spun at 1000 Hz. The power output is only 10^{-22}W. As this couples very weakly to a detector it is unlikely that any laboratory source could generate enough energy for detection.

The most likely sources of gravitational radiation are astrophysical in nature. Astrophysical sources, involving accelerations to velocities close to c and masses of the order of the sun, are required because of the factor $\frac{G}{c^5}$ in the equation for energy production. Astrophysical sources have already provided indirect evidence of gravitational waves. Indeed, it has been shown that the spin down rate of a binary pulsar was consistent with energy loss from gravitational radiation [Taylor et al 1979]. Both periodic and continuous sources are expected, along with a stochastic background. In the following pages a brief review of the most probable sources is given.

1.6 Astrophysical Sources of Gravitational Waves

1.6.1 Supernovae

Supernovae exist in two forms, type 1 and type 2. Type 2 supernovae are created by the gravitational collapse of the core of a massive highly evolved star into a neutron star or a black hole. The collapse is characterised by the core bouncing

outwards due to nucleon repulsion, producing a shock wave that causes an optical shell to expand outwards. Type 1 supernovae are thought to occur in white dwarfs after accretion of mass from a close companion star. The supernova is thought to result from a nuclear explosion. The white dwarf can collapse to a neutron star but does not have sufficient mass to form a black hole. The event rate of type 1 and type 2 supernovae out to 10 Mpc (the Virgo cluster of galaxies) is expected to be several per year. The amplitude of the gravitational radiation emitted depends on the symmetry of the collapse: the more asymmetric the event the larger the wave amplitude. For sources such as supernovae there are a wide range of potential mechanisms influencing the collapse. The wave form is not known to any certainty and the wave amplitude is commonly expressed as an approximation in terms of the total energy radiated E. The amplitude at distance r and at frequency f, for a given energy is [Thorne 1987]

$$h = 2.7 \times 10^{-20}(\frac{E}{M_{\odot}c^2})^{1/2}(\frac{1000}{f})^{1/2}(\frac{10Mpc}{r})$$

Gravitational radiation may be generated after the collapse has ocurred in the newly formed object. For example if the collapse forms a black hole, infalling matter can excite the normal modes of vibration and produce gravitational waves.

1.6.2 Coalescence of Compact Binaries

A large fraction of all stars exist in binary systems. As the two objects orbit around each other they emit gravitational waves. Binary systems are an abundant source of periodic gravitational radiation. Unfortunately the orbital period is long and the generated gravitational wave is at a frequency of less than a millihertz, far below the frequency range of terrestrial detectors. However, the energy loss from the gravitational radiation causes orbital decay and eventually they will coalesce. Close to coalescence the frequency and amplitude of the gravitational wave becomes potentially detectable. To provide terrestrialy detectable gravitational wave frequencies from a binary coalescence the binary system must comprise of neutron stars or black holes.

It is difficult to estimate how many such systems exist because of difficulties in finding them using conventional astronomy. It is likely that gravitational wave observations will be required to determine how many suitable systems exist. However, here are three known neutron star binaries that should coalesce within the lifetime of the universe. An example is binary pulsar 1913 + 16.

The signal from these systems is characterised by a 'chirp', whose amplitude and frequency increases with time. The amplitude and rate of frequency change depends on the total mass of the individual stars, $m = m_1 + m_2$, the reduced mass $\mu = m_1 m_2/(m_1 + m_2)$ and the distance from the source to the earth, r, measured in hundreds of Mpc. The amplitude and time scale that the signal frequency changes over are given by [Schutz 1988]

$$< h >= 10^{23} m^{2/3} \mu f^{2/3} r^{-1}$$

$$\tau = \frac{f}{\dot{f}} = 7.97 \mu^{-1} m^{-2/3} f^{-8/3} sec$$

The total mass and reduced mass appear in both equations. If the character of the signal is measured with an array of gravitational wave detectors, then the equations can be solved to give the distance to the source [Schutz 1988]. If the source can be optically detected and its red shift found, an accurate determination of Hubble's constant can be obtained from the distance and the red shift.

1.6.3 Rotating Neutron Stars

Rotating neutron stars are sources of periodic gravitational waves. A rotating neutron star, for example a pulsar, emits gravitational radiation if it is either non-axisymmetric or is axisymmetric but rotating around an axis that is not the symmetry axis. The greater the asymmetry and the faster the rotation the greater the wave amplitude. The deviation from symmetry can arise for several reasons. The crust of the neutron star may have lumps on it due to a star quake or from an asymmetric collapse in its formation. Neutron stars accreting matter from a companion star may develop an instability from the spin up associated with transfer of angular momentum from the matter accretion. The radiation is generated by

hydrodynamic waves on the surface of the star travelling in the opposite direction to the star's rotation. These are known as Wagoner stars.

1.6.4 Stochastic Sources

It is possible that there is a background of gravitational waves which may be detected by looking for correlations between independent detectors. This background may be the result of the superposition of many sources or the result of violent events at the beginning of the Universe. Possible sources may be binary stars in nearby galaxies: the abundance of binary sources at low frequencies should superimpose to produce a strong background signal. Also, it is thought that there may have been a pre-galactic population of massive stars, known as population 111 stars. The violent astrophysical destruction of these through supernovae and collapses to black holes may have produced gravitational waves that are currently present in the Universe. A third possible background source is primordial gravitational radiation which is the residue of the very early history of the Universe. Caused by the decoupling of matter and gravitons, inflation may have amplified this to detectable levels. Other possible sources worth mentioning here are the cosmic strings predicted by several Grand Unified theories. The vibration of such closed cosmic string loops would add up to produce an effective stochastic signal.

1.7 The detection of gravitational waves

The detection of gravitational waves relies on sensing the strain in space induced by the gravitational waves. There are currently two classes of detector being developed in laboratories around the world, bar detectors and laser interferometers. The bar detectors sense the reaction of a solid body to the internal stresses caused by gravitational waves, while the laser interferometer senses the influence that a gravitational wave has on the separation of two essentially free test masses.

1.8 Bar detectors

The first gravitational wave detection experiment was carried out with a bar detector by Joseph Weber at the University of Maryland in the 1960's. The principle behind such a detector is that an elastic body will resist changes of its proper length, such as those that are caused by gravitational waves. The induced motion can then be sensed as a measure of the gravitational wave amplitude. In practice the detector consists of a large mass, usually a cylinder weighing a few tonnes with the resonant frequency of the first longitudinal mode chosen to overlap with the expected wave frequency. Bar detectors are narrow bandwidth detectors because they rely on the excitation of the fundamental mode of the bar, but this could be overcome by an array of detectors, each tuned to different frequencies. The motion of the bar was originally sensed by Weber [Weber 1969] by bonding piezoelectric transducers (PZT) to the middle of the bar, the electrical signal providing the information on the movement. Later the motion was sensed by other techniques which have included using a PZT sandwich between two masses and using capacitive transducers.

The detector is isolated from both seismic and acoustic noise by suspending the mass in a vacuum. Another important noise source in a bar detector is thermal noise. The thermal energy of any mode is kT. This is equivalent to a displacement amplitude at the resonant frequency of the bar of

$$dx = (\frac{kT}{m\omega_o^2})^{1/2}$$

where T is the temperature, k is Boltzmann's constant, m is the mass and ω_o is the resonant frequency of the fundamental mode. However, if short pulses are being searched for, then for a detector with a high Q (that is a low coupling with the environment) and if the measurement time is much smaller than the storage time given by $\tau = Q/\omega_o$ then the detectable displacement becomes

$$dx = (\frac{kTt_{meas}}{mQ\omega_o})^{1/2}$$

where t_{meas} is the measurement time and the bar is treated as a simple harmonic oscillator. The sensitivity can be improved by lowering the bar temperature, in-

creasing the mass, increasing the Q and lowering the measurement time. Most research groups currently involved with bar detectors cool the bars to around 4K. The reduction of the measurement time improves the sensitivity. However, the measurement systems rely on amplifying the signal and when the measurement time is reduced the bandwidth of the measurement amplifier is increased. This increases the amplifier noise and means some balance must be found. Currently the most sensitive bar detectors operate at a detection level of h of 10^{-18} at around 1 kHz.(Stanford University and CERN-the University of Rome.)

The ultimate sensitivity of the bar detector is limited by the Heisenberg uncertainty principle. This places a limit of around 10^{-20}on the detectable gravitational wave amplitude for a 1000 kg bar. It is possible that the use of 'quantum nondemolition' techniques [Braginsky 1977, Caves et al 1980] will reduce that limit. When a measurement is made, it is normally a linear measurement of a pair of conjugate observables. They are measured symmetrically and are subject to the Heisenberg uncertainty limit. If an observable is used that allows a nonlinear measurement to be made, where back action occurs in one quadrature only then the quantum limit can be avoided. An example is the complex amplitude x+iy. If a phase sensitive transducer is used to measure only x, then x can be as accurate as required still satisfying the quantum limit (the error goes in to y). A second bar detector can then be used to measure y as accurately as required and so apparently removing the quantum limit.

1.9 Laser Interferometers

The strain in space induced by a gravitational wave can be measured using an electromagnetic wave. The simplest technique is based on the use of a Michelson interferometer, as shown in figure 1.2. To eliminate some of the effects of environmental noise the beam splitter and mirror masses are suspended as pendulums in a vacuum tank.

A beam splitter divides the laser beam into two equal components, travelling in orthogonal directions. Arms are formed by placing mirrors along the beam path

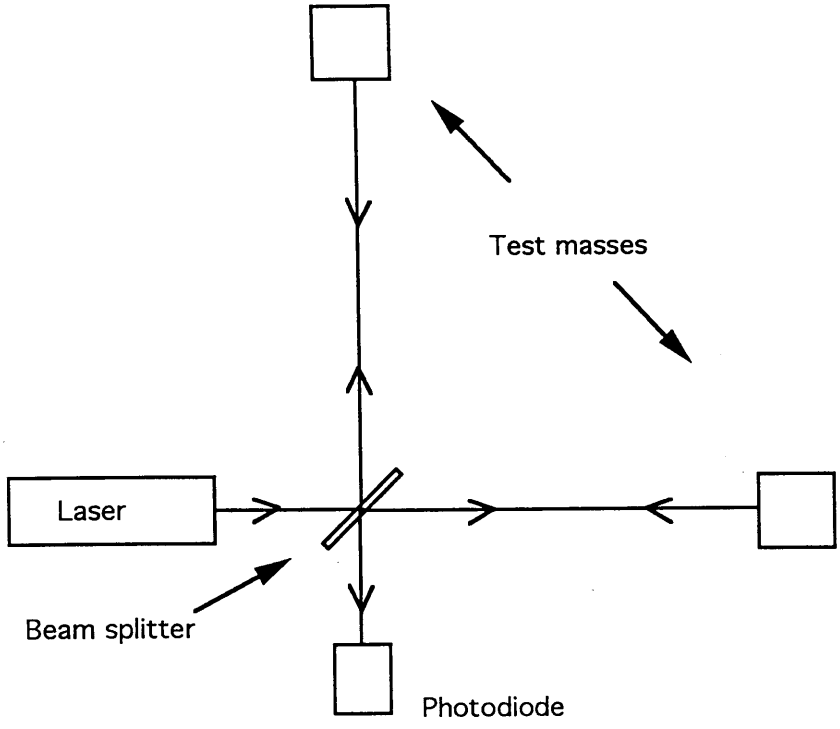

Figure 1.2: Michelson interferometer.

after the beam splitter. These have the effect of reflecting the light back to be recombined on the beam splitter. Any differential change of the path length in the arms of the interferometer leads to a relative phase change in the returning light. This phase change becomes an intensity change when the recombined beams are detected on a photodiode. The detector senses a differential change between the two arms. In fact, this is ideal because the quadrupole nature of gravitational waves means that in orthogonal directions, for the correct polarisation, there are length changes of the opposite sign.

The interferometer sensitivity to the gravitational wave can be maximised by having the arm length of the detector equal to quarter the wave length of the gravitational wave; thus for gravitational wave frequencies of around 1kHz the optimum path length is 150 km. However because the detector must be placed in a vacuum to reduce the effect of refractive index fluctuations, such an arm length is technically too difficult to achieve. This has resulted in the development of two path folding techniques to achieve an effective path length of 150 km: a multipass

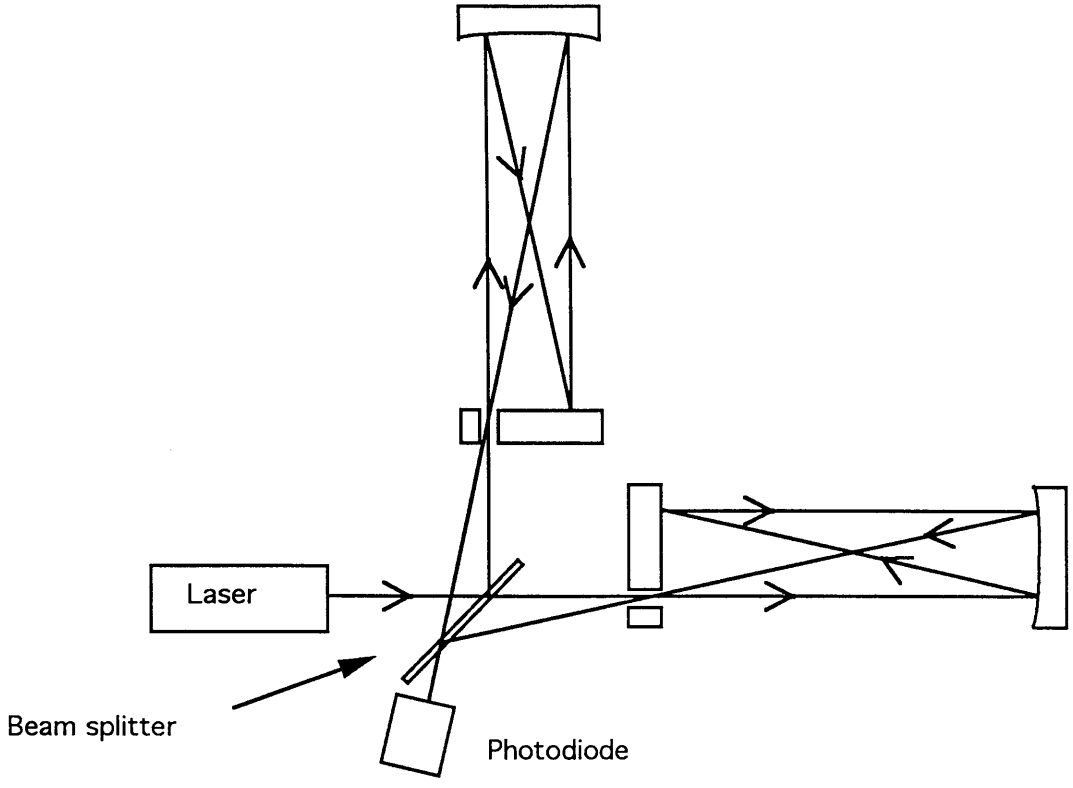

Figure 1.3: Delay line interferometer

Michelson or Delay line and a Michelson with Fabry-Perot cavities in each arm.

1.10 Delay Line Detectors

A multipass or Delay line detector, figure 1.3, was first suggested by Weiss [Weiss 1972]. The Max Planck Institute for Quantum Optics (MPQ) and Massachusetts Institute of Technology (MIT) have both developed prototype delay line detectors. In a delay line system the laser beam is reflected many times between two mirrors before recombining on a beam splitter. This has the effect of increasing the differential optical path length change by N, the number of bounces, over a 1 bounce system. The main drawback of such a system is the larger mirror diameter required. Noise from the mirror resonances may be introduced at frequencies close to signal frequencies if the mirror is too large. Another problem is scattered light in the delay line introducing phase noise at the output. This can be reduced

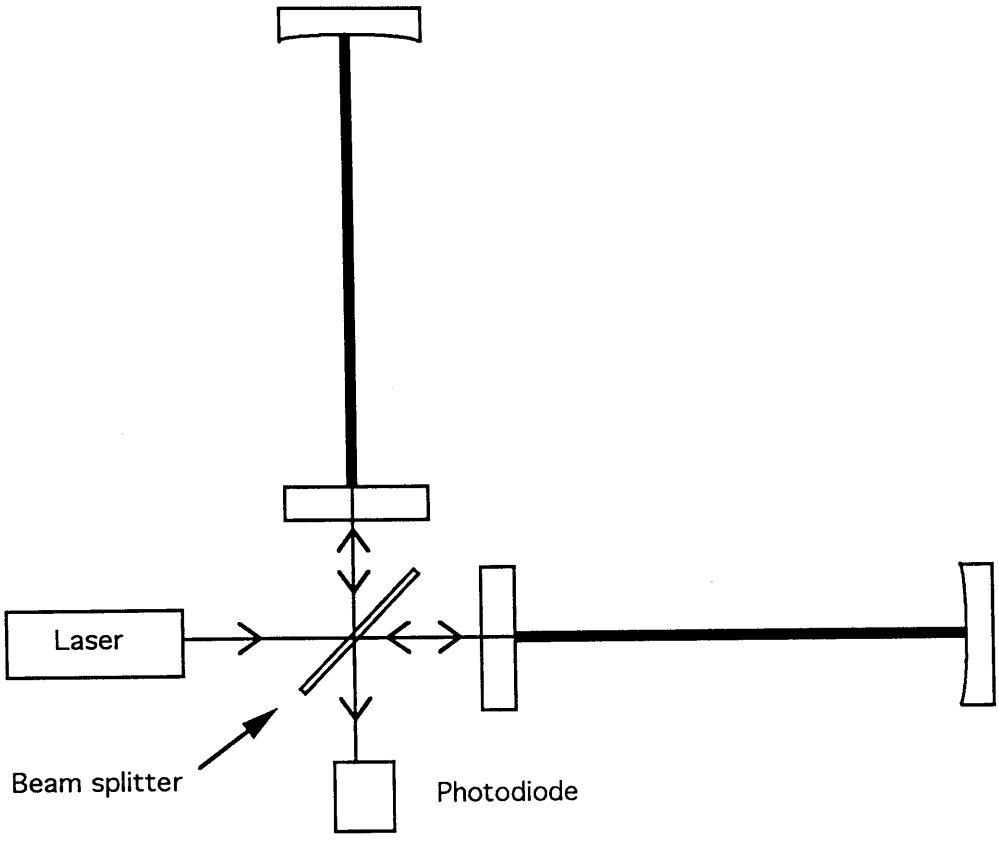

Figure 1.4: Fabry-Perot Michelson interferometer

by frequency stabilising the laser light [Schilling et al 1981]. The MPQ detector which has arm lengths of 30 m has a gravitational wave amplitude sensitivity of $1.1 \times 10^{-19}/Hz^{1/2}$ above 1.5 kHz [Shoemaker et al 1988].

1.11 Fabry-Perot detectors

The Fabry-Perot Michelson interferometer was first developed at Glasgow University on a 10m prototype and later at Caltech on a 40m detector. The Fabry-Perot system works by achieving a longer effective path length by use of a Fabry-Perot cavity in each arm. This is shown in figure 1.4. The Fabry-Perot cavity in each arm is held on resonance with the laser light. Fluctuations in arm length produce large phase fluctuations in the returning light. The comparison of the phase of the light from the two arms can be carried out by recombining the light on a beam

* Alternatively the light from each cavity may be detected separately; the resulting signals may then be subtracted electronically to give a measure of the relative length of the two cavities.

splitter. As both cavities have to be held on resonance with the laser light, precision control of the orientation of the test masses is required as well as much greater frequency stability of the laser. The Fabry-Perot system has the advantage that much smaller mirrors can be used. Additionally scattered light is less of a problem because of the overlap of the multiple bounces.

The Glasgow prototype is composed of two 10m optical cavities. In this system one cavity is used to frequency stabilise the laser by locking the laser to the cavity. The other cavity is held on resonance with the laser light by a control system that adjusts the Fabry-Perot cavity length. There is no optical recombination; instead the gravitational wave signal is derived from the feedback signal required to keep the cavity on resonance as the gravitational wave changes the cavity length. The current detector has a gravitational wave amplitude sensitivity of $0.7 \times 10^{-19}/Hz^{1/2}$[Morrison et al 1991] and the current amplitude sensitivity of the Caltech detector is $2.5 \times 10^{-20}/Hz^{1/2}$[Zucker et al 1991].

1.12 Noise sources in interferometric detectors

The sensitivity of an interferometer is limited by several noise sources. These are important for the current detectors and for the next generation of gravitational wave detectors planned by several research groups [Hough et al 1989], [Vogt et al 1989], [Giazotto et al 1989], [Blair et al 1989]. These detectors are interferometers with arms up to 3 km long, giving strain sensitivities of 10^{-22} in a frequency range of a few tens of Hz to a few kilohertz. The main noise sources for interferometers are described below, along with estimates of the technology required for the gravitational wave detectors of the future.

1.12.1 Heisenberg Uncertainty Principle

A fundamental limit to the detection process is the Heisenberg Uncertainty Principle applied to the measurement of the test mass displacement. Any measurement of the position, x, affects the momentum of the test mass, p. In a time τ the smallest measurable displacement of a mirror of mass M may be calculated from

$\Delta x \Delta p \geq \hbar$ using $\Delta p \sim M\Delta x/\tau$

$$\Delta x = (\hbar\tau/M)^{1/2}$$

For a mirror of mass 400 kg the minimum detectable wave amplitude is around $10^{-24}/Hz^{1/2}$ at 1 kHz; far below limits set from other noise sources.

1.12.2 Photon shot noise

An important fundamental noise source in interferometric detectors is shot noise in the measurement of the light intensity. The gravitational wave signal induces an intensity change and so the smallest signal detectable depends on the smallest intensity change detectable. This is determined from the fluctuations in the number of photoelectrons produced in the photodetector. The signal to noise ratio increases with the square root of the laser power. To achieve a sensitivity high enough to detect a wave of amplitude of 10^{-22} around 1 kW of input laser power is required. Fortunately there are schemes that have been proposed to reduce the demands on the laser power. One technique is power recycling or standard recycling [Drever 1983]. If an interferometer is operated on a null fringe the light, for a low loss system, is returned towards the laser and wasted. In power recycling, figure 1.5, a mirror is placed between the laser and the beam splitter to recycle the light back to the interferometer. This effectively increases the available light power. With power recycling a long base line detector will require approximately 100 W of light to detect a wave of amplitude of 10^{-22} . Other schemes which have been proposed are dual recycling [Meers 1988] and using squeezed light [Caves 1981].

1.12.3 Radiation pressure

A fundamental limit is radiation pressure fluctuations on the interferometer mirrors. Radiation pressure is due to random fluctuations in the number of photons striking the mirrors and leads to a momentum uncertainty. Caves [Caves 1980] has shown that radiation pressure and shot noise in a Michelson can be minimised to

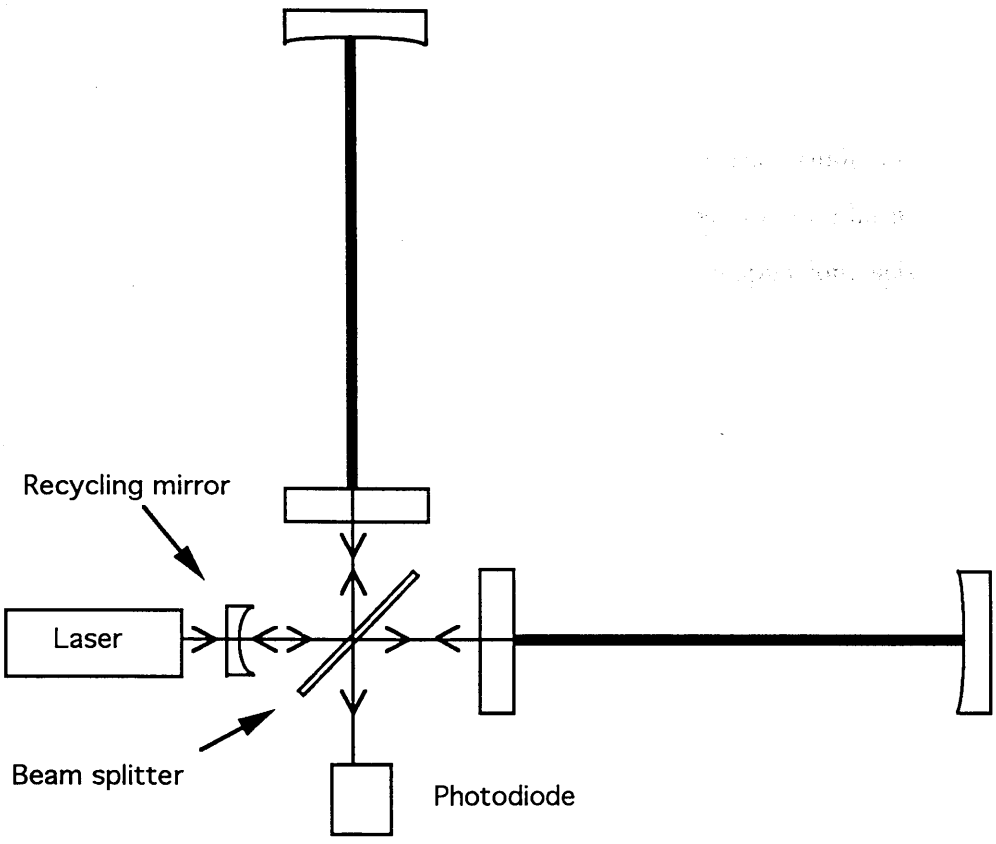

Figure 1.5: Power recycling in a Fabry-Perot interferometer

the limit of the uncertainty principle. The noise from radiation pressure whenever 100 W of laser light is used with power recycling should be far below the shot noise limit.

1.12.4 Technical noise

There are many noise sources that arise for technical, rather than fundamental, reasons that limit the performance of a detector. These include laser beam geometry fluctuations, thermal noise in the masses and suspension, seismic noise refractive index fluctuations in the vacuum, laser intensity fluctuations and laser frequency fluctuations. Figure 1.6 summarises the main noise sources as a function of wave amplitude and frequency expected in a 3 km baseline detector as proposed by [Hough et al 1989]. Laser frequency noise and intensity noise are important to this thesis and are described in further detail.

1.12.5 Frequency noise

A Michelson interferometer with arms of identical length is insensitive to laser frequency fluctuations. However, due to scattered light and arm length differences the laser light has to be frequency stabilised. The level of stabilisation required is not as great as that for a Fabry-Perot system. As mentioned earlier the cavities in a Fabry-Perot must be kept on resonance with the laser light. For Fabry-Perot cavities the required frequency stability of laser light of frequency ν is

$$\frac{d\nu}{\nu} = hD$$

where $d\nu$ is the frequency deviation, h is the gravitational wave amplitude and D takes account of variations in the two cavities mode matching, visibility and storage times. The proposed detectors will require a frequency stability of $3 \times 10^{-8} Hz/Hz^{1/2}$ at 1 kHz if a sensitivity to h of 10^{-22} is required [Hough et al 1989]. Currently the stabilised Argon ion lasers used in the Glasgow prototype have a frequency stabilised level of $2 \times 10^{-5} Hz/Hz^{1/2}$ at 1 kHz [Robertson 1990].

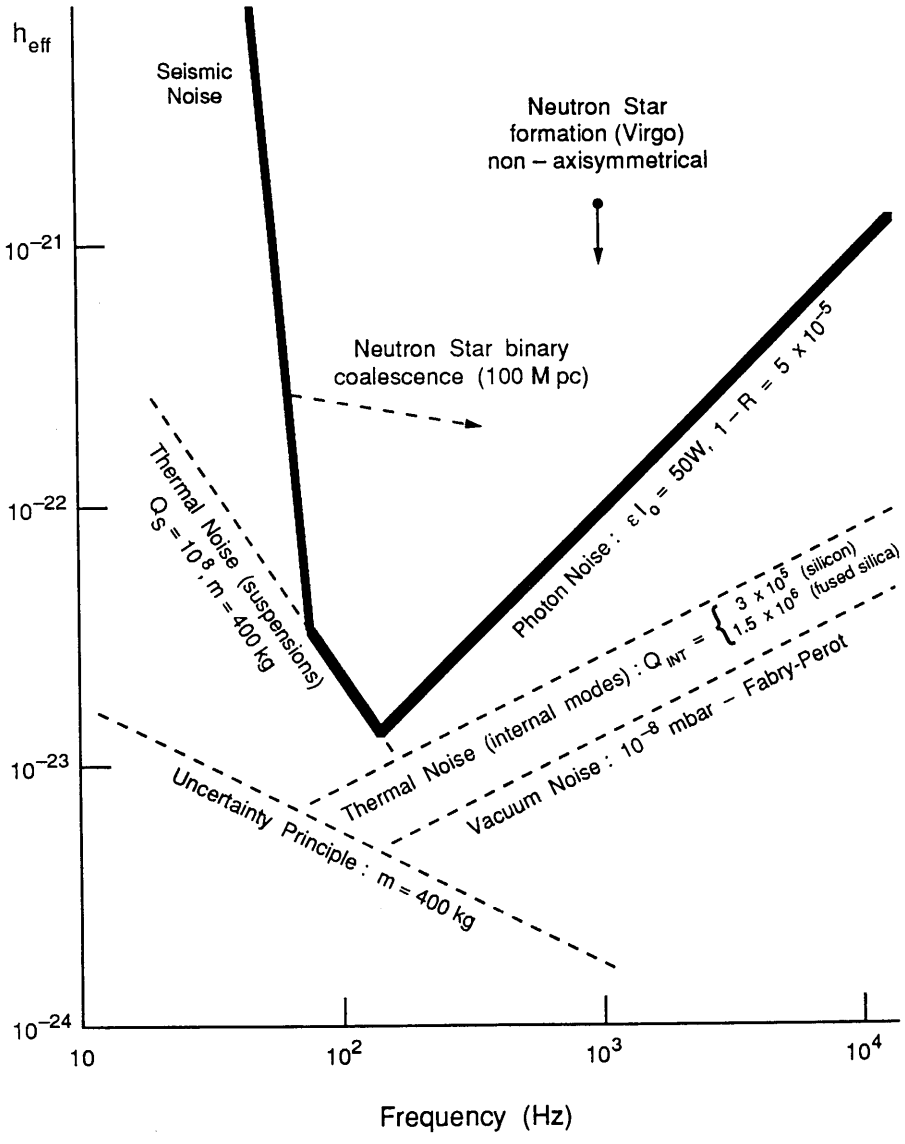

Figure 1.6: The figure shows some burst sources and noise levels in a 3 km interferometer. h_{eff} is the rms amplitude for pulse signals of frequency f measured over a bandwidth of f/2. The photon noise was calculated assuming standard recycling and ϵI_o is the laser power efficiently coupled into the detector. The quality factors used to calculate the thermal noise correspond to the suspension and to the mass (either silicon or fused silica). The graph is taken directly from the GEO proposal [Hough et al 1989].

1.12.6 Intensity noise

The intensity noise from a laser is generally much larger than shot noise for low frequency Fourier components. If a cavity and laser are held exactly on resonance the detection system is independent of intensity fluctuations. If there is an offset in the feedback system the intensity noise will couple in. The present system at Glasgow has an intensity stability of $\frac{dI}{I} = 10^{-7}/Hz^{1/2}$ at 1 kHz [Mangan 1988]. This should be stable enough for the next generation of long base line detectors.

1.13 Summary

The requirements of a laser to operate an interferometer are high power, frequency and intensity stability. In order to reach a sensitivity to h of around 10^{-22} the laser must supply around 100 W with a frequency stability of $3 \times 10^{-8} Hz/Hz^{1/2}$ at 1 kHz and an intensity stability of $\frac{dI}{I} = 10^{-7}/Hz^{1/2}$. The present generation interferometric detectors use Argon ion lasers. It is unlikely that these lasers will be scaled up to provide the necessary power, although the frequency and intensity stability could be achieved. The following chapters describe some experiments towards the development of an alternative to the Argon ion laser.

Chapter 2

Diode Pumped Nd:YAG Lasers

2.1 Introduction

The demands placed on a laser for interferometric gravitational wave detection suggests that the currently used argon ion lasers will be able to meet the criteria for laser power only if a number of lasers are coherently added. Although these lasers are potentially capable of reaching the requirements for frequency and intensity stability, the difficulty is in scaling up the system from a few watts of single frequency light to about a hundred watts.

Of the currently available alternative lasers a solid state Neodymium based system is the most promising. Both crystal and glass hosts for Neodymium are available, each with different properties. Nd:Glass is available and the non-crystal structure allows higher fractional doping and hence gain, but tends to be inhomogeneously broadened. The most widely used crystal host is Yttrium Aluminium Garnet, YAG. Nd:YAG lasers are available with multimode powers of up to a few kilowatts and the scaling of a single frequency Nd:YAG laser to the 100 W level is very likely. Others are available and being developed, for example Nd:YLF, but seem to lack the robustness required for general use.

The most common and efficient operational wavelength of Nd:YAG is 1064 nm. Compared with the 514 nm wavelength of the Argon ion laser the Nd:YAG suffers from increased beam diffraction ($\sqrt{2}$ larger), a costly and technologically important point when vacuum systems and mirror sizes have to be increased accordingly. However, it is possible to operate the Nd:YAG laser at its second harmonic using the nonlinear susceptibility of a crystal material so that a high power second har-

monic Nd:YAG laser looks to be a promising alternative to an argon ion laser. Several recent developments have enhanced the prospects of such a laser. Namely the development of laser diode pumping in the past few years and the availability of new nonlinear materials, such as LBO for second harmonic generation. Recently diode pumped slab lasers have been demonstrated at power levels of a few watts [Burnham and Hays 1989] and a cw second harmonic efficiency of over 30 % (6.5 W second harmonic from 18 W of fundamental) has been demonstrated [Yang et al 1991].

This chapter describes the nature of Nd:YAG lasers followed by a description of a low power longitudinally pumped Nd:YAG laser.

2.2 Nd:YAG lasers

Neodymium doped Yttrium aluminium garnet or Nd:YAG is chemically stable, robust, has good optical quality and good thermal conductivity, all of which are desirable properties for a laser material. The Yttrium in YAG is doped with approximately 1% Neodymium, the optimum for cw operation. At higher doping levels the efficiency of the laser material decreases because of inhomogeneities from crystal strain, reduced heat conductivity and concentration quenching. Concentration quenching arises from cross relaxation, where an upper lasing level is destroyed leaving two ions in a lower nonlasing level and so destroying the inversion. The limited doping restricts the gain available from a Nd:YAG laser. Co-doping can be applied to improve the characteristics, either to improve absorption of the pump or to allow increased doping. However, such schemes have inevitable drawbacks for example line broadening and pumping difficulties. If chromium is used as a co-dopant then for efficient pumping the pump wavelength must be less than 600 nm which causes damage to the crystal structure of Nd:YAG.

Nd:YAG is a four level laser, as shown on the simplified energy level diagram of figure 2.1. The main lasing transition of 1064 nm corresponds to the transition of the $4F_{3/2}$ level to the $4I_{11/2}$ level. Other lasing transitions are available, for example 1300 nm.

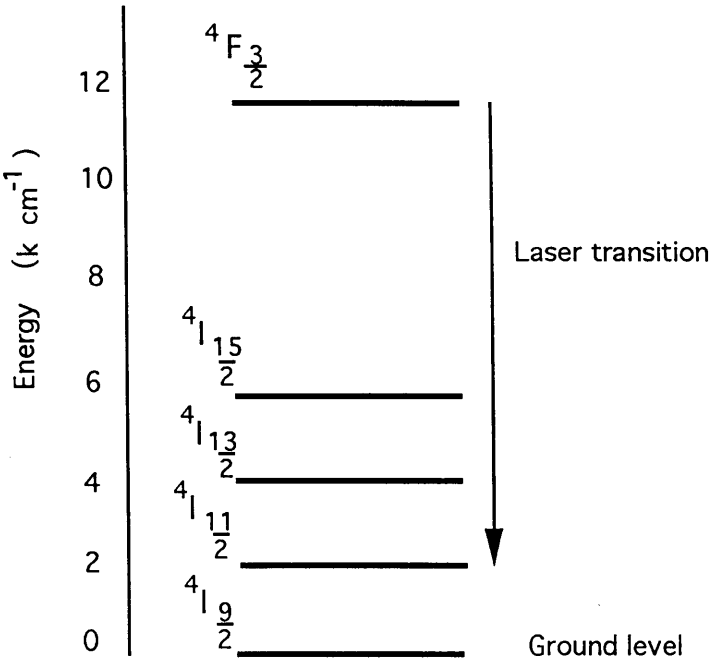

Figure 2.1: Energy level diagram of Nd:YAG [Yariv 1975].

2.3 Pumping

Nd:YAG must be pumped optically. The absorption spectrum is shown on figure 2.2. The lowest pump bands that can be used if the four level nature of the Nd ion is to be applied are around 800 nm, the higher pump levels beyond 600 nm lead to degradation of the Nd:YAG. Pumping can be achieved with tungsten lamps or gas discharge lamps. The life time of such pumping schemes is a few hundred hours. The lamp emission is not well matched to the absorption spectrum of Nd. This poor spectral match means that most of the electrical input energy ends up as heat in the Nd:YAG rod and thus requires water cooling for continuous operation. Chapter 4 deals with a flash lamp pumped Nd:YAG laser and some of the associated thermal problems.

Pumping can be achieved using a laser diode. This is significantly more efficient than a flash lamp, due to the narrow band emission of the laser diode. The strongest absorption band can be utilised by tuning the diode emission to match it exactly which helps eliminate the heating problems that a flash lamp generates. At

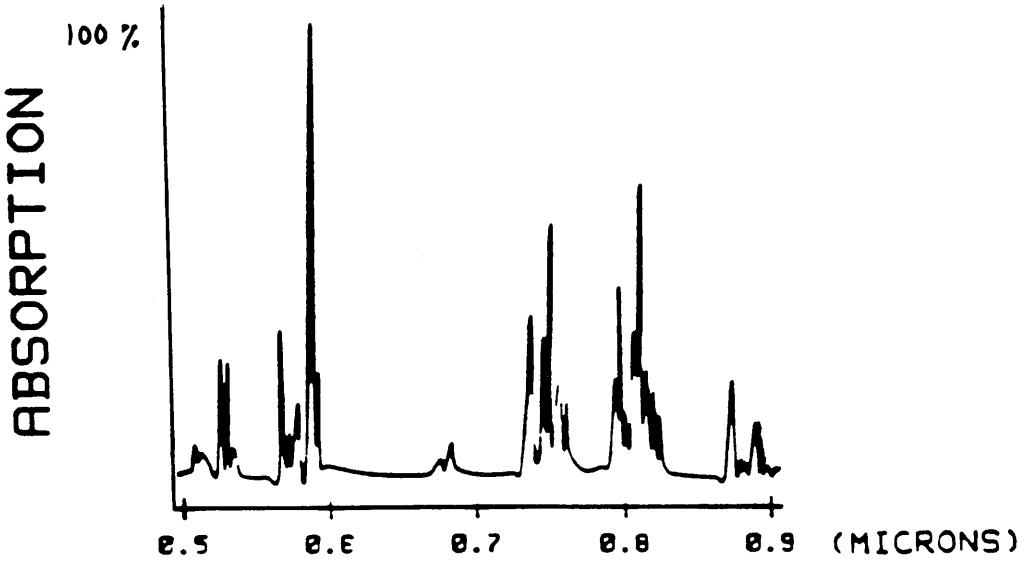

Figure 2.2: Absorption spectrum of Nd:YAG

high power levels some active cooling may be necessary but will be significantly less than if flashlamp pumping is used. The Nd:YAG can be pumped either in a radial direction to the Nd:YAG rod or can be pumped along the axis. If longitudinal pumping is used then the efficiency of the pumping can be improved through spatial overlap of the pump and the laser mode; in addition this eliminates any requirement for transverse mode control. At higher power levels longitudinal pumping becomes impractical because of the number of diodes required and some form of transverse pumping is required. Diode pumping has allowed electrical power to light power efficiencies of around 10 % [Hanover 1990]to be achieved. This is significantly higher than for flashlamp pumping which achieves less than 1% efficiency.

2.4 Development of a diode pumped Nd:YAG laser

As discussed in the previous section the criteria for efficient diode pumping are spectral overlap with the absorption peak of Nd:YAG and spatial overlap with the Nd:YAG mode. To achieve spectral overlap the pumping was carried out using a single strip Sony gallium aluminium arsenide double hetero-junction laser

diode. The diode was specified at a power level of 500 mW and at a wavelength of 810 nm, in order to match the 808.5 nm absorption peak of the Nd:YAG. The wavelength of a laser diode is both temperature and current dependent. The cavity length changes with temperature and hence wavelength, either from the increased current or from an external temperature change. (The semiconductor is so small that axial mode spacing is around 0.1 nm.) The wavelength changes by about 0.3 nm per $^{\circ}C$ and by about 0.025 nm per mA. In order to gain spectral match the diode temperature was actively controlled.

The wavelength of the diode, for a current of 620 mA and temperature of 24 $^{\circ}C$, was measured at only 805 ± 1.5 nm, a little off the absorption peak. This could have been improved by increasing the temperature but can be counter productive due to the operational lifetime of the diode reducing with temperature. However, the absorption of the pump was examined in a 3×5 mm cylindrical piece of Nd:YAG as a function of temperature and current. The transmission was measured with varying temperature as the current was held constant. The results are shown on figure 2.3. This enabled the optimum diode parameters for pumping to be determined. From the graph the higher temperature is the most efficient, at all currents. This further indicates that the wavelength of the diode is just off the absorption peak of Nd:YAG.

2.5 The Nd:YAG laser cavity

The Nd:YAG laser cavity design was a linear arrangement. As will be discussed in chapter 4, Nd:YAG lasers are susceptible to running more than one longitudinal mode so that either a twisted mode or ring cavity is more desir able. However for simple design and construction a linear cavity was used. The laser cavity consisted of a flat mirror and a 15 cm radius of curvature mirror spaced by 12 cm. The Nd:YAG rod itself was used as the plane mirror. A longitudinal pumping scheme was used to take advantage of the improved efficiency. Figure 2.4 shows a schematic diagram of the cavity and pumping arrangement. This cavity arrangement has a waist of 285 μm positioned on the plane mirror. The rod was a cylinder of diameter

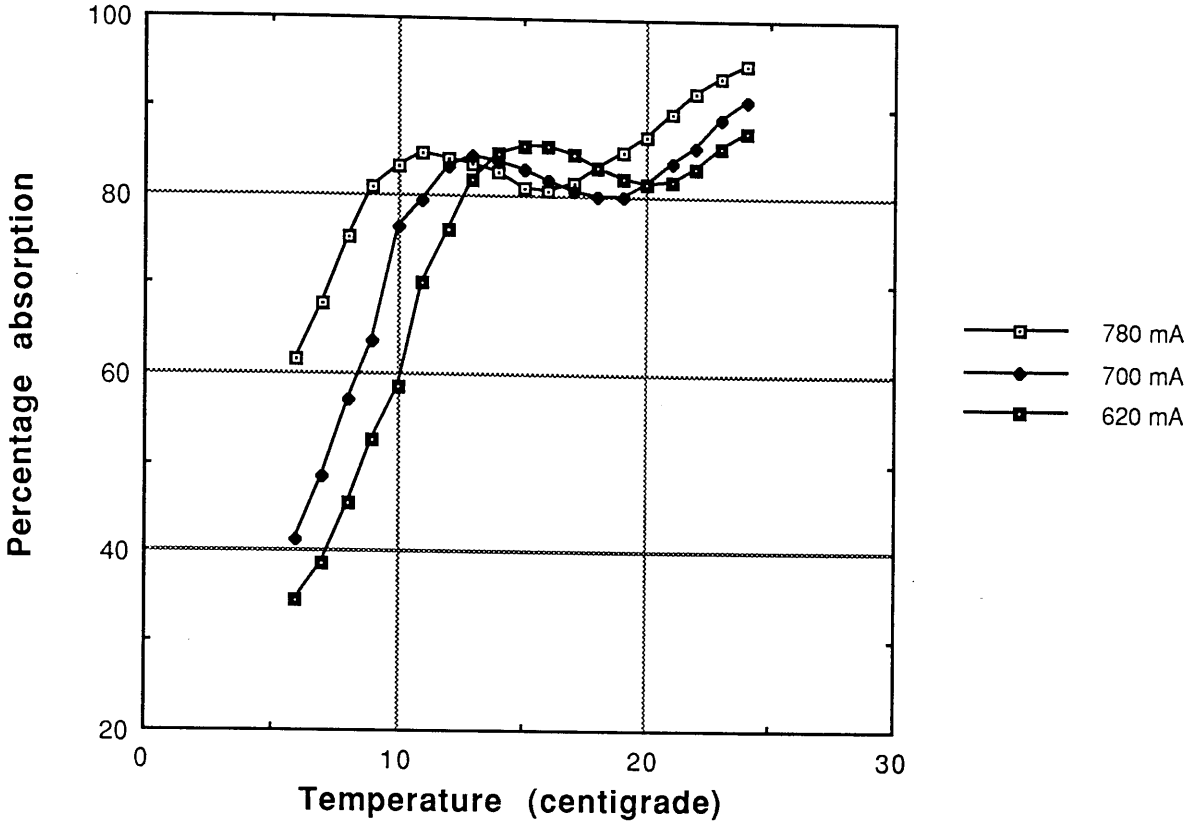

Figure 2.3: Absorption of diode laser light by Nd:YAG as a function of temperature for various diode currents.

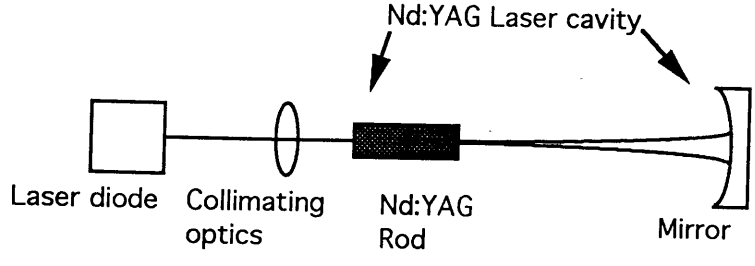

Figure 2.4: Schematic diagram of the linear Nd:YAG laser cavity and pumping arrangement.

3 mm and length 5 mm, doped with 1 % Nd. It was antireflection coated for 810 nm and coated for high reflection at 1064 nm on the end that the pump was incident, thus transmitting the pump but acting as a cavity mirror for the Nd:YAG. The opposite end of the rod was antireflection coated for 1064 nm to minimise any cavity losses. The curved mirror was 1% transmitting and served as the output coupler.

Longitudinal pumping was used. In order to take full advantage of the efficiency and to force a TEM 0,0 mode to run, the pump profile and the laser mode profile should match. If the pump and the laser had identical wavelengths then for optimum overlap the two beams should have a waist of the the same size in overlapping positions. However the wavelength variation will lead to different diffraction rates. The absorption of the pump occurs over a small length and the beams undergo a very small size change. In this situation, matching the two waists as well as possible is probably the most efficient technique.

The laser diode has a beam shape that is not dependent on a conventional cavity geometry but on the structure of the cavity defined by the semiconductor sandwich used. The active region of the laser is a thin layer, which uses waveguide confinement effects to keep the beam in the active region. This results in a profile that is asymmetric and astigmatic. The small size of the semiconductor results in a quickly diverging beam. The beam divergence and astigmatism must be compensated for to allow efficient pumping. The collimation was achieved as shown in figure 2.5. An initial lens of 8 mm focal length was placed at the diode output to slow the beam divergence. This was followed by an anamorphic prism pair, of approximately three times contraction along one axis. This was used to produce a symmetric beam and correct the astigmatism. The anamorphic prism pair was used in place of a cylindrical lens. Along one axis the prisms have no effect on the beam, whereas in the orthogonal direction they act like a lens. (They behave as a cylindrical lens, the orientation of the prisms defining the power of the lens.) A 48 mm lens and a 6.5 mm lens were then used in a telescope arrangement to allow the beam to be experimentally reduced. The lenses formed a beam waist of aproximately 0.14 mm on the surface of the Nd:YAG rod, the size and position of

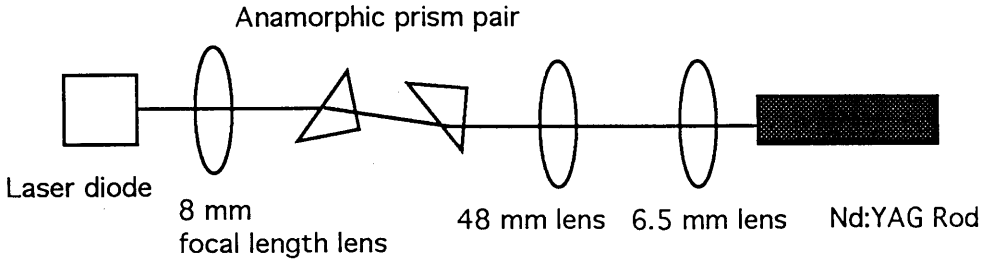

Figure 2.5: Pumping optics used to obtain matching of the laser diode and Nd:YAG laser.

the cavity laser waist. The use of several components in the pumping arrangement had the disadvantage of introducing loss, this loss being as much as 47 %. It is possible that fewer optical compone nts giving a lower quality pump beam could have been tolerated with advantage of less loss; an arrangement that replaced the prisms and initial lens with a single cylindrical lens may have been a simple way to restrict the losses. The laser diode power had already been restricted to 340 mW to extend the diode life time and with the loss from the pumping optics the useful pump power was limited to 180 mW.

The Nd:YAG laser power output was 75 mW of Tem 0,0 for a diode temperature of 24 °C. The variation of power output as a function of diode temperature is shown for various diode currents on figure 26. From consideration of these results and the previous pump absorption results it is probably better to use an attenuation of the pump rather than varying the diode current (which changes the absorption character) to control the output of the Nd:YAG laser.

To provide a single mode and a polarised output an etalon and Brewster angled

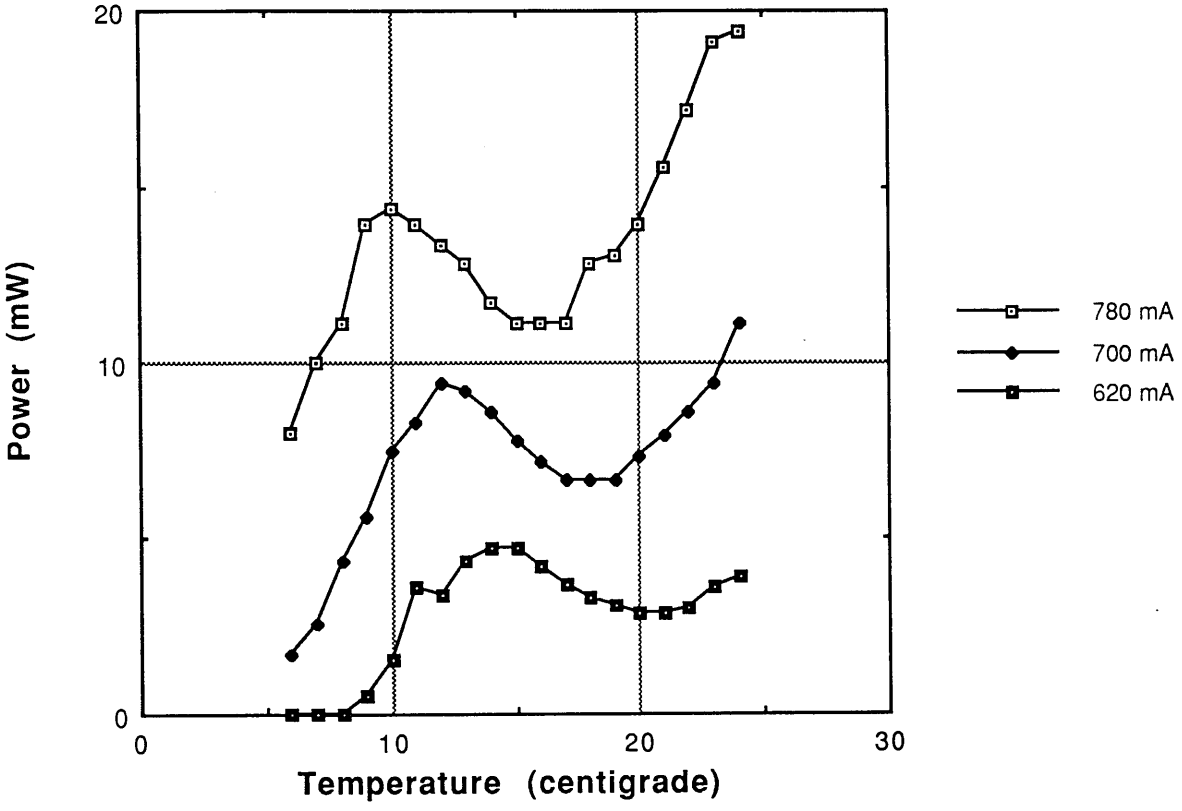

Figure 2.6: Power output of Nd:YAG laser as function of the temperature of the laser diode pump for various diode currents. (For a single longitudinal mode)

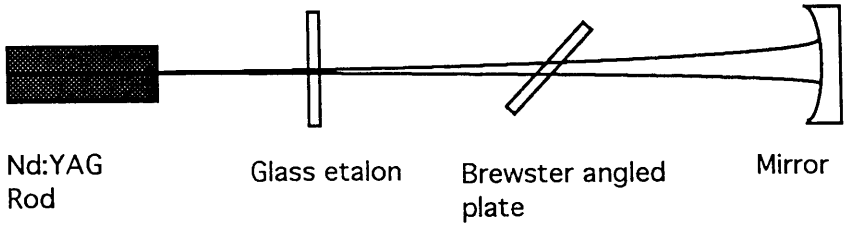

Figure 2.7: Nd:YAG laser cavity with etalon and Brewster angled plate added to provide a single mode and a polarised output.

plate were added to the cavity, as shown in figure 2.7. This gave a single mode output but the loss associated with each component resulted in a power drop to around 20 mW maximum output. The single mode power as a function of useful pump power (pump power after the collimating optics) at 24 $°C$ is shown in figure 2.8. The overall electrical efficiency of the laser is 5.5% when running multimode. This drops to 1.2% when the etalon and brewster plate are added to the cavity.

2.6 Summary

A low power diode pumped laser was developed and its maximum electrical efficiency shown to be 5.5%. This could have been improved if the losses from the pumping optics could be eliminated or reduced. It is possible that a reduction in the number of elements in the pumping scheme, for instance replacing a lens and the anamorphic prism pair with a cylindrical lens, would have reduced the loss.

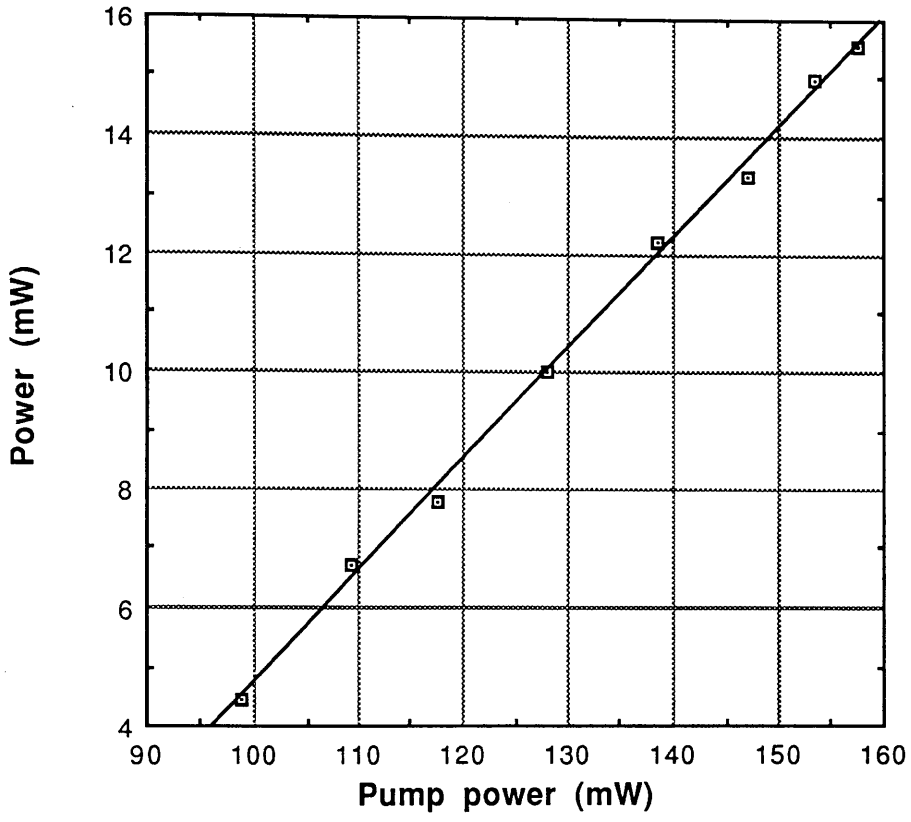

Figure 2.8: Single mode power from a Nd:YAG laser as a function of useful pump power.

Chapter 3

Frequency noise measurement and intensity stabilisation

3.1 Introduction

Chapter 1 outlined the requirements of a laser for use in an interferometric gravitational wave detector. Two criteria which are examined here are frequency noise and intensity noise.

One of the possible applications of a low power diode pumped Nd:YAG is its use as a highly frequency stable oscillator for injection locking of a high power laser, either pumped with a flashlamp or diodes. A diode pumped Nd:YAG laser is expected to have a lower level of frequency fluctuations than either a flashlamp pumped Nd:YAG laser or an Argon ion laser. The solid state nature of the Nd:YAG is a possible advantage over the plasma gain medium of the Argon laser in terms of noise performance. However, it is the reduction and possible elimination of the water cooling in a diode pumped laser that may make the greatest contribution to its potential for low noise. The first part of this chapter describes the stabilisation of the laser described in Chapter 2 to a Fabry-Perot cavity and the subsequent measurement of the natural frequency fluctuations.

The second noise source examined is intensity noise. It has been demonstrated that the intensity noise of an Argon ion laser can be stabilised to a very high degree [Mangan 1988]. A flash lamp pumped Nd:YAG laser has a low frequency intensity noise level very similar to an Argon ion laser (see chapter 7). A diode pumped Nd:YAG has a significantly lower noise level [Campbell 1991]. However,

Nd:YAG lasers have a particular intensity noise peak at around a few hundred kHz, that arises from the dynamics of the lasing process. This is known as a relaxation oscillation and may cause intensity noise of up to 1 % of the dc intensity at the oscillation frequency. The removal of this intensity may have important consequencies as it has been reported [Kazovsky and Atlas 1990] that the relaxation oscillation may couple from intensity noise into frequency noise. The second part of this chapter describes a servo technique which, applied to a diode pumped Nd:YAG laser, removes the oscillations at source rather than using an amplitude modulator as an external noise filter.

3.2 Frequency fluctuations

The measurement of the frequency fluctuations of a laser relies on making a comparison with a reference source; this is commonly a Fabry-Perot cavity. A technique that can be applied to measure such a signal is to use a feedback control system where a correction signal is applied to maintain the laser and the reference in a fixed state. The correction signal can then be used as a measure of the quantity under examination. The laser frequency can be corrected by either changing the cavity length mechanically, with for example a piezoelectric transducer (PZT), or changing the optical length with an electro-optic or acousto-optic modulator. The optical fractional path length change $\frac{\Delta l}{l}$ corresponds to a fractional frequency change of $\frac{\Delta f}{f}$, where Δl and Δf are the changes in length and frequency respectively, and l and f, are half a wavelength and the free spectral range c/2l (where c is the velocity of light in the medium) respectively. The selection of the feedback element is generally made with the bandwidth of the control system in mind.

A block diagram of a negative feedback control system is shown in figure 3.1. G and H are control elements with transfer functions G(s) and H(s). The error signal is v_ϵ defined by $v_n - v_f$, where v_n is the noise source and v_f is the feedback signal. The relationships

$$v_f = \frac{GHv_n}{1+GH}$$

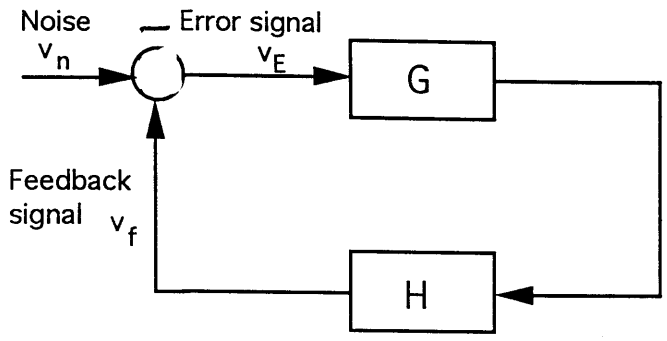

Figure 3.1: Block diagram of Control system.

and

$$v_\epsilon = \frac{v_n}{1 + GH}$$

can easily be obtained. From this it can be seen that the control system reduces the natural fluctuations by a factor $1 + GH$, and that the value of v_f is a direct measure of the natural frequency fluctuations whenever the loop gain, GH, is much larger than 1. Such a system may not necessarily be stable. For stability, the phase delay in the feedback loop must be less than π when the loop gain is unity. For example, in a PZT used as a feedback element the mechanical resonance can be accompanied by a large phase change. This may result in an oscillating system if the unity gain point is not restricted to be below the PZT resonance frequency. As mentioned earlier, the control system has the effect of reducing the frequency fluctuations by the loop gain of the control servo. The system is in fact suppressing the frequency fluctuations of the laser whenever the correction signal is applied to the laser cavity. Applying the correction signal to the reference cavity would yield only the laser noise relative to the cavity.

Optical cavities, such as a Fabry-Perot cavity, may be used as a reference source for laser stabilisation. There are several ways to generate an error signal to use in a feedback loop, but the two most useful are transmission locking and radiofrequency (RF) reflection side band locking. The transmission intensity of a Fabry-Perot cavity is a strong function of frequency whenever the cavity is close to resonance. This allows an error signal to be generated. The point half way up

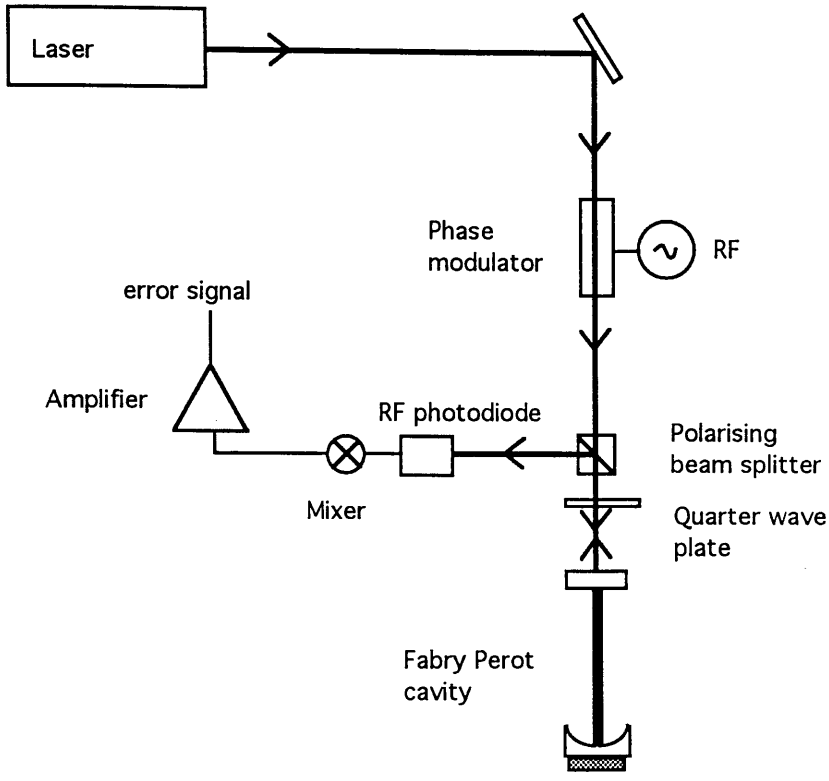

Figure 3.2: Locking scheme using RF sideband reflection locking.

a fringe is used as the reference point. This allows a bipolar error signal to be derived since any deviation from the half way position of the fringe generates a change in intensity, either an increase or decrease depending on the frequency shift. If this signal is subtracted from a second signal that depends on the laser intensity, then an intensity free error signal can be derived. One of the disadvantages of this system is that if the frequency shift is larger than half the cavity line width the error signal may switch polarity and lock will be lost. A second difficulty is having to match the response of the two photodiodes.

Figure 3.2 shows a block diagram of the RF reflection locking scheme [Drever et al 1983]. The incident laser light is phase modulated at a radio frequency greater than the cavity linewidth. This results in sidebands being added to the incident light at the modulation frequency. The light directly reflected from the Fabry-Perot cavity and the light that leaks from the cavity combine on a photodiode. The leakage light contains no sidebands, due to the modulation frequency being

larger than the cavity linewidth and hence being suppressed. The interference produces an amplitude modulated signal at the original modulation frequency. The amplitude and phase of the modulation depend on the difference in frequency between the laser light and the cavity resonance for laser fourier components below the line width of the cavity. Above the linewidth of the cavity the signal is proportional to the integral of the frequency difference (the phase). The demodulation of this signal produces an error signal with a magnitude and sign that is linear with the frequency offset (or phase offset for frequencies higher than the linewidth) of the laser and the cavity. This system uses only one photodiode and so eliminates any matching of response. It has the further advantage that there is a wide servo band width independent of linewidth. In such a system the cavity has a transfer function that is equivalent to a low pass filter that has a 3dB point at a frequency of half the cavity linewidth. This results in a $\frac{\pi}{2}$ phase shift at frequencies greater than the cavity linewidth. However, if the phase shift is accounted for, the transition is smooth and the bandwidth may be many times larger than the linewidth.

3.3 Frequency fluctuations of the diode pumped Nd:YAG

The frequency fluctuations of the diode pumped laser described in Chapter 2 were measured by locking the laser to a cavity using RF reflection locking to generate the error signal. Figure 3.3 shows the experimental apparatus used.

The laser light was phase modulated at 10 MHz, and was incident on a reference cavity of finesse approximately 200. To extract the reflected light and the light returning from the cavity, a polarising beam splitter and quarter wave plate were used as an optical diode. The signal was then detected on an RF photodiode. Once demodulated and filtered, the generated error signal was amplified, filtered and applied to a PZT controlled laser cavity mirror. The electronics of the control system were designed to maintain the stability of the control loop. The bandwidth of the servo was not too important because the frequency of interest in the noise spectrum of the laser is around 1 kHz. The electronics used in the control system

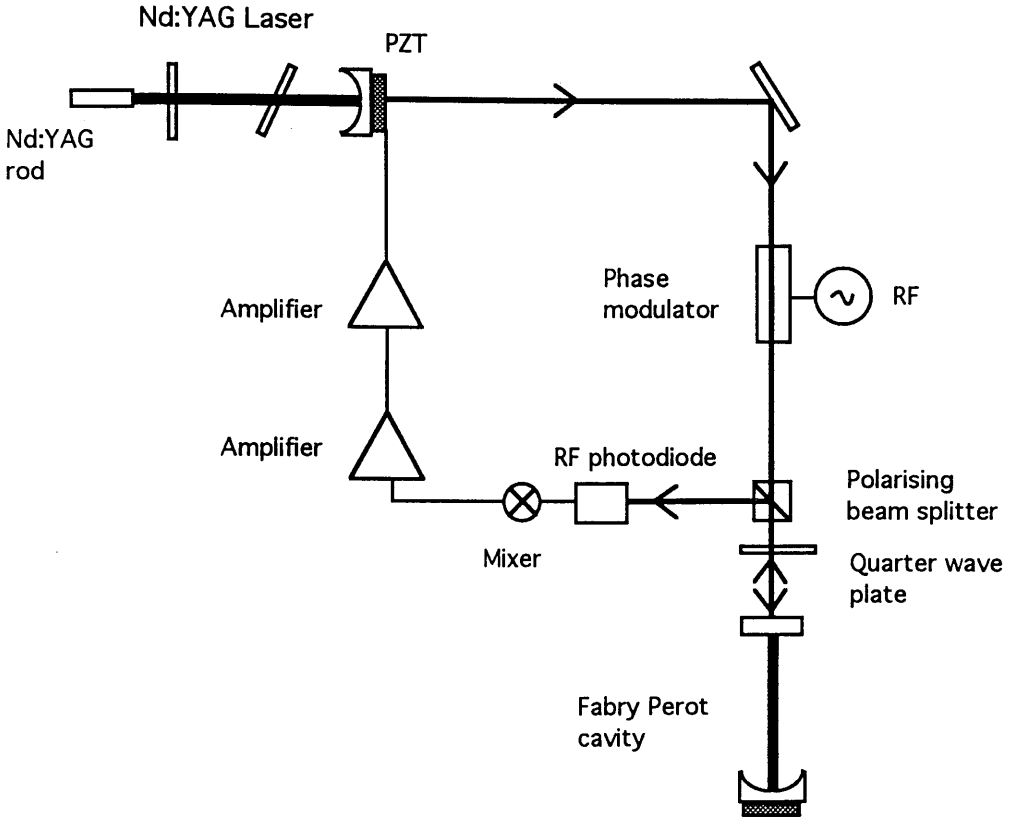

Figure 3.3: Experimental apparatus to measure frequency fluctuations of the Nd:YAG laser using the RF locking technique.

are shown on figure 3.4. The unity gain point of the servo was around 20 kHz which was much lower than the cavity roll off frequency of several megahertz. The electronics used a 12 dB rolloff from 50 Hz to around 5 kHz, and then used a 6dB rolloff through to the unity gain point.

When measuring the frequency noise, considerable effort was made to eliminate background noise from the laboratory: this involved acoustic isolation of the laser and Fabry-Perot cavity and switching off excess equipment in the lab. This cut down the frequency fluctuations by around a factor of ten at 1kHz. The laser diode pump was isolated from back reflection but this made no difference to the noise level. Figure 3.5 shows the spectrum of the feedback signal, the representation of the laser noise. The spectrum shows a frequency fluctuation level of 50 $Hz/Hz^{1/2}$ at 1 kHz. This is significantly lower than the 2-3 $kHz/Hz^{1/2}$ noise level of an argon ion laser. The excellent noise performance of the diode pumped system makes it suitable for interferometry and establishes its potential for injection locking, a role described in Chapter 5.

3.4 Relaxation oscillations

Relaxation oscillations occur due to the interaction between the oscillation field of the laser cavity and the atomic inversion of the laser medium. An increase in the field intensity reduces the inversion due to increased stimulated emission. This consequently reduces the gain and decreases the field intensity. This arises when the laser is perturbed by a small change in gain, cavity loss or alignment. The effect is generally not seen in gas lasers, for example an Argon ion laser, because the recovery time of the excited state population inversion is shorter than the laser cavity decay time. The relaxation oscillations can be responsible for intensity peaks of as much as 1% of the dc intensity. The oscillation occurs at a frequency that is dependent on the losses, the pumping level and the upper state lifetime of the laser transition. Figure 3.6 shows spectra of intensity noise for both the diode pumped Nd:YAG laser of Chapter 2 and the flashlamp pumped Nd:YAG laser of Chapter 4. In both cases relaxation oscillations can be seen. Yariv [Yariv 1975]

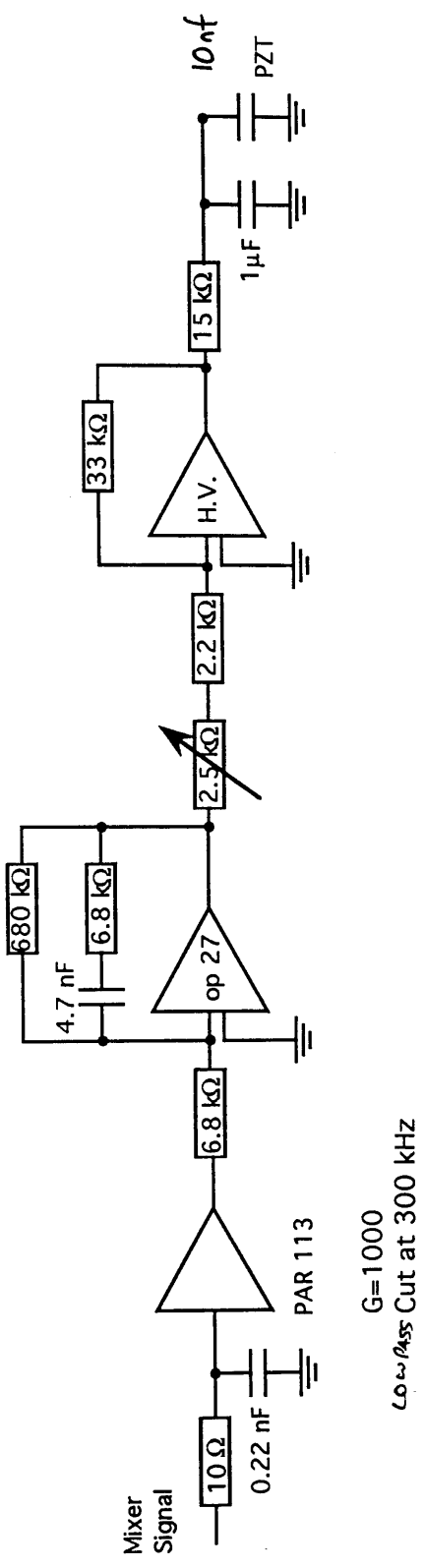

Figure 3.4: Feedback electronics used for locking the Nd:YAG laser.

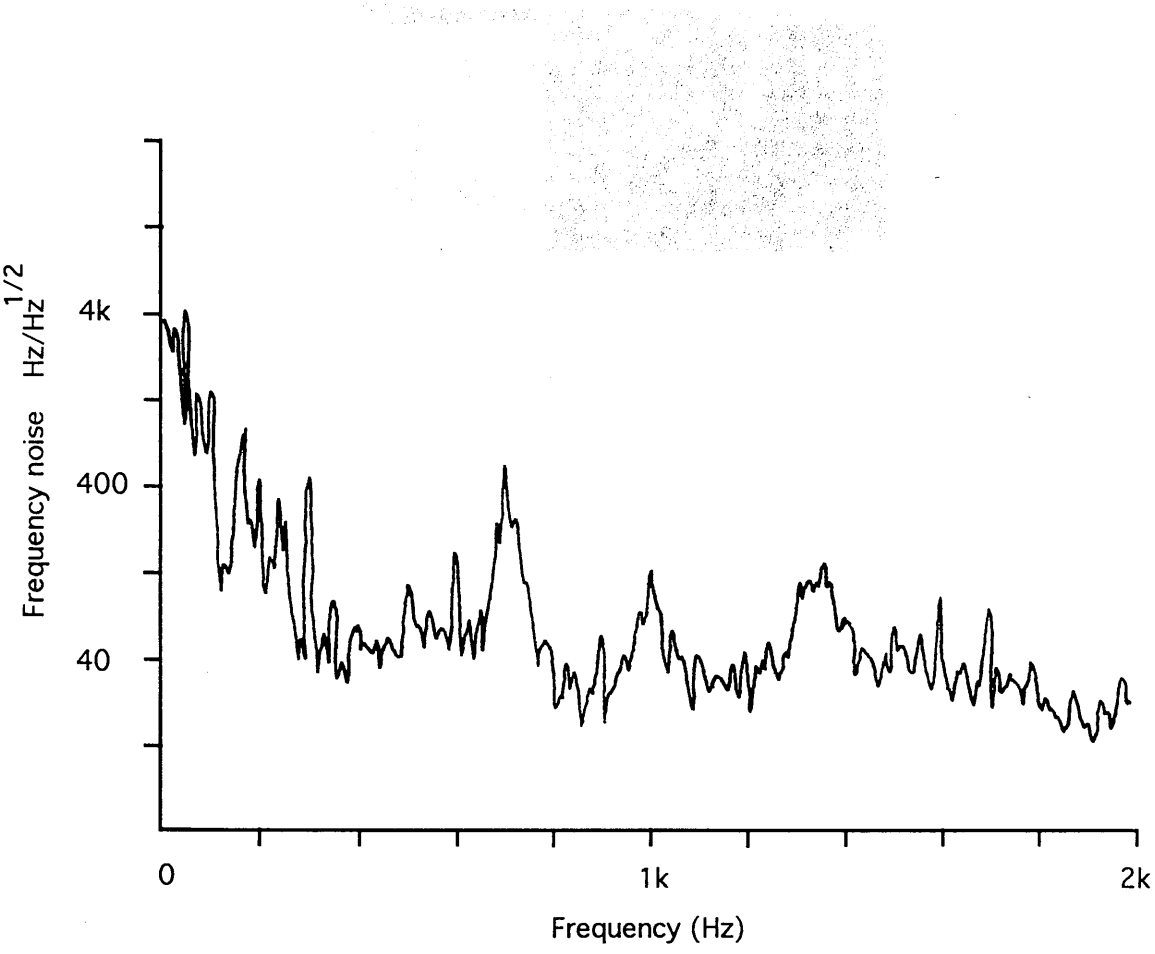

Figure 3.5: Spectrum of frequency noise of the diode pumped Nd:YAG laser.

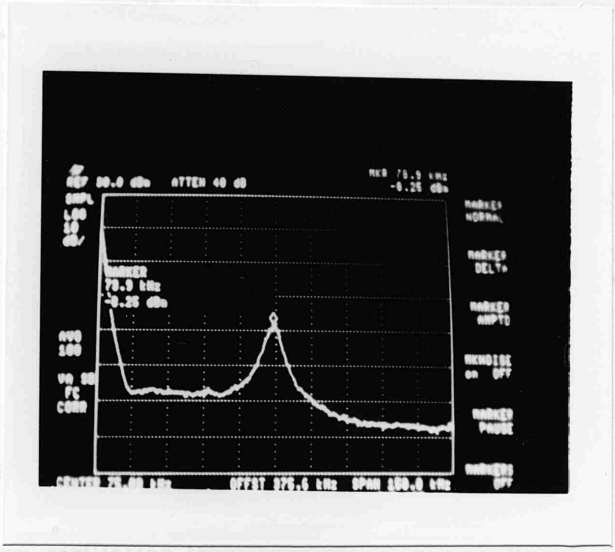

FULL SCALE 150 kHz

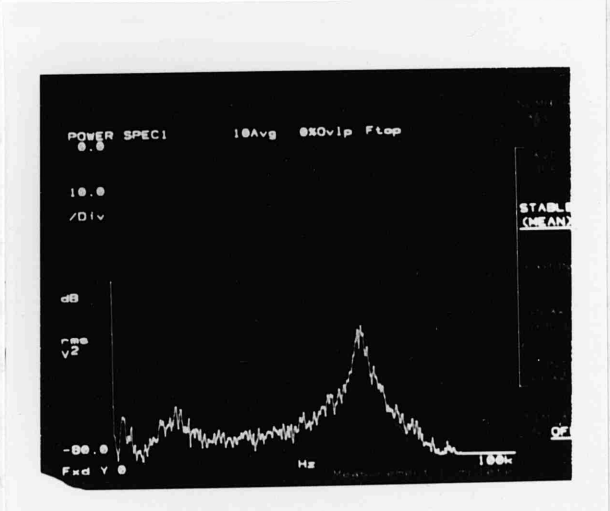

FULL SCALE 100 KHz

Figure 3.6: Spectra of Intensity noise in a flashlamp pumped Nd:YAG (upper figure) and a diode pumped Nd:YAG laser.

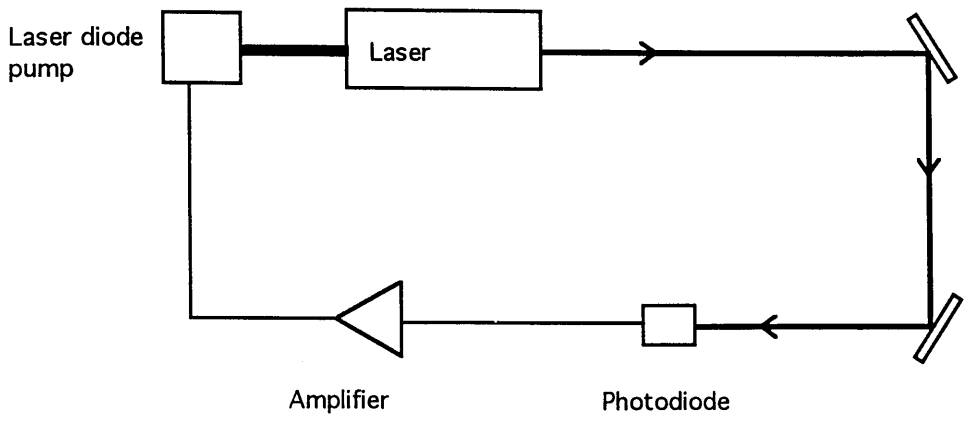

Figure 3.7: Block diagram of feedback system to remove intensity noise in a diode-pumped laser.

gives the relaxation oscillation frequency as

$$\omega = \sqrt{(\frac{r-1}{\tau t_c})}$$

where t_c is the cavity storage time, τ is the upper level lifetime and r is the ratio of the pump rate to the threshold pump rate. An intensity noise peak is a problem itself in a laser used for operating a gravitational wave interferometer but additionally may complicate the frequency stabilisation of the laser. This complication may arise from the possibility that the relaxation oscillations may couple to frequency fluctuations. As mentioned earlier the intensity fluctuations can be removed using an amplitude modulator, but this has the disadvantage that the intensity noise is not eliminated at source. An alternative technique to that is to remove the intensity oscillations using a feedback servo that applies a correction signal directly to the pump [Kane 1990]. This is particularly suitable for a laser diode pumped system, where the pump may be modulated by controlling the laser diode current. Figure 3.7 shows a block diagram of such a feedback system. The servo control loop gain is a product of the transfer function of the electronics and of the laser itself. In order to account for any phase changes the transfer function of the system must be known. The transfer function of the laser undergoing change in pumping rate may be calculated as follows. Yariv [Yariv 1975] gives the photon

density of a 4 level laser subjected to small perturbations from equilibrium as

$$\frac{d^2q}{dt^2} + \frac{r}{\tau}\frac{dq}{dt} + \frac{1}{\tau t_c}(r-1)q = \frac{1}{\tau}(r-1)R$$

where q is the photon density, τ the upper level life time, t_c is the cavity storage time and the pumping rate R is of the form $R = R_o + R_1$ where R_1 is the deviation from equilibrium. The above equation describes a driven simple harmonic oscillator. The laplace transform of the above equation gives the transfer function as

$$\frac{W}{E} = \frac{t_c}{\frac{s^2}{\omega_o^2} + \frac{rs}{\tau\omega_o^2} + 1}$$

this may be written as

$$\frac{W}{E} = \frac{t_c}{\frac{s^2}{\omega_o^2} + \frac{s}{Q\omega_o} + 1}$$

where W is the laplace transform of the photon density and E the transform of the pump perturbation R_1 and $\omega_o^2 = \frac{r-1}{\tau t_c}$, $\gamma = \frac{r}{\tau} = \frac{\omega_o}{Q}$ and the phase is given by $\tan\delta = \frac{\gamma\omega}{\omega_o^2 - \omega^2}$. In terms of intensity the transform is

$$\frac{I_o}{\frac{s^2}{\omega_o^2} + \frac{s}{Q\omega_o} + 1}$$

where I_o is the dc intensity. The above shows that beyond the relaxation frequency ω_o there is a phase change of π. As discussed earlier, to maintain a servo stability for frequencies that exceed the relaxation frequency this phase shift must be partially compensated for. This can be achieved through the phase change of a differentiator (or high pass filter).

3.5 Electronic servo to remove relaxation oscillations

The work on the electronic servo was initiated and carried out in Orsay, France. The servo was designed for a diode pumped twisted mode Nd:YAG laser. The laser was longitudinally pumped with a 1 watt Sony laser diode and had a maximum

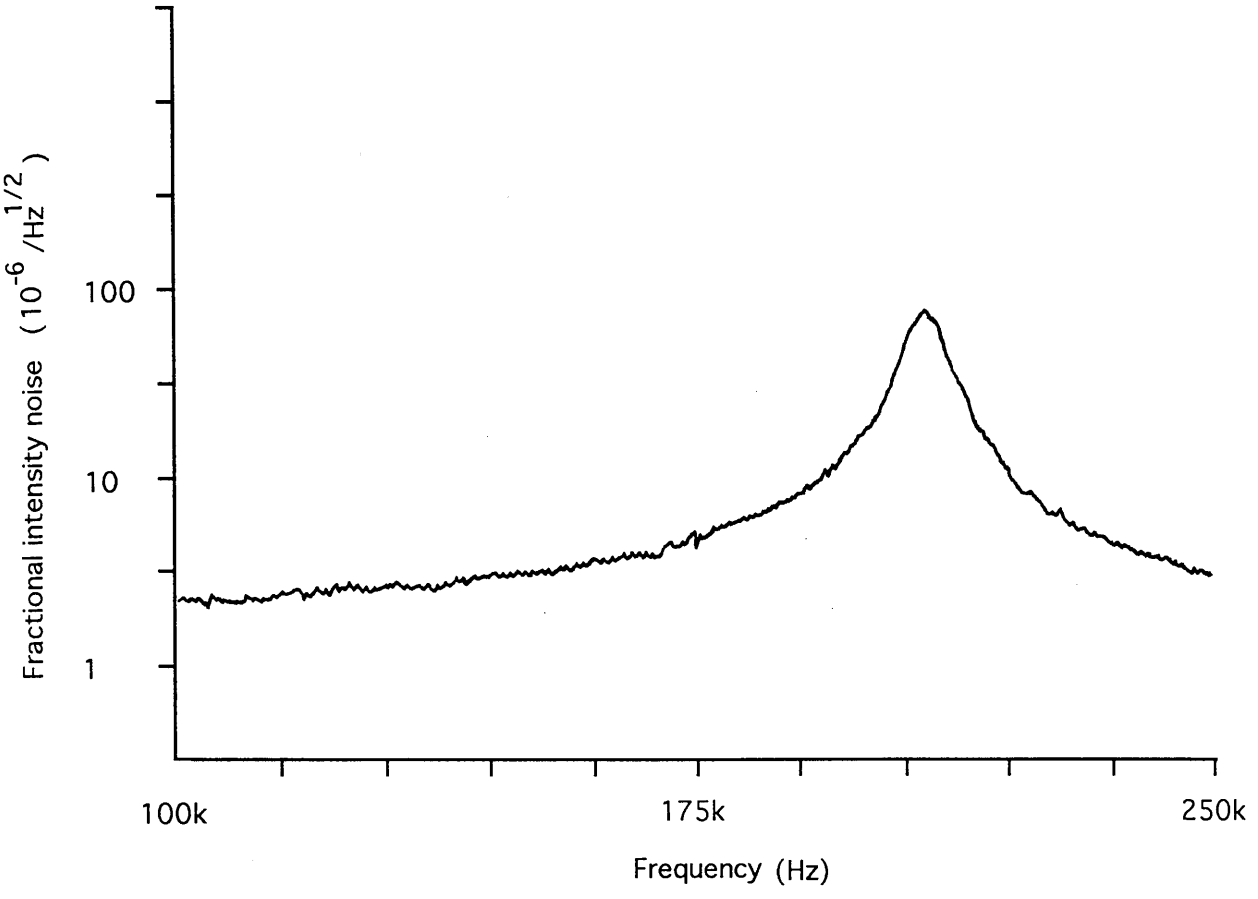

Figure 3.8: Spectrum of intensity noise of a twisted mode Nd:YAG laser.

single frequency output power of 100 mW. The cavity was twisted mode to provide single mode operation (see Chapter 4). The laser had a relaxation oscillation at around 200 kHz at full power, as shown in figure 3.8. To eliminate this, a servo was designed that would provide the necessary phase change beyond the relaxation frequency. The essential element in this was a differentiator with a 3dB point at 1.85 MHz. The differentiator advances the phase by $\pi/2$ up to 1.8 MHz, cancelling some of the π phase change beyond the relaxation oscillation frequency. The experimental layout to eliminate the relaxation oscillations is shown in figure 3.9. Part of the output was sampled on an RF photodiode. The signal was then amplified and filtered to introduce the necessary phase delay to maintain stability. The electronics produced a current that was then applied directly to the laser diode, changing the pump rate. The electronics used are shown in figure 3.10.

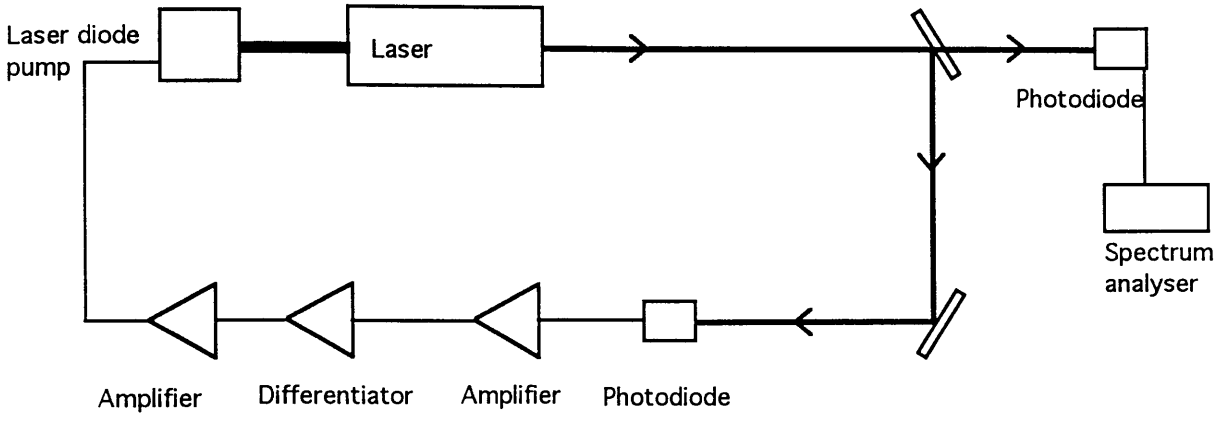

Figure 3.9: Experimental apparatus used to eliminate relaxation oscillations in a twisted mode Nd:YAG laser.

The circuit consisted of two amplification stages, a differentiator and a current generator. The overall gain at 200 kHz was approximately 140.

3.6 Results

A separate photodiode was used to examine the intensity noise. Examining the intensity noise directly rather than using either the feedback or error signal of the servo was experimentally very simple and eliminates the possibility of any error in the calibration of the error point.

Figure 3.11 shows spectra of the intensity noise with and without the feedback applied. As can clearly be seen the servo eliminates the intensity noise peak, reducing the level by around 30 dB. The successful elimination of the oscillation confirms the suitability of such a laser for use in interferometry. This technique could be applied to a higher power system.

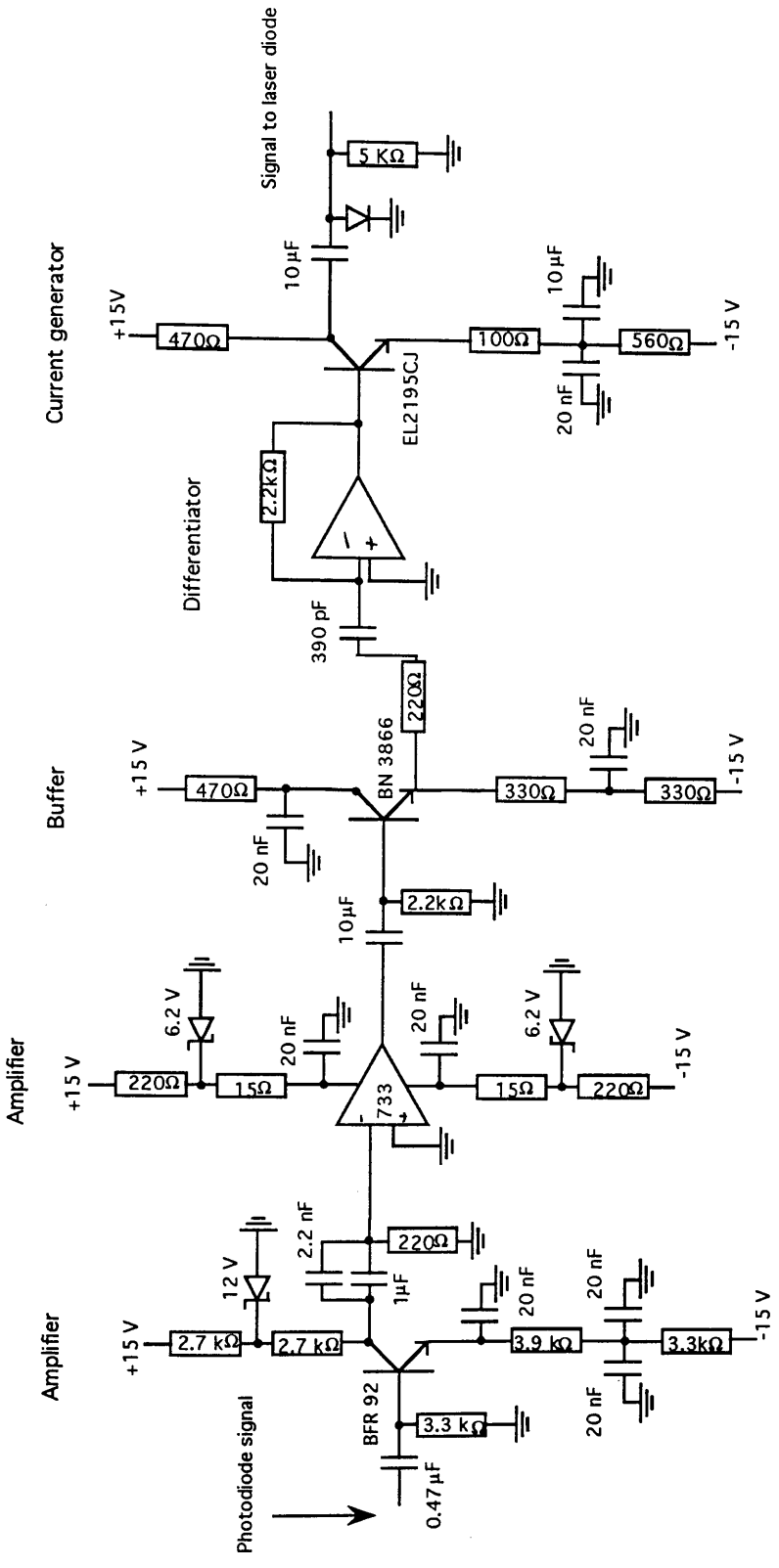

Figure 3.10: Servo electronics used to remove relaxation oscillations.

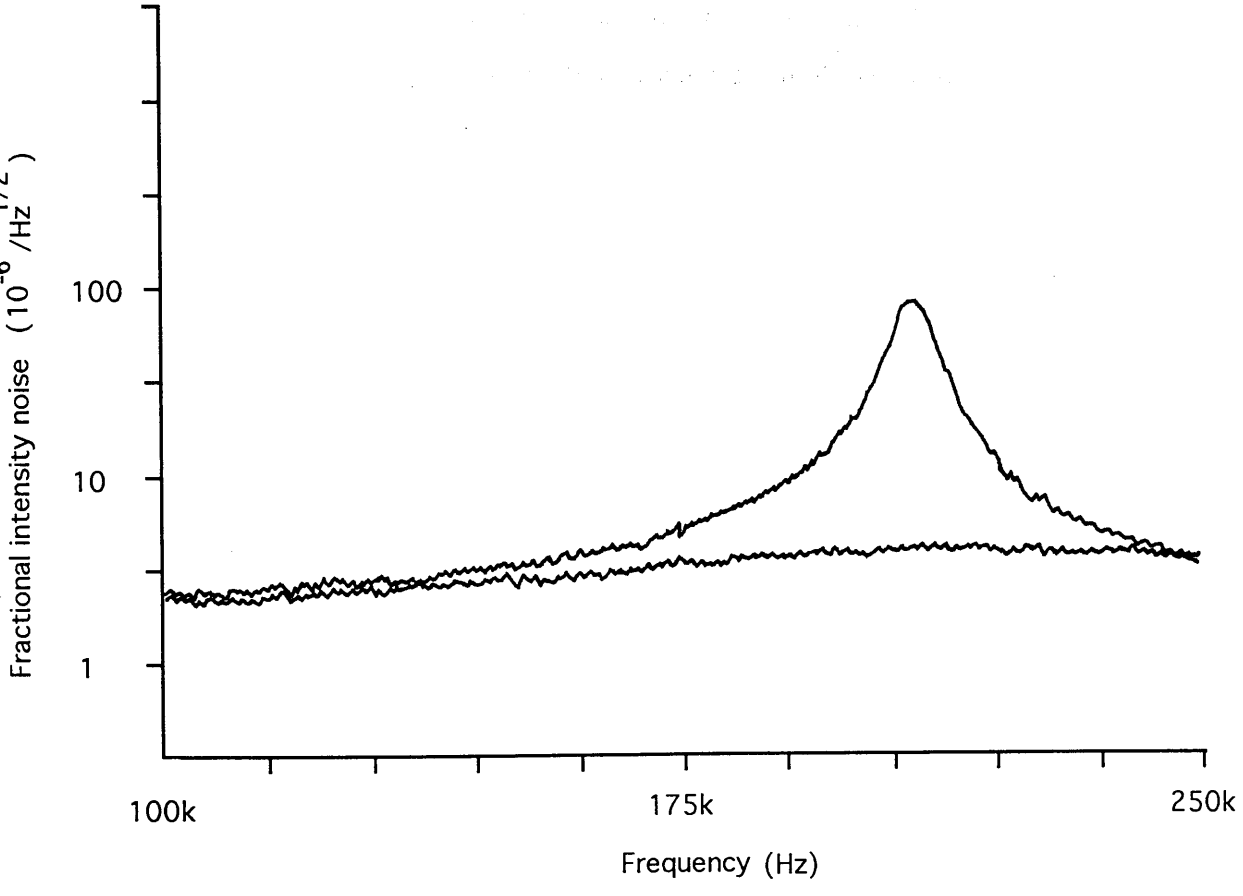

Figure 3.11: Spectra of intensity noise in the twisted mode laser with and without the feedback on. The lower plot shows the result with the feedback on.

3.7 Summary

The diode pumped laser had a lower frequency noise level than an Argon ion laser, only 50 $Hz/Hz^{1/2}$ at 1 kHz compared with the 2-3 $kHz/Hz^{1/2}$ noise level of an Argon ion laser. This may be due to the diode pumped laser having no water cooling. In addition the possible drawback of the relaxation oscillations in diode pumped Nd:YAG lasers has been shown to be easily eliminated giving the possibility of a very stable laser in both frequency and intensity.

Chapter 4

Flash Lamp Pumped Nd:YAG Lasers

4.1 Introduction

In Chapter 2 Nd:YAG lasers were discussed and in particular the pumping of Nd:YAG with laser diodes. Currently diode pumps are limited, due to cost and availability, to low power lasers. This chapter describes the rebuilding of a commercial high power multimode flash lamp pumped Nd:YAG laser into a single frequency ring laser. The commercial laser used for this was a SPECTRON SL903 Nd:YAG laser. The Nd:YAG rod was 4 mm in diameter and 100 mm long. It was pumped in a close coupled chamber by a 4 kW c.w. Krypton arc lamp.

4.2 Linear lasers

Conventionally Nd:YAG lasers are based on linear cavities. This is a disadvantage if the laser is to be operated with a single longitudinal mode because, although homogeneously broadened, the Nd:YAG laser is prevented from running in a single mode by spatial hole burning associated with a linear cavity. The spatial hole burning is caused by the standing wave field of a longitudinal mode. Where the field is a minimum the inversion is large and this allows parasitic longitudinal modes to run [Siegman 1986]. To force a single mode requires an intracavity etalon. The etalon introduces loss that eliminates the parasitic longitudinal modes, but this is inefficient, since it does not allow access to the inversion that the standing wave pattern leaves.

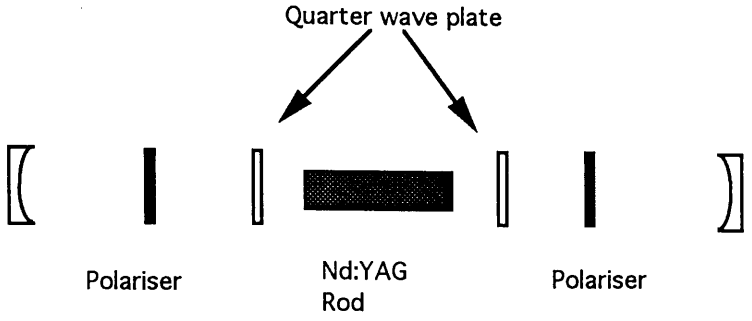

Figure 4.1: Twisted mode Nd:YAG laser cavity

It is more efficient to eliminate spatial hole burning by using either a travelling wave cavity or a twisted mode cavity. If a travelling wave is used, as in the case of a unidirectional ring laser, there is no standing wave pattern and so the entire gain medium is used. Alternatively, for a laser where thermal birefringence is not important a linear cavity can be converted to a twisted mode cavity using two quarter wave plates and two polarisers. The quarter wave plates are placed on each side of the Nd:YAG rod and a polariser is placed between each quarter wave plate and the cavity mirror, as shown in figure 4.1. When the quarter wave plates are orthogonal and at 45 degrees relative to the polarisers then each cavity mode splits in to two orthogonally polarised components. The spatial distribution of the standing wave pattern of each component is separated by a quarter wave length. The two average and give a spatial distribution independent of position.

4.3 Ring lasers

In addition to preventing spatial hole burning in a solid state laser a unidirectional ring has several other advantages. The ring design is very useful for a laser system that involves either injection locking or intracavity second harmonic generation, as discussed in Chapters 5 and 6. In the first case if an external signal is directed into a ring laser there is no optical feedback to the injection source and so no isolation is required. In the second case the unidirectional pass through the intracavity elements means light is generated in one direction only, and this allows the simple collection of any intracavity second harmonic that is generated.

The main disadvantage of a ring laser is that the gain medium is traversed only once during a round trip compared with a similar linear system in which it is traversed twice. Another problem with a ring design is the astigmatism produced by non normal incidence on curved mirrors.

4.4 Thermal effects from a flashlamp

Most of the power from a flashlamp pump ends up as heat. For continuous operation the laser rod must be cooled by water pumped around the rod. However, as the thermal conductivity of the rod is finite, a radial temperature gradient occurs. Since the refractive index is temperature dependent,the temperature gradient produces a radial parabolic index profile which is equivalent to a lens [Koechner 1970]. This lensing must be included in any cavity design. For a pump lamp power of 4 kW the lens can be equivalent to a simple lens of focal length 25 to 30 cm.

Stress and thermal gradients can cause birefringence and astigmatism of the thermal lens. The birefrigence can reduce the available power out of a polarised laser. Since the outer part of the rod is subjected to the most stress the outer rod becomes unusable and the useful volume of the laser rod that the mode occupies is limited [Spectron 1990].

The flow of cooling water can also restrict the volume of the rod that can be occupied by the laser mode [Koechner 1972]. Fluctuations in the flow can cause temperature changes which in turn change the thermal lens and cause output power fluctuations. This can be avoided by reducing the beam diameter to allow the thermal inertia of the outer area of the rod to provide damping of the temperature fluctuations.

4.5 Thermal lens measurement

A measurement of the thermal lens was made by examining the change in the beam profile of a Helium Neon laser beam directed through the centre of the rod while the lamp was on. To calculate the lens value, the results were compared

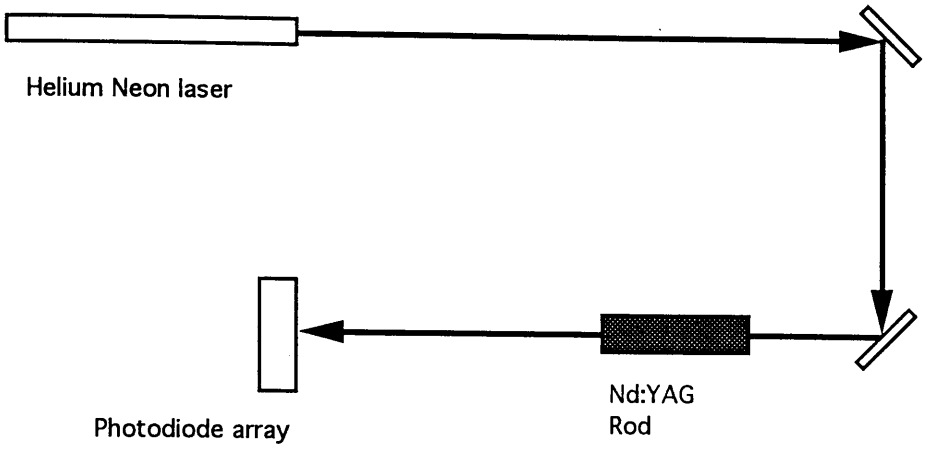

Figure 4.2: Experimental layout to measure the effect of the thermal lens of a Nd:YAG rod.

with the effect that a simple lens would have had on the beam. This gave both the magnitude of the lens and a check of the accuracy of the simple lens approximation.

The experimental apparatus is shown in figure 4.2. To check for the effects of astigmatism the shape of the Helium Neon laser beam after being passed through the thermal lens was examined. The beam remained circular and the effects of astigmatism were considered negligible. The beam diameter was measured at several positions using a photodiode array of 256 strips. Each diode was 15 μm wide and separated by 10 μm. This allowed the gaussian diameter to be accurately measured. The procedure was repeated for several different lamp currents. To analyse this data the original Helium Neon laser beam diameter and curvature were used to calculate the beam diameter as a function of distance after passing through a thin lens. The experimental data of beam size as a function of distance from the Nd:YAG rod was then plotted beside the calculated values. The results are shown on figure 4.3. The graph shows that a simple lens equivalent is probably adequate to describe the thermal lens. The expected increase in lens power with increasing lamp current can also be seen. The graphs indicate that the thermal lens has a focal length of around 35 cm for a lamp current of 21 amps, the lamp current found later to be the most useful.

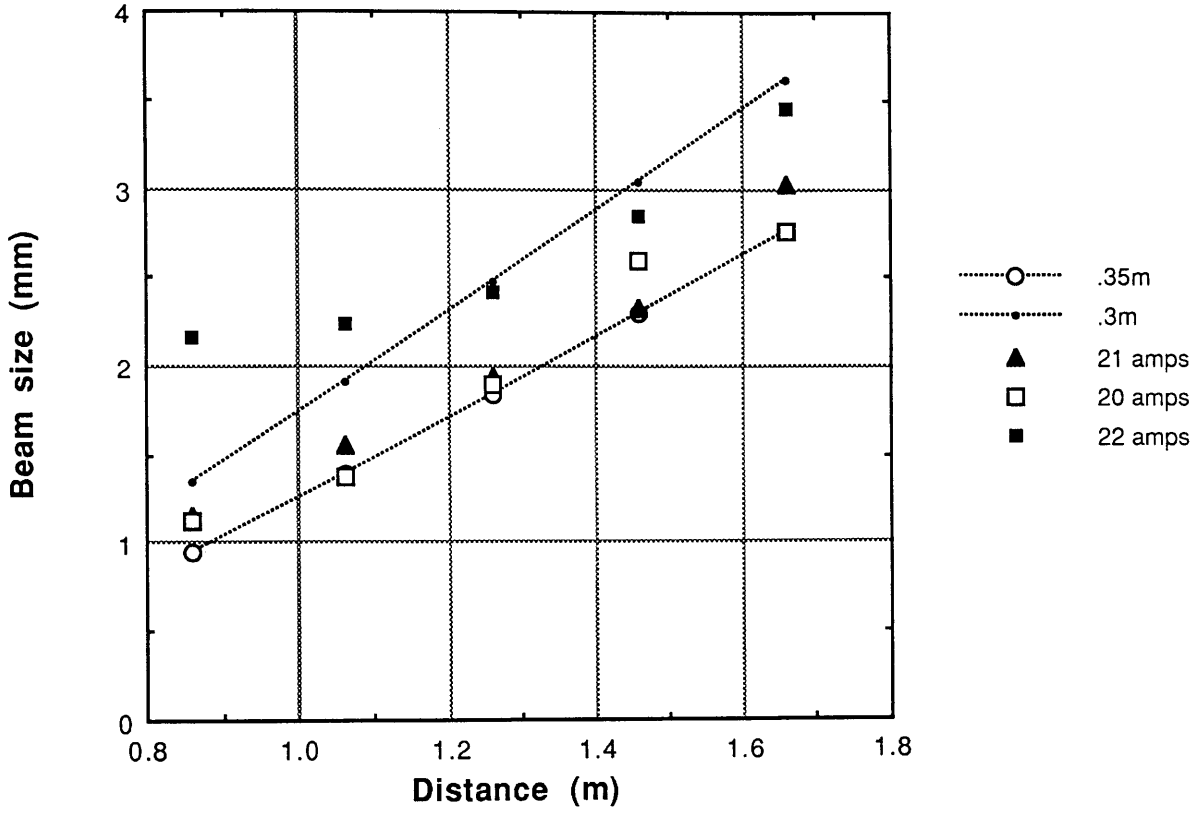

Figure 4.3: Graph of HeNe beam diameter as a function of lamp current. Shown on the graph are experimental points for lamp currents of 20,21 and 22 amps and points calculated from thin lenses of focal length 35 cm and 30 cm.

This technique is limited by two factors. The first is that it does not take into account the effect that the circulating laser power has on the thermal lens. The gaussian beam profile of the circulating laser power reduces the temperature gradient of the rod and so lowers the effective power of the lens. The second limitation is that the measurement is for a wave length of 633 nm not for the Nd:YAG wavelength of 1064 nm.

4.6 Cavity design

Two important features of a cavity design are stability and the mode profile. The cavity must be designed to provide a path that will not lead to loss through diffraction of the beam, that is the cavity must be stable. The mode profile should, because of saturation of the gain, occupy as large an area of the gain medium as possible.

The stability and mode profile can be calculated using the ray transfer matrix for the cavity $\begin{Bmatrix} a & b \\ c & d \end{Bmatrix}$. This the matrix that is used in geometric optics and in gaussian optics to relate the defining parameters of a beam before and after a given optical arrangement. While the defining parameters of a paraxial geometrical ray are its distance from the optic axis and the angle the ray makes with respect to that axis, it is the complex q parameter that is transformed in gaussian optics. The q parameter is defined by

$$\frac{1}{q} = \frac{1}{R} - j\frac{\lambda}{\pi W^2}$$

where R is the radius of curvature, λ is the wavelength and W is the beam radius. In geometric optics the parameters are related by a matrix transformation, whereas in gaussian optics the q parameter transfers according to

$$q_2 = \frac{aq_1 + b}{cq_1 + d}$$

where q_1 and q_2 denote q before and after the optical structure.

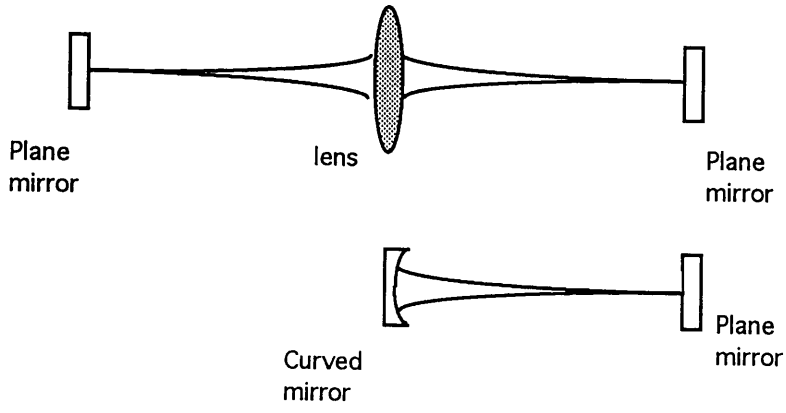

Figure 4.4: A linear cavity containing a lens and its cavity analogue using a curved mirror to replace the lens.

The stability condition for the above transfer matrix is [Kogelnik and Li 1966],

$$-1 < \frac{1}{2}(a+d) < 1.$$

To form an adaptable, stable and easily understood cavity the design was based closely on the cavity of the original commercial linear laser. The original cavity consisted of a plane mirror and a mirror of 10 m radius of curvature, with the thermal lens placed almost centrally in the 1.2 m long cavity. This linear cavity arrangement is very close to a cavity consisting of two plane mirrors and a centrally placed lens. It is simple to understand this cavity by comparing it to its analogue of one flat mirror and one curved mirror, as shown in figure 4.4.

A ring cavity was devised that would have a mode volume in the gain medium, and a stability close to that of the original linear laser. The form of the design selected was a four mirror cavity, comprising of one curved mirror and three plane mirrors, with a path in the shape of a figure of eight. As shown in figure 4.5 the cavity re-routes the return trip of the linear cavity via two mirrors. The return through the lens is replaced by reflection off a curved mirror.

The number of curved mirrors was limited to one to simplify the cavity and minimise the effects of astigmatism. To further reduce any astigmatism the cavity was chosen to have a beam path which had the shape of a figure of eight, since

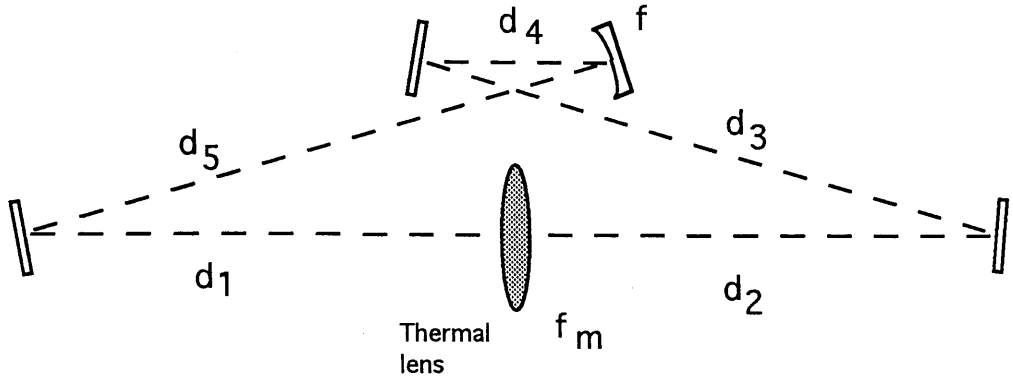

Figure 4.5: Four mirror ring laser cavity containing a curved mirror.

this reduced the angle of incidence on the curved mirror. A four mirror cavity as described above is shown in figure 4.5. The ray transfer matrix for such an arrangement has components

$a = 1 - \frac{d_5}{f_m} - \frac{1}{f}(d_5 + d_4 + d_3 + d_2) + \frac{d_5}{f f_m}(d_2 + d_3 + d_4)$

$b = T - \frac{d_5}{f_m}(d_1 d_2 + d_3 + d_4) - \frac{d_1}{f_m}(d_5 + d_4 + d_3 + d_2) + \frac{d_1 d_5}{f f_m}(d_2 + d_3 + d_4)$

$c = -\frac{1}{f_m} - \frac{1}{f} + \frac{1}{f f_m}(d_2 + d_3 + d_4)$

$d = 1 - \frac{d_1}{f} - \frac{1}{f_m}(d_1 + d_2 + d_3 + d_4) + \frac{d_1}{f f_m}(d_2 + d_3 + d_4)$

where T is the total path length, f is the focal length of the thermal lens, f_m is the lens equivalent of the curved mirror and d_1 to d_5 are the distances shown in figure 4.5. The stability condition for such a matrix is, $-1 < \frac{1}{2}(2 - \frac{T}{f_m} - \frac{T}{f} + \frac{(d_1+d_5)(T-d_1+d_5)}{f f_m}) < 1$.

The ring cavity evolved into a cavity of total length 203 cm with a curved mirror of radius 0.5 m as shown in figure 4.6. The cavity had two waists; one waist had a radius of 240 μm and was positioned 58 cm to the left of the thermal lens and the other had a radius of 290 μm and was positioned 70 cm to the right of the thermal lens.

Unidirectional operation was provided by an optical diode [Johnson and Proffitt 1980]. This consisted of a Faraday rod and three quartz rotating plates mounted at Brewsters angle. The quartz plates rotate the polarisation using optical activity. If

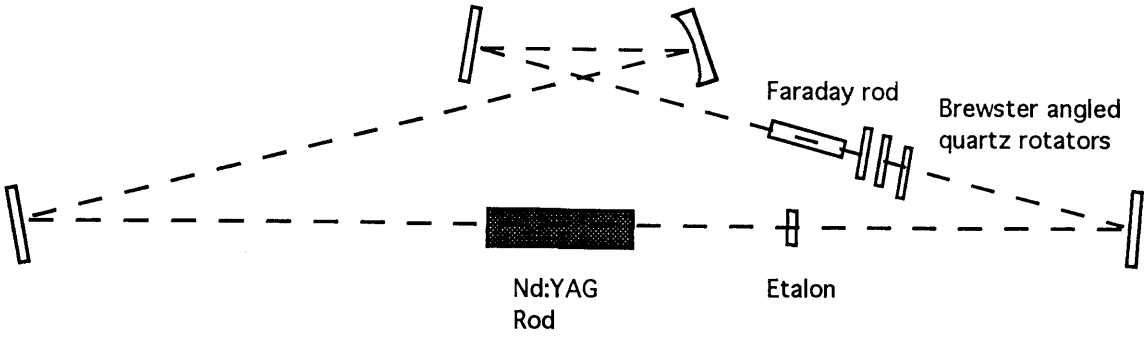

Figure 4.6: Cavity design of 4 mirror ring laser with unidirectional and single longitudinal operation.

the rotation of the polarisation by the quartz rotators is matched to the magnitude of the rotation caused by the Faraday rod then in one direction the total rotation of the cavity polarisation cancels and in the other direction it is summed. The rotation from each part of the optical diode could be matched by varying the number of quartz plates and varying the length of Faraday rod influenced by the magnetic field. The Brewster angled quartz plates thus provided a direction dependent loss which resulted in unidirectional operation.

The laser had a single transverse mode but to provide single longitudinal operation the laser required a low finesse etalon. The laser had a maximum single frequency polarised output power of 6.5 W with an 8% transmitting output coupler. The graph in figure 4.7 shows how the output power varied with lamp current. This does not follow a straight line but levels off as the current is increased. This could be due to the increase in the power of the thermal lens changing the mode volume in the gain medium.

4.7 Mode hopping

While the laser was single mode, it was prone to mode hopping, often on a time scale of less than 30 seconds. A suspected source of the mode hopping was vibration

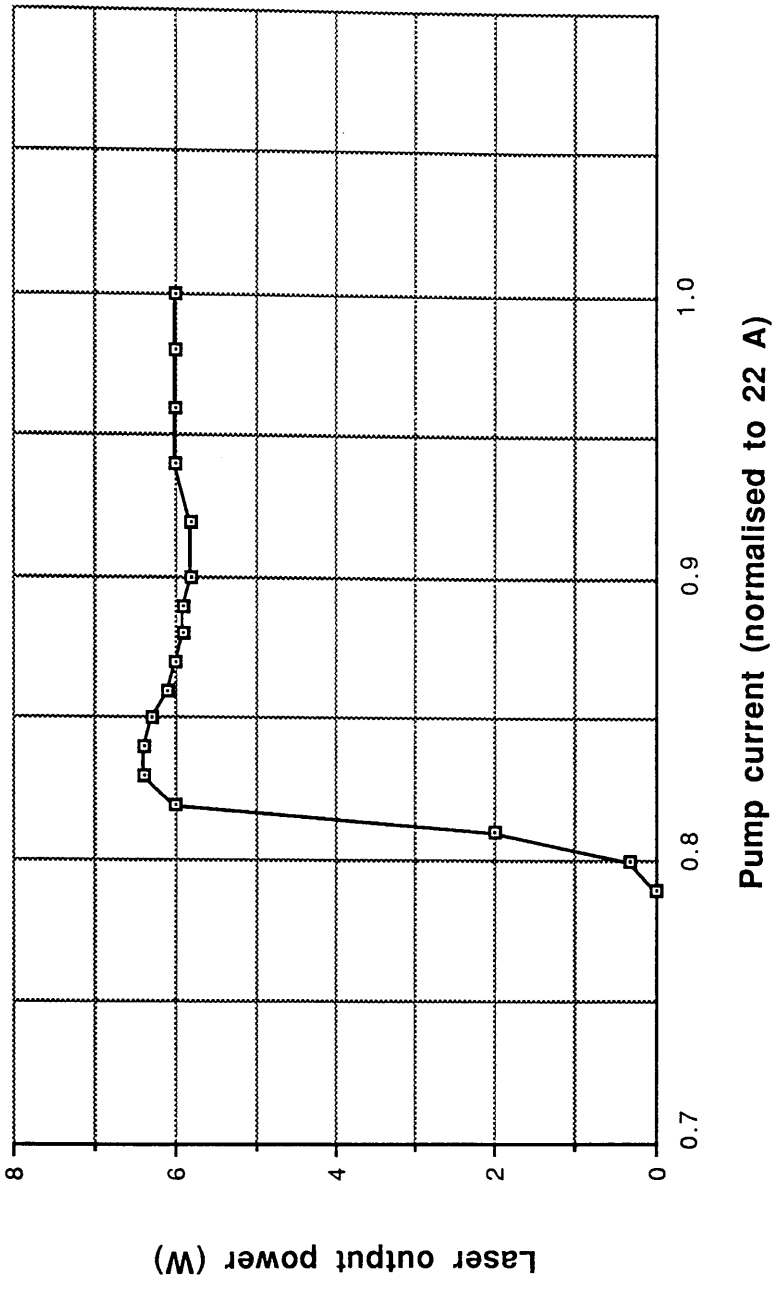

Figure 4.7: Graph of output power of 4 mirror ring Nd:YAG laser as a function of lamp current.

caused by the flow of cooling water through pipes fixed to the laser frame. It has previously been shown that mechanical isolation can improve the intensity and frequency stability of a laser [Kerr 1986]. This was tried in an attempt to eliminate mode hopping. The unit containing the lamp and rod was separated from the laser frame and mounted directly on to the optical bench using a lead and rubber stack. This isolated the vibration produced by the flow of cooling water from the laser frame, and also isolated the pumping chamber from ground based mechanical disturbance. The laser frame, which supported the cavity mirrors and intracavity components, was mounted on the optical bench with a similar arrangement of lead and rubber stacks. This greatly improved the stability of the laser. The mode hopping still occurred but it was now on a much longer time scale; the laser was stable for one to five minutes or longer. The mode hopping that did occur was a short burst of oscillatory jumping between two adjacent modes. This was followed by stable operation and then another burst of mode hopping. This is shown in figure 4.8 which shows the mode structure measured using a scanning Fabry-Perot cavity. Several attempts were made to improve the stability further. A temperature stabilised etalon was tried, as were higher finesse etalons and to eliminate drafts and room noise, a possible source of mode hopping, an acoustic isolation box of lead backed foam was made to cover the laser. However, these changes made little or no improvement to the laser stability.

4.8 Discussion

The cavity design had two problems associated with it. Even with mechanical isolation the laser was prone to mode hopping, often holding only one mode for a few minutes. This made it difficult to frequency stabilise the laser or to measure the frequency noise of the laser. The other drawback was that it had a beam shape that was elliptical with a ratio of 2:3, due to the curved mirror in the cavity. This complicated operations such as injection locking and intracavity focussing, see Chapters 5 and 6. The ellipticity could have been compensated for by using an intra cavity compensating plate but would probably have reduced the output

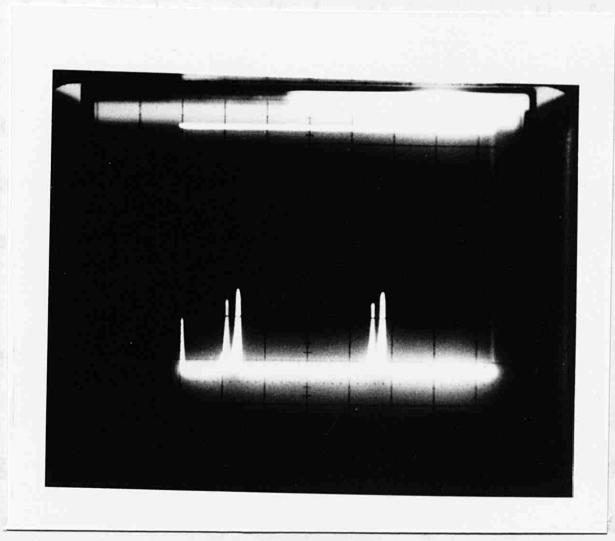

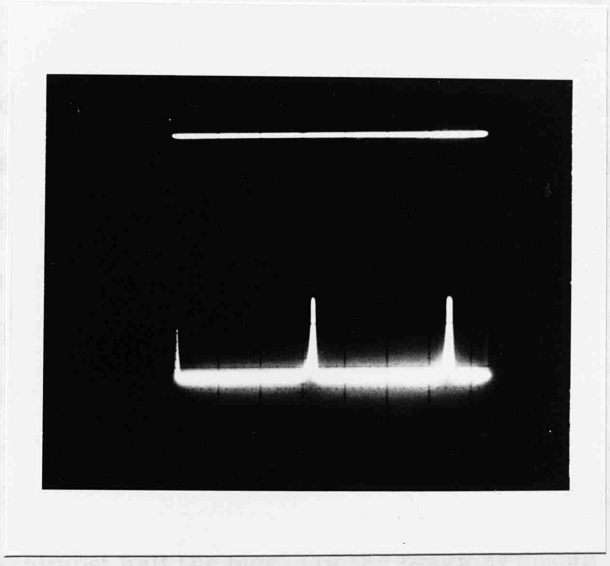

Figure 4.8: The upper figure shows the output of a scanning Fabry-Perot cavity while the laser is oscillating between two modes. The lower figure shows the steady state condition.

power of the laser.

Mode hopping in the laser can be made more difficult by reducing the length of the laser cavity. A shorter laser cavity length increases the free spectral range of the laser, which increases the space between adjacent longitudinal modes and decreases the gain of these modes. The problem of astigmatism in a ring laser can be removed if no curved mirrors are used in the laser cavity design. Using these criteria the laser cavity was redesigned.

4.9 Improved ring cavity design

A three mirror ring cavity was chosen so as to reduce the path length, and all the mirrors were chosen to be flat. The cavity stability was provided by the thermal lens alone.

This cavity is an exact analogue of a linear cavity that has two flat mirrors and a centrally placed thermal lens. As shown in figure 4.9, the path was re-routed by a third mirror to pass through the thermal lens, eliminating the curved mirror used in the previous ring design. In a symmetric cavity, such as this, the waist is half way around the path length starting from the thermal lens. To allow the waist to be accessed for second harmonic generation the cavity was arranged so that the third mirror was not placed half way around the path length.

The transfer matrix for such a system has components $a = 1$, $b = T$, $c = -\frac{1}{f}$ and $d = 1 - \frac{T}{f}$. The stability criterion is $0 < 1 - \frac{T}{2f} < 1$.

One advantage of this simple cavity was that it could be easily altered to try to optimise the mode volume in the gain medium. This was done by changing the cavity length and observing the power and stability. The cavity length was optimised at 1.1 m, almost half the length of the previous design. This gave a waist size of 310 μm.

If the cavity was too long the power out was reduced when the polarisers were introduced to the cavity. This effect was due to the mode occupying the stressed outer area of the rod where birefringence prevents any useful use of the gain medium.

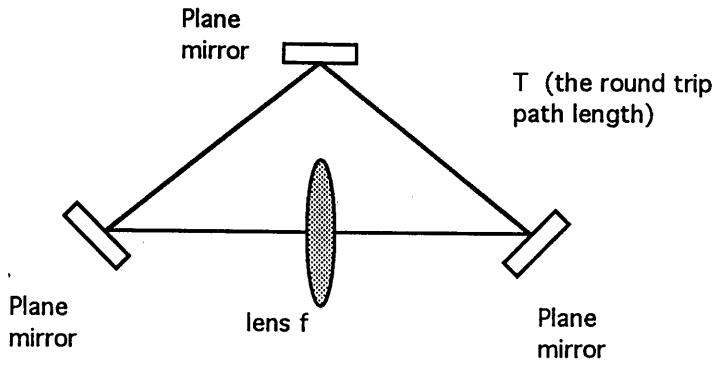

Figure 4.9: Three mirror ring cavity.

As in the previous design the laser had an intracavity etalon for single mode operation and an optical diode for unidirectional operation. A diagram of the laser is shown in figure 4.10. The scanning Fabry-Perot picture in figure 4.11 shows the laser running multimode and running single mode. At high powers the laser does not quite behave as if it is completely homogeneously broadened as the multimode picture shows.

As expected the new design improved both the beam shape to a ratio of 6:7 and eliminated the mode hopping.

With an 8% output coupler the laser had a single frequency polarised output of between 8 and 10 watts. A graph of power output as the lamp current is altered is shown in figure 4.12. Again the output power levelled out due to the effect of the increase in thermal lens, as shown by the shape of the curve.

4.10 Summary

A stable single mode high power ring Nd:YAG laser was developed. A three mirror ring was constructed using flat mirrors; stability was provided by the thermal

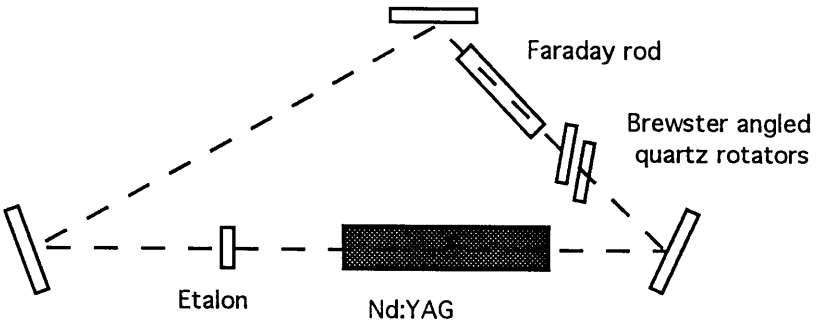

Figure 4.10: Three mirror ring laser cavity containing an etalon and optical diode.

lens of the Nd:YAG rod. The three mirror design allowed a short cavity length to eliminate mode hopping and the flat mirrors allowed a design that did not introduce the astigmatism associated with curved mirrors in a ring laser.

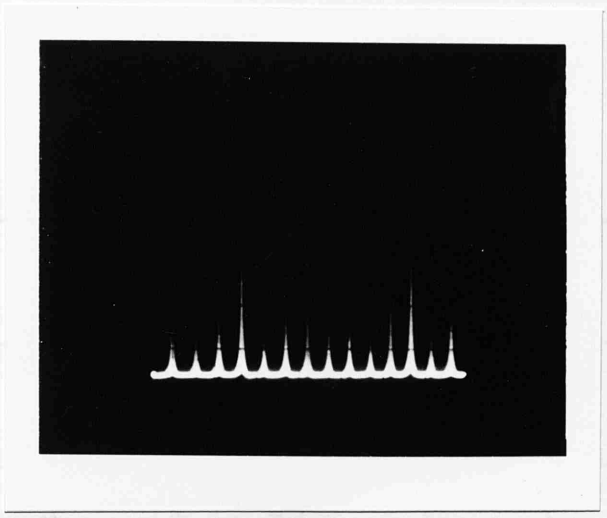

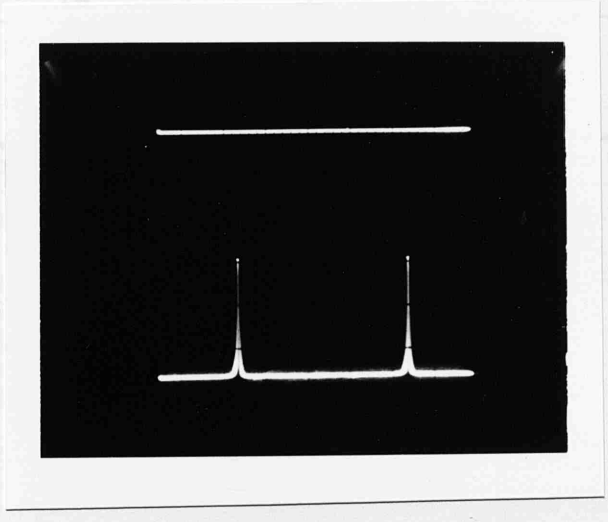

Figure 4.11: The upper plot shows the multimode structure of the 3 mirror ring without the intracavity etalon. The lower plot shows the single mode operation when the etalon is in place. The requirement of an etalon demonstrate the laser is not homogeneously broadened.

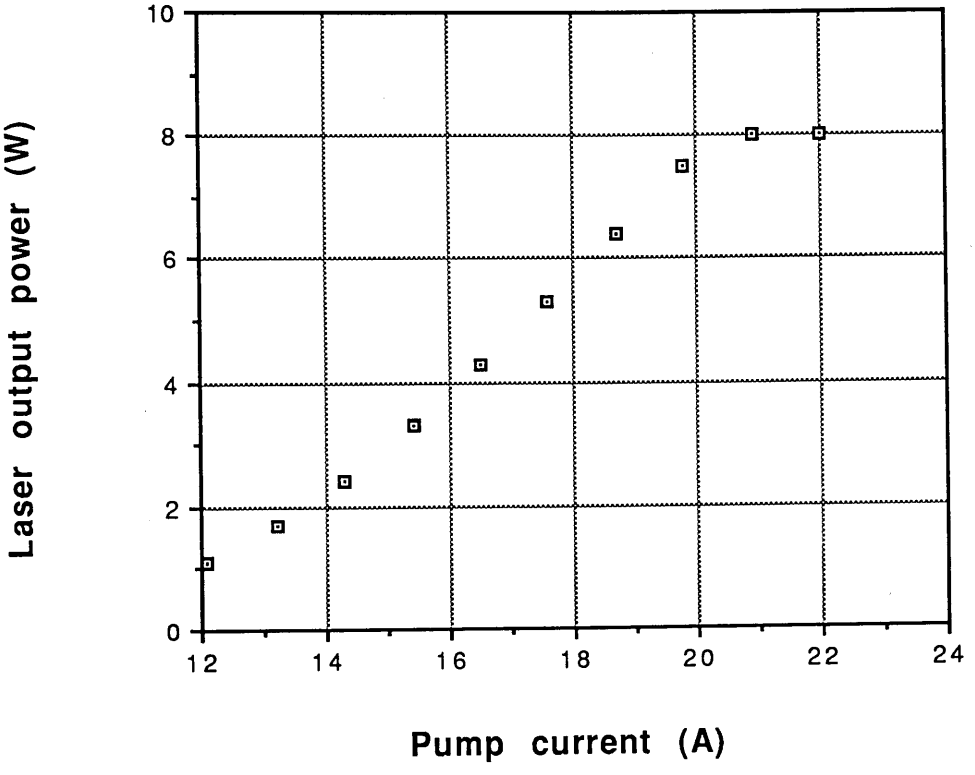

Figure 4.12: Graph of output power of 3 mirror ring laser as a function of lamp current.

Chapter 5

Injection locking experiments

5.1 Introduction

In Chapter 1 the demands placed on a laser for use in a long baseline interferometric gravitational wave detector were discussed. The important criteria are, a laser power of 50 to 100 Watts and a frequency noise level, after stabilisation, of around $3 \times 10^{-8} Hz/Hz^{\frac{1}{2}}$ at a frequency of 1 kHz. Injection locking of two or more lasers has been suggested as a possible application to meet both these criteria.

It has been shown that a laser can be frequency stabilised to a very high level by use of an electronic control system. In such a control system a correction signal is applied to frequency control elements, for example a piezoelectric transducer(PZT), an acousto-optic modulator or an electro-optic modulator [Kerr 1986] [Robertson 1990]. In such schemes the bandwidth may be limited by the response of the control element. The bandwidth limit places strict demands on a control system, if very high gain and hence low noise is to be achieved. If injection locking is used to transfer the frequency stability of a small ultrastable laser, such as that developed in Chapter 2, to a high power laser [Nabors et al 1989], then the demands on any electronic servo system will be reduced.

For technical reasons it is unlikely that an argon ion laser will be scaled up from providing 2 to 3 W of single frequency power to around 100 W. However, it has been suggested [Kerr,Hough 1989] that the coherent addition of several lasers, made possible by the phase correlation from injection locking, could be used to supply the power. Although high power Nd:YAG lasers exist and a diode pumped single mode high power laser is under development [Hanover 1990 b], a coherent

addition scheme could be applied as easily to Nd:YAG lasers.

This chapter describes the injection locking of the high power flash lamp pumped Nd:YAG laser described in Chapter 4 with a low power diode pumped Nd:YAG laser, and the subsequent examination of the effect on the frequency fluctuations of the high power laser.

5.2 Injection Locking

Injection locking involves the synchronisaton of two oscillators by coupling a signal from one oscillator into the other. This is generally done by coupling a weak signal from a highly stable source, known as the master oscillator, into a more powerful oscillator, known as the slave. This allows the more powerful oscillator to be controlled by the the weaker oscillator signal.

Consider the case of two lasers, a small stable master laser and a high power slave laser. A weak signal of angular frequency ω from the master laser injected into the the slave laser will circulate inside the cavity and be amplified in the presence of the cavity resonance angular frequency ω_1. If ω moves close enough to ω_1 the signal will have an intensity approximately equal to the intensity of ω_1 and the amplified injected signal will start to saturate the gain to the extent that ω_1 no longer oscillates, leaving only the injected signal ω. The full range in frequency (around the cavity resonance) over which this can occur is given by Siegman [Siegman 1986] as

$$\Delta F = \frac{\eta T f sr}{\pi}(\frac{P_m}{P_s})^{1/2}$$

where P_m, P_s are the respective powers of the master and slave lasers, T is the coupling transmission, fsr the free spectral range of the slave laser and η is a term to acc ount for spatial and polarisation overlap of the two lasers. The injection locking process allows the phase of the two lasers to be highly correlated inside the locking range, thus allowing processes such as the coherent addition of lasers. It has been shown that the frequency stability or narrow linewidth of a laser can be transferred to another laser through injection locking [Chow 1982], [Nabor

et al 1989]. In addition, injection locking can be used to induce single frequency operation in a high power laser eliminating the need for an etalon, and its associated losses [Cregut et al 1989].

5.3 Injection locking of high power ring laser

The laser used as the master oscillator was a LIGHT WAVE 120-03A diode pumped monolithic Nd:YAG ring laser [Kane,Byer 1985] with a single frequency polarised output power of 40 mW. The frequency of this could be adjusted by controlling the temperature of the Nd:YAG crystal. The cavity consisted of a Nd:YAG slab; changing the temperature controlled the laser cavity length and consequently the frequency. It was possible to tune the frequency over a range of several GHz to within 0.1 MHz. Tuning the frequency of the laser allows the lasing transition of the master laser to lie on the peak of the gain curve of the slave laser.

The slave laser was the flashlamp pumped Nd:YAG described in Chapter 4. The cavity was a 4-mirror ring with a beam path in the shape of a figure of eight (the first configuration described in Chapter 4, figure 4.6). The laser had an intracavity optical diode for unidirectional operation, but the etalon was removed, so that the laser was running with more than one longitudinal mode. (It was hoped to use injection locking, in place of the etalon, to force a single mode.)

The experimental arrangement used to injection lock the two lasers is shown in figure 5.1. The output of the master laser was injected into the slave laser through the output coupler. The two lasers were mode matched and care was taken to ensure good spatial overlap of the injected beam and the slave laser beam around the path length of the slave laser. The polarisation of the lasers was also matched. It was difficult to get perfect overlap because both lasers had elliptical beam shapes. Light from one of the other slave laser mirrors was split to produce two beams. One beam was directed into a scanning Fabry-Perot cavity and the other on to an RF photodiode. The RF photodiode output was monitored with a spectrum analyser to allow the beat signal between the two lasers to be seen. Using this, the master laser frequency could be tuned to within the locking range.

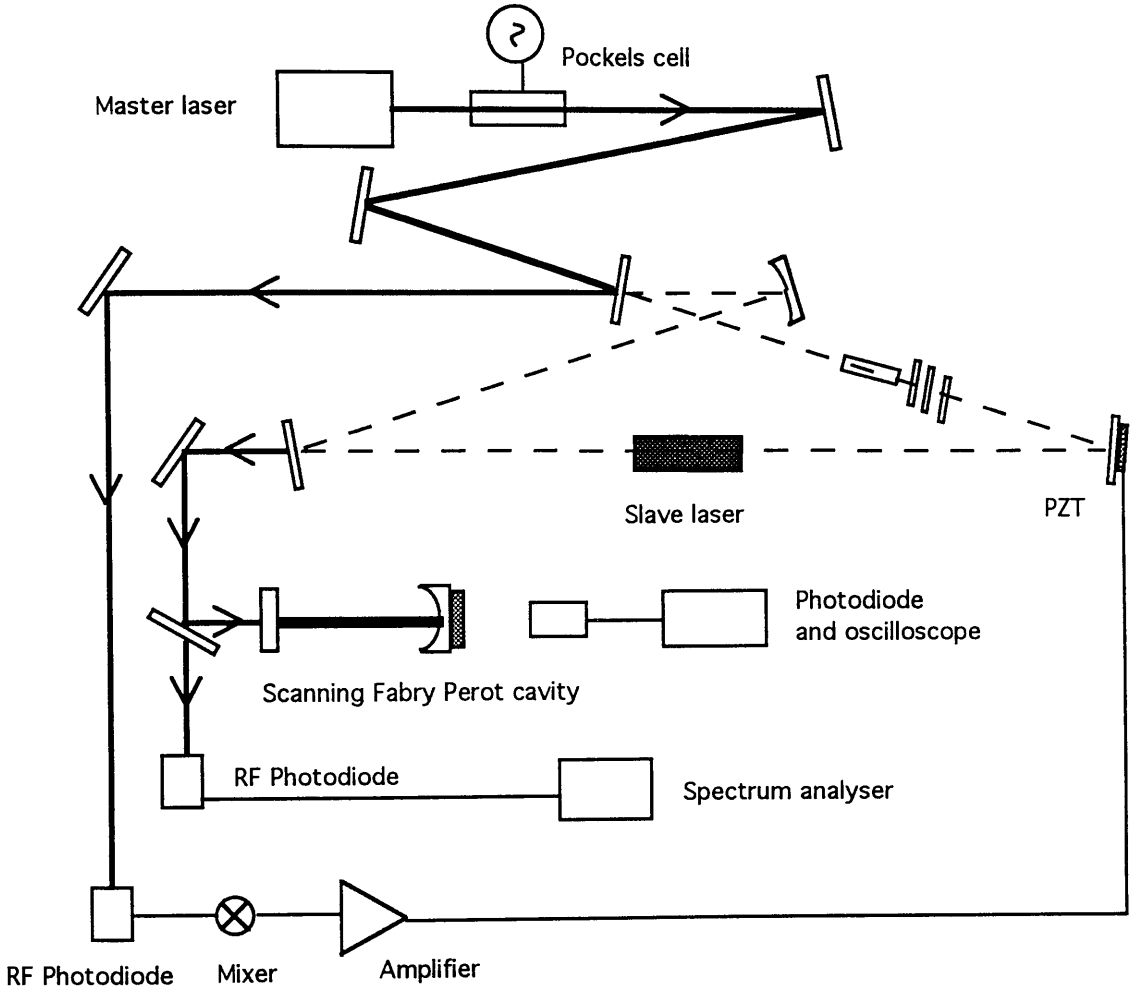

Figure 5.1: Experimental apparatus used to injection lock the 4 mirror ring laser with a diode pumped ring laser. The diode pumped laser light is injected through the output coupler into the 4 mirror ring. Also shown is a scanning cavity and RF photodiode for analysis of the laser state and a control system to maintain locking.

The scanning Fabry-Perot cavity was used to observe the mode structure of the laser. Injection locking should induce single frequency operation and this was used to indicate when locking occurred.

Injection locking was first tried with an 8% transmitting output coupler on the slave laser but there were no signs of locking. This was replaced with an output coupler of 20% transmission to increase the locking range of the laser. The locking range for an 8% transmitting output coupler, a master laser power of 40 mW and a slave laser power of 6.5 W is 0.3 MHz. Increasing the transmission of the coupler to 20 % additionally reduces the slave power, and so the locking range increases to 1.2 MHz. To find lock, the master laser frequency was changed using the thermal controller until the beat signal between the two lasers was found. The laser was then further tuned to within the locking range. The locking occurred, but only briefly, due to the frequency fluctuations of the slave laser. The locking was indicated by the single mode operation of the laser. (Without injection locking the laser was running two modes, or sometimes three.)

To maintain locking, an electronic servo was used to hold the two lasers within the injection locking range. The external influences on the laser, such as mirrors shaking from external disturbances and the subsequent frequency change may cause loss of lock. The servo was used to sense and correct these effects, allowing lock to be maintained. The servo worked in much the same way that a laser is frequency stabilised to a Fabry-Perot cavity using RF sideband reflection locking. When a Fabry-Perot cavity is locked to a laser using the RF sideband technique, the interference between the sidebands and the light exiting the cavity produces a signal that has an amplitude modulation, at the initial modulation frequency, that is proportional to the frequency difference between the incident light and the cavity resonance frequency. In the injection locking case the master laser light is phase modulated as before but the laser cavity does not act as the frequency discriminator. However, it can be considered as an analogous situation to RF locking with a Fabry-Perot cavity, with the laser output substituting for the leakage light from the Fabry-Perot cavity. The error signal is formed from the beat signal of the sidebands (that are reflected off the coupling mirror) and the slave laser output,

which, when injection locked, should be equal in frequency to the injected signal. This, as before, resulted in an amplitude modulated signal that when demodulated gave a bipolar error signal, with magnitude proportional to the frequency offset. The error signal with appropriate amplification and filtering, for servo stability, was fed back to a PZT controlled cavity mirror in the slave laser. The electronics used for the servo are shown in figure 5.2.

If the frequency fluctuations of the laser are too large or too fast for the servo to respond then lock will be lost, because the servo will not have been able to follow the frequency shift through the injection locking range. Once the injection locking has been lost the servo is unable to reforce locking, as the error signal will be unintelligible due to the multimode operation of the laser. The situation where the system could be forced to re-lock by the servo by using the slave laser cavity as a frequency discriminator (exactly as if locking to a Fabry-Perot) is prevented by the lack of a suitable error signal. The servo relies on initial locking to work.

5.4 Results

With the 20% transmitting output coupler, the servo held the two lasers injection locked for up to 15 minutes with an output power of 2.5 Watts. The lower power was due to overcoupling of the laser, the 20% loss of the mirror was too high for the laser gain. The beat signal for the lasers when almost locked is shown in figure 5.3 and pictures of the mode structure while locked and unlocked are shown on figure 5.4. To allow more power out, the laser should be locked with a lower transmitting output coupler on the slave laser. This would narrow the locking range of the two lasers and would either require more power from the master laser or possibly a better electronic servo. In the first case the increased power would widen the locking range cancelling the effect of the lower output coupler. Improving the servo (more gain and a wider bandwidth) would allow a narrower locking range to be tolerated despite intrinsic laser frequency fluctuations that could be larger than the locking range.

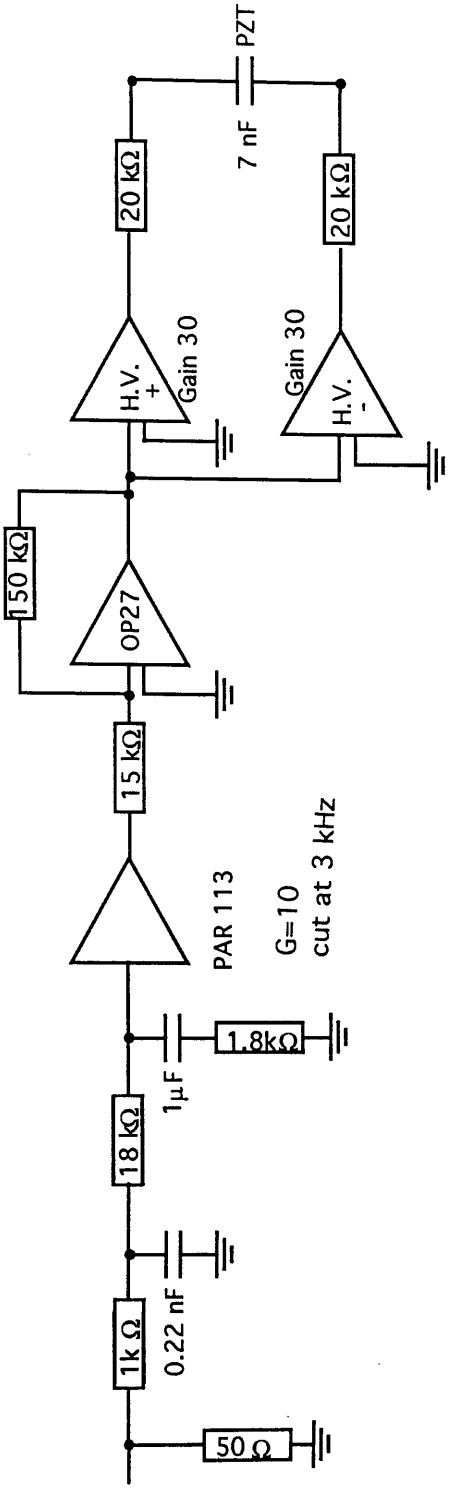

Figure 5.2: Servo electronics used to maintain injection locking of the laser system of figure 5.1.

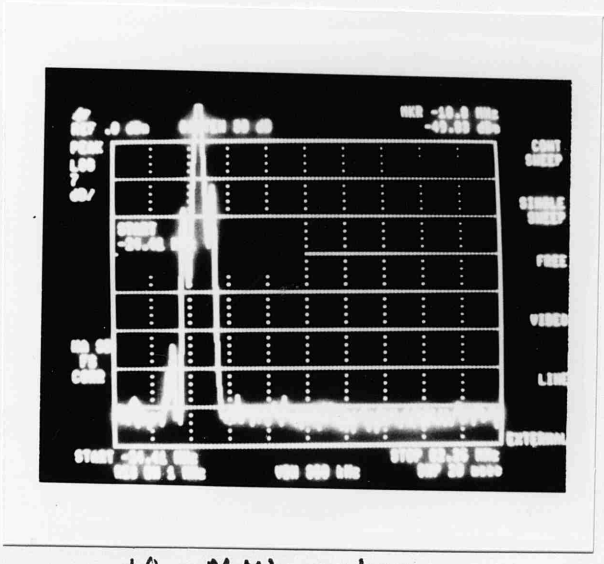

10 MHz per box

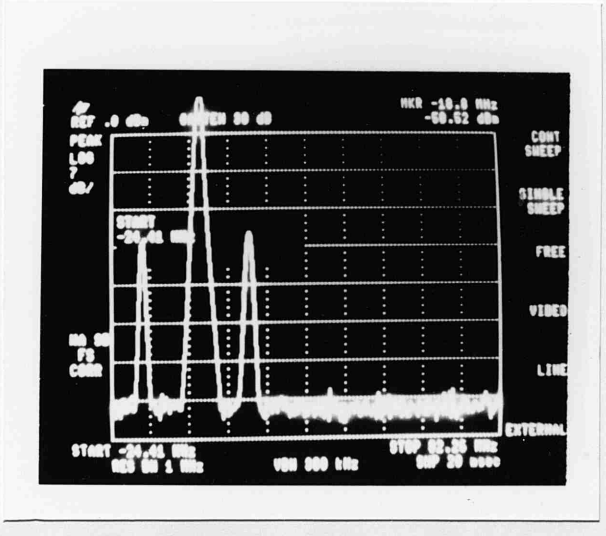

10 MHz per box.

Figure 5.3: The upper figure shows the beat signal from an RF spectrum analyser when the system is almost locked. The beat signal between the master and slave lasers can be seen approaching zero. The lower figure shows the beat signal between the master and slave lasers out side the locking range.

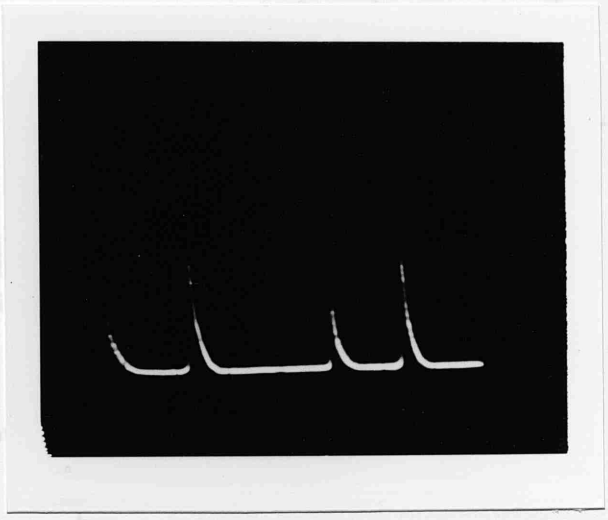

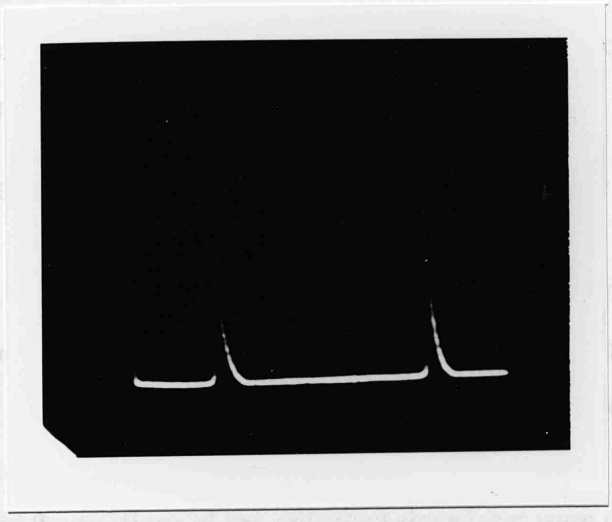

Figure 5.4: The upper figure shows the multimode structure of the slave laser when unlocked and the lower figure shows the single mode structure when locked (lower). Both were taken using a scanning Fabry-Perot cavity.

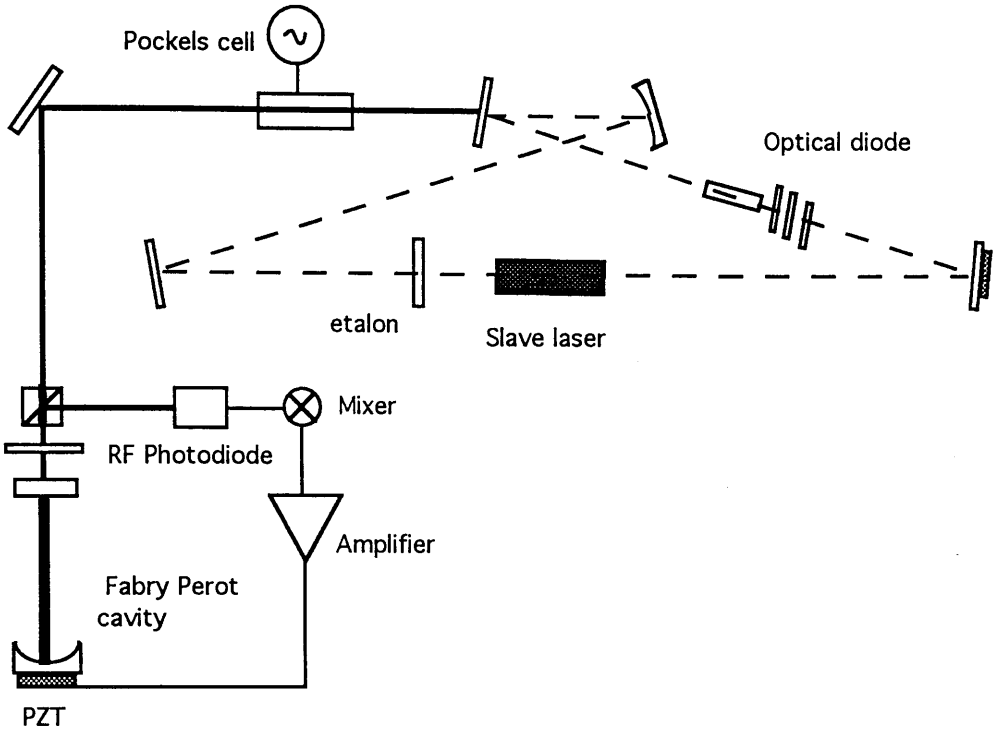

Figure 5.5: Experimental apparatus used to measure the frequency noise of the unlocked slave laser using the RF sideband technique.

5.5 Frequency fluctuations

To observe how the injection locking suppressed the frequency fluctuations of the high power slave laser, the frequency fluctuations of the unlocked slave laser and the locked slave laser were measured and compared. Additionally the master laser frequency fluctuations were measured.

The frequency fluctuations of the unlocked slave laser were measured by locking a Fabry-Perot cavity to the laser using the RF sideband reflection locking technique described in Chapter 3. The error signal formed was amplified and fed back to a PZT controlled mirror in the Fabry-Perot cavity. The experimental arrangement is shown in figure 5.5, and details of the servo electronics are shown in figure 5.6.

When the frequency noise of the unlocked slave laser was measured, the laser cavity contained an etalon for single mode operation and had an 8% transmitting

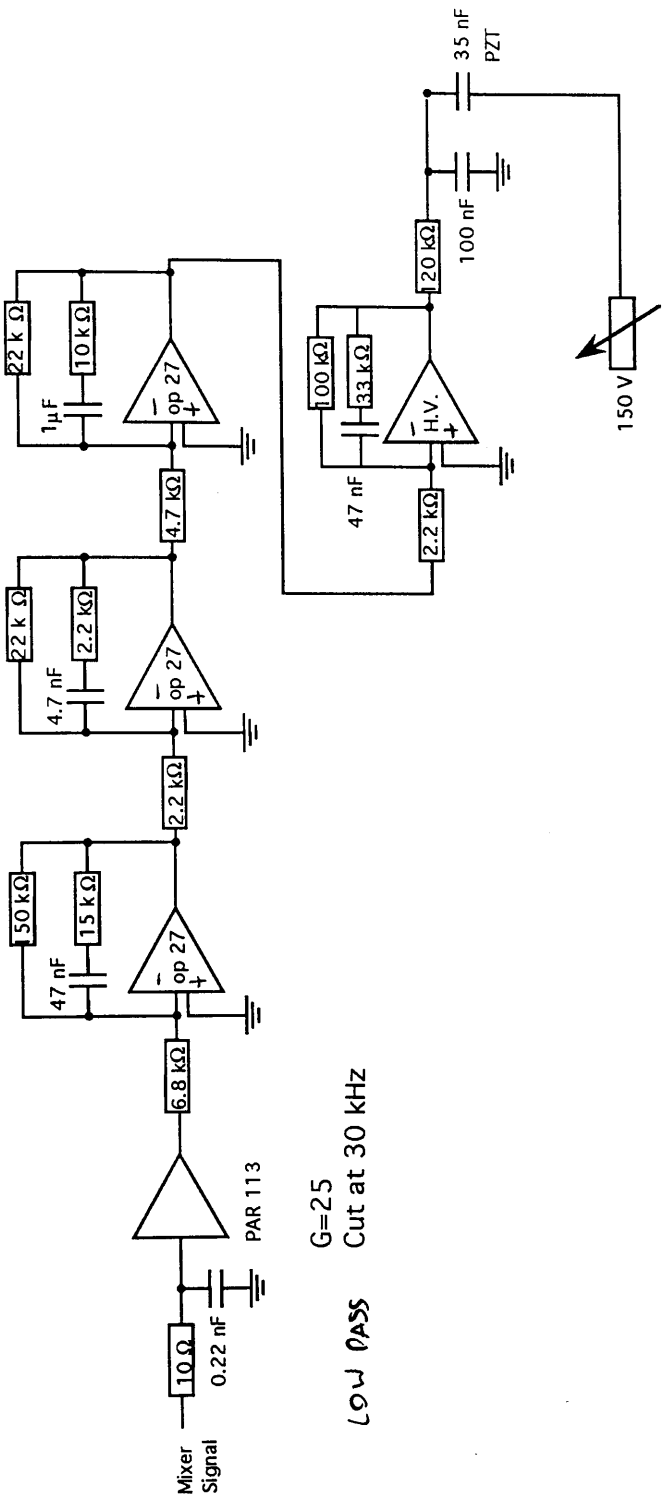

Figure 5.6: Servo electronics to measure the frequency noise of the unlocked slave laser using the RF sideband technique.

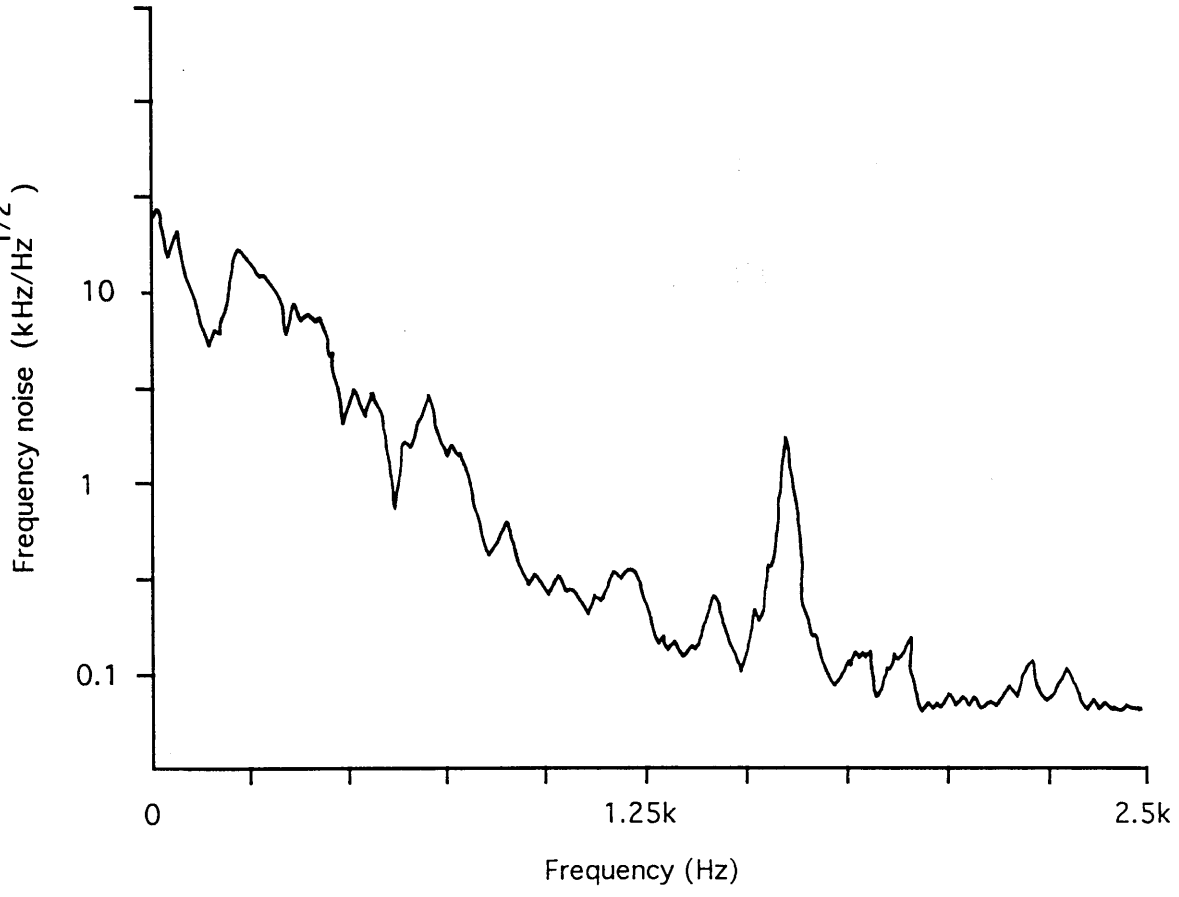

Figure 5.7: Spectrum of frequency fluctuations of unlocked slave laser

output coupler. The unity gain point of the servo was around 5 kHz so the spectrum of the feedback servo to the PZT up to 5 kHz represents the frequency fluctuations of the laser. The spectrum is shown in figure 7.

The frequency fluctuations of the Nd:YAG laser are similar in magnitude to an argon ion laser*. At 1kHz the noise from an argon laser is 2 to 3 $kHz/Hz^{\frac{1}{2}}$[Kerr1986]. It is likely that the water cooling found in both lasers introduces the dominant noise source to each at this frequency.

* The best small frame argon ion laser.

5.6 Frequency fluctuations of injection locked laser

The frequency noise of the slave laser, while injection locked, was measured by electronically servo-locking a Fabry-Perot cavity to the laser using transmission locking to the side of a fringe. (Transmission locking was used in place of RF reflection locking only because there were no more phase modulators available.) The experimental arrangement is shown in figure 5.8. The output of the laser was split to form two beams; one was used to keep the laser injection locked via the RF locking servo and the other was again divided to form two beams. One beam was incident on a reference photodiode, and the other on a Fabry-Perot cavity, which had a photodiode monitoring its transmission. The light incident on the reference photodiode was attenuated using a polarising beam splitter and a half-wave plate until the photodiode signal was equal to half the signal height of a fringe transmitted by the Fabry-Perot cavity. The signals from the photodiodes were subtracted from each other using a difference amplifier to produce an error signal that was independent of intensity fluctuations. The cavity was locked to the laser by suitably amplifying the error signal and feeding it back to a PZT controlled mirror in the Fabry-Perot cavity. The electronics for the locking servo are shown in figure 5.9. This procedure was repeated to measure the noise of the master laser, the diode pumped Nd:YAG laser. The electronic servo used was identical to that used for the injection locked laser.

Figure 3.2 shows the block diagram of a negative feed-back system. G and H are control elements with transfer functions G(s) and H(s). As described in Chapter 3 the relation

$$v_\epsilon = \frac{v_n}{1+GH}$$

and

$$v_f = \frac{GHv_n}{1+GH}$$

can easily be obtained. If the loop gain, GH, is much greater than 1 then $v_f = v_n$ and when the loop gain is much less than 1, $v_\epsilon = v_n$. Whenever the gain is low, the phase of the loop gain is also important. If the gain is close to 1 then both the

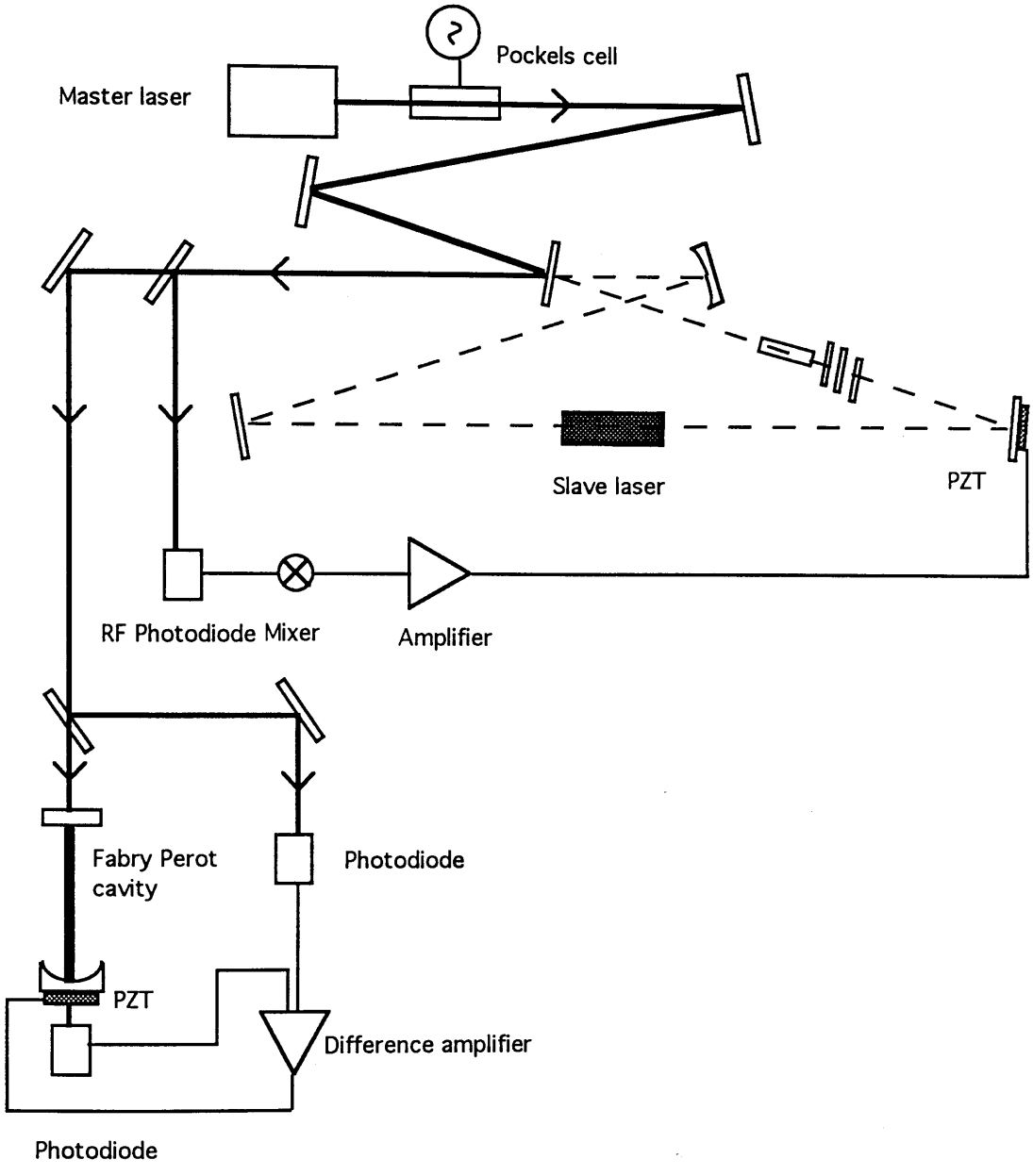

Figure 5.8: Experimental apparatus used to measure injection locked slave laser frequency fluctuations.

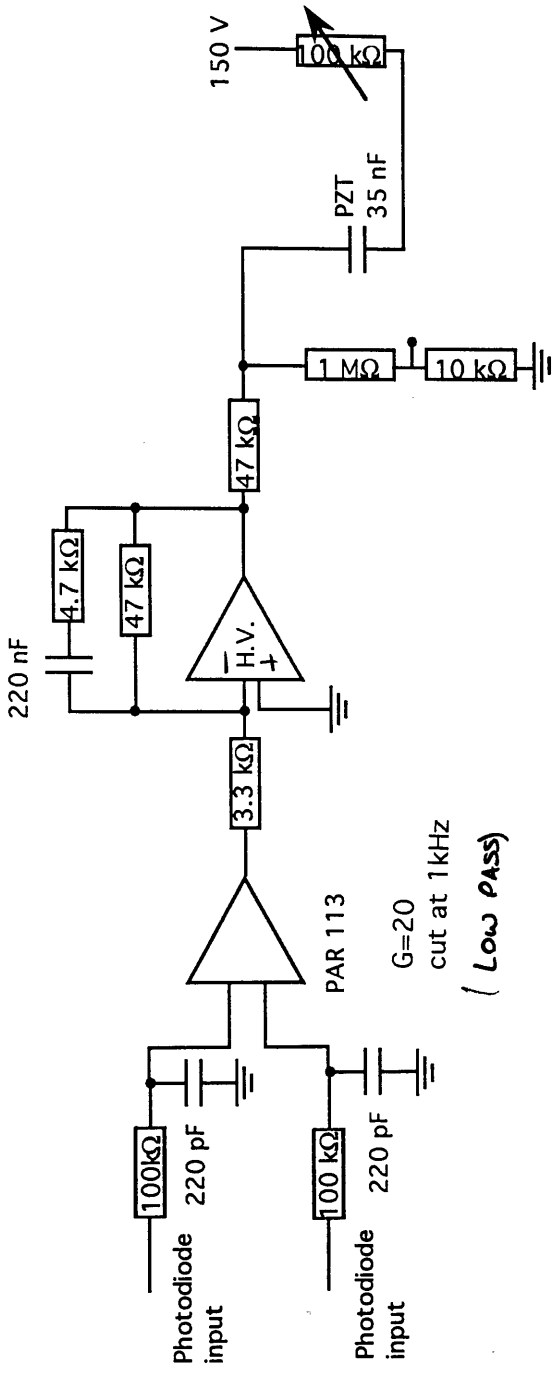

Figure 5.9: Servo electronics for frequency noise measurement of the injection locked laser.

error and feedback signals, together with the loop phase and gain must be used to determine the frequency noise.

The servo used to measure the frequency fluctuations of the injection locked laser, and the master laser, had a unity gain point of around 1 kHz. To make a comparison of the noise, of the locked and unlocked laser, the error signal and feedback signal, shown in Appendix A, were used to calculate the frequency fluctuations up to around 1 kHz for both the locked slave laser and the master laser. The error signal and the feedback signal were used to calculate the magnitude of the loop gain;this is v_f/v_n. The phase of the loop, calculated from the electronics, was then used to calculate the magnitude of 1+GH, thus allowing the frequency noise to be calculated.

5.7 Results

The frequency fluctuations of the locked slave and the master laser are shown, in figure 5.10, plotted, on to the same graph as the spectrum of the unlocked slave laser. The results show an approximate factor of ten improvement in the noise performance of the slave, and also that the injection locked laser is at a noise level comparable with the master laser. The results do confirm the transfer of frequency stability from the master laser to the slave. Four points were plotted to show the bulk structure of the noise. The error in the calculations made any fine structure impossible to show. However, it is unlikely that comparing the fine structure of the frequency noise would be useful as environmental changes between measurements (several days occurred between measurements) would dominate the fine structure.

5.8 Shot noise

The servo used to maintain the locking uses an error signal that has a magnitude that depends on the size of the sidebands on the master laser light and the size of the slave laser output. As the slave laser output is so large, this can result

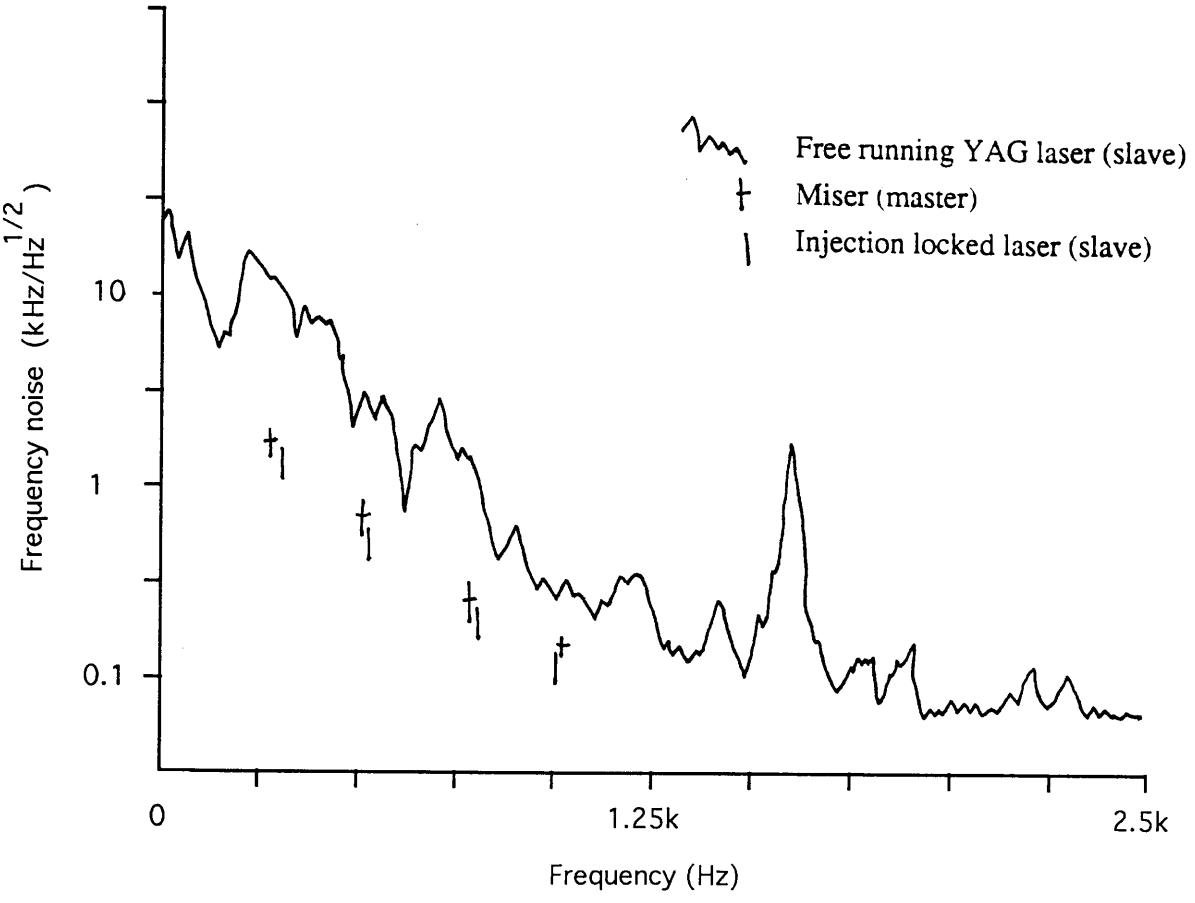

Figure 5.10: Frequency noise of slave laser, master laser, and injection locked slave laser. The complete curve is the frequency noise spectrum of the unlocked slave laser. The calculated noise for the master laser and injection locked slave laser has been plotted onto the graph.

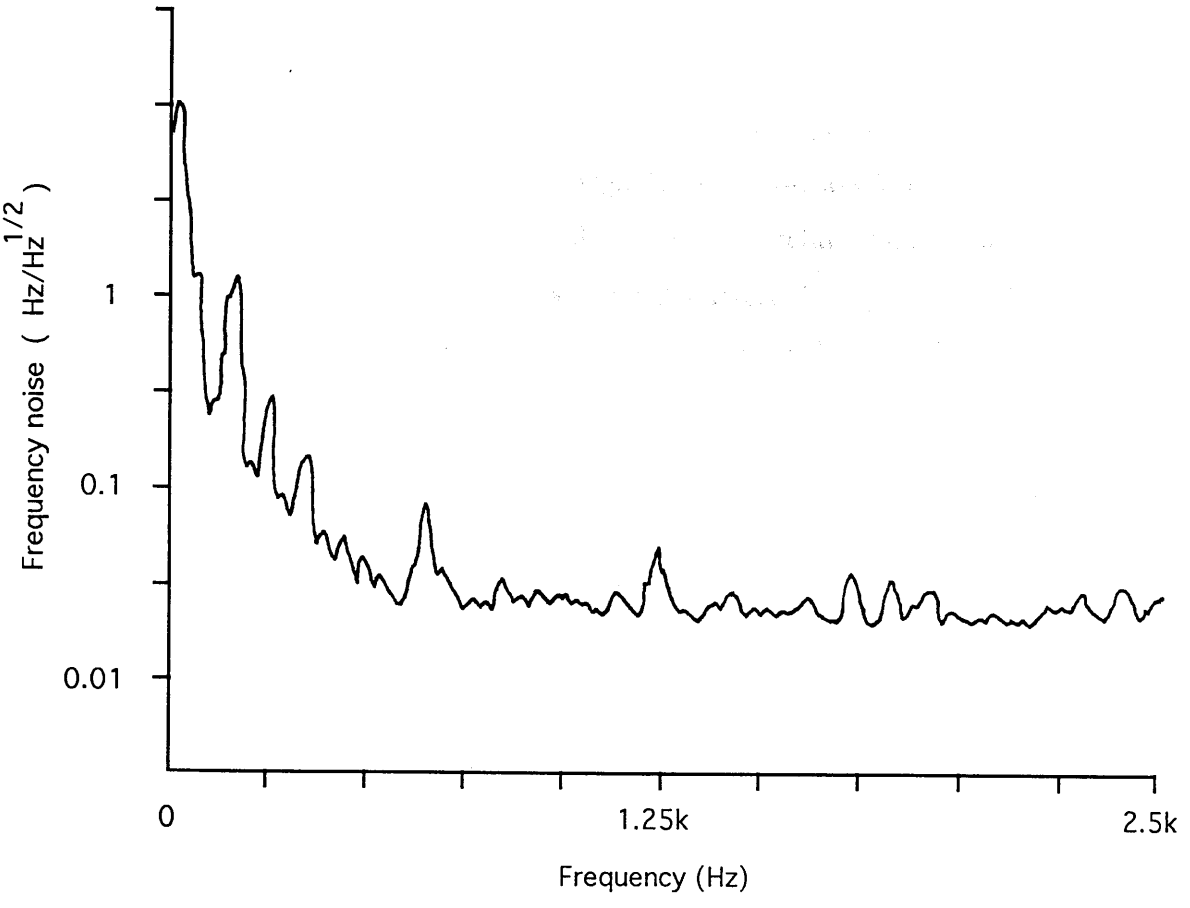

Figure 5.11: Spectrum of frequency noise corresponding to the shot noise level in the servo system used to maintain injection locking.

in shot noise at the photodiode being imposed back on the laser through the servo system. This was measured to check the possible limitations that could be imposed on frequency stability. To calculate this, the shot noise at the error point was measured by using a torch to supply the same photodiode current that occurs when locked using the laser light. The spectrum is shown in figure 5.11. At 1 kHz the frequency noise corresponds to $11 \times 10^{-3} Hz/Hz^{1/2}$, far below the fluctuations of the injection locked laser.

5.9 Further injection locking experiments

The injection locking technique was further examined at a later stage using a higher power master laser. The LIGHTWAVE diode pumped laser was replaced with a similar laser from the Laser Centre, Hanover that was capable of supplying a single mode output power of 400 mW. Although 400 mW was available the polarisation ratio was approximately 3:1 so only 300 mW was useful. The frequency tuning control of the high power laser was also much coarser.

The flashlamp pumped Nd:YAG laser was again used as the slave laser but by this time the cavity had been rearranged. The cavity was in the form of a three mirror ring laser, the second cavity described in Chapter 4. As before, the cavity had an optical diode in place but the intracavity etalon was removed. A similar technique to that used previously was tried in order to lock the laser, but even with the increased locking range it was unsuccessful. This technique failed for a variety of output couplers, up to 25% transmitting. As before, an electronic servo very similar to the one described earlier, was used to try to maintain any injection locking.

The problem appears to have been the coarse temperature tuning of the master laser. The master laser frequency was unable to be controlled delicately enough to allow its frequency to remain in the locking range. The coarse temperature tuning forced the laser in and out of lock as the locking range was swept through when ever the temperature was changed. This occurred too quickly for the servo to be able to operate and retain locking. A larger bandwidth or higher gain servo may be a potential solution. The larger bandwidth would hopefully allow the locking range to exceed the frequency shifts, and the servo, if improved, would hold lock as the frequency was swept through.

An alternative technique was tried where, rather than trying to tune the master laser to within the locking range of the dominant free running mode, the master laser was used to try to seed the free running mode from below threshold. This allows the servo to operate and lock before the injection locking has occurred. Whenever the slave laser is below threshold, the slave laser cavity is locked to the

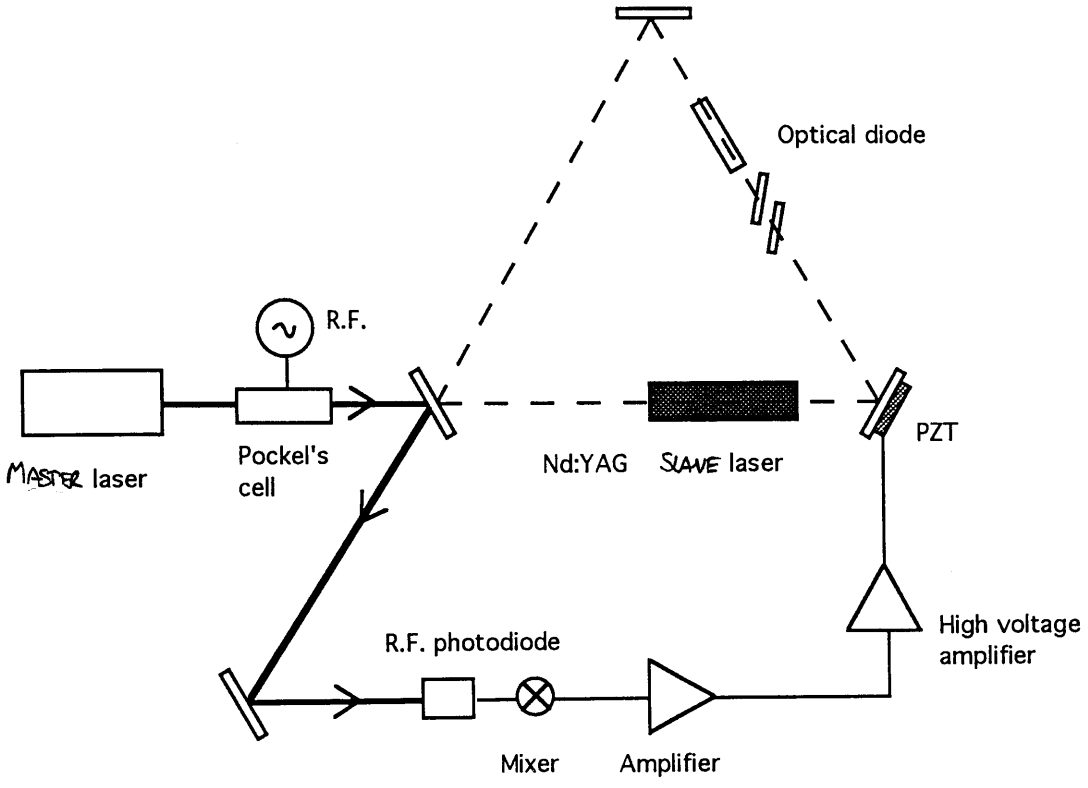

Figure 5.12: Experimental arrangement used to injection lock 3 mirror ring laser.

master laser light. This is identical to the case of locking a Fabry-perot cavity to a laser, as the laser cavity below threshold is simply a Fabry-perot cavity. Once locked, if the laser is raised above threshold, there is enough gain for lasing action. However, the master laser light will be amplified as it circulates in the slave cavity. If the master laser frequency is close enough to the gain peak of the slave laser the master laser light will saturate the gain and the lasing will occur at a frequency controlled by the master laser; the system is then injection locked. In the case of Nd:YAG the large gain bandwidth means that the seeding of the mode should be relatively simple.

The experimental arrangement used is shown in figure 5.12. The two lasers were initially mode matched, and a first level of spatial overlap was obtained. Reducing the lamp current to operate the laser below threshold was tried initially but the lamp current affected the thermal lens and changed the cavity characteristics too much to allow locking to hold when the current was increased. The change in

thermal lens was accompanied by a small beam displacement and this may have prevented the locking. Instead the slave laser was switched below threshold by using an intracavity variable aperture. The variable aperture was used to increase the losses, pushing the laser below threshold. When the laser was below threshold, the laser cavity was scanned by driving the cavity PZT mirror. The laser had a reflected output that was identical to a Fabry-Perot cavity, and the observed fringes were used to optimise the lining up procedure, making the laser cavity resonant with the master laser light. The servo was connected after alignment and the slave laser cavity was locked to the master laser. The aperture was slowly opened allowing the master laser to seed the slave laser mode. This was repeated for several master laser frequencies, to allow the gain centres to be overlapped.

This technique allowed the laser to lock when a 25% output coupler was used; this gave a power of approximately 2 watts. Unfortunately it did not work for any other output coupler. Thus, similar results to the first experiment were obtained although the locking range was increased.

5.10 Summary

The frequency noise from the flash lamp pumped Nd:YAG laser was shown to be at a similar level to an argon ion laser*. This is probably due the water cooling found in both systems.

The second set of injection locking experiments involved a larger locking range than before, but was not any easier. It appears that the servo must be of a high enough standard to allow locking to occur, as it is possible that the fast laser fluctuations dominate the locking. Results from Hanover [Frietag 1990] suggest that the locking range can be very narrow if the servo has enough gain and a wide enough bandwidth.

The overall results are encouraging, the frequency stability has been shown to be transferred from the master laser. This makes a locking scheme an attractive proposition as part of a laser frequency stabilisation system.

* similar to the best small frame argon laser.

Chapter 6

Second Harmonic Generation

6.1 Introduction

The development of a high power Nd:YAG ring laser has been described in the preceding chapters. Although an interferometer can be operated using infrared illumination, as proposed in several funding applications [Giazotto et al 1989], the longer wavelength has several disadvantages; for example the wavelength is invisible to the human eye and the beam diffraction is larger. The larger beam size requires not only a larger mirror but a larger vacuum pipe, as discussed in Chapter 1; both of these requirements are expensive and technologically more difficult.

This chapter describes some experiments in second harmonic generation using a nonlinear crystal with the aim of developing a high power intracavity doubled Nd:YAG ring laser. In such a laser the infrared output is converted to a visible green output. A brief review of the process of second harmonic generation, sometimes known as frequency doubling, is also given.

6.2 Second harmonic generation

The electric field of a monochromatic plane wave with angular frequency ω is defined in terms of its Fourier components by

$$E(r,t) = \{E(r,\omega)\exp\ i(kr - \omega t) + cc\}/2 \tag{6.1}$$

where cc is the complex conjugate, k is the wave vector and r is the displacement vector.

When this electric field is applied to a medium with a second order nonlinear susceptibility, it results in a polarisation at the harmonic frequency 2ω of

$$P(r,2\omega) = \sum_{ijk} \epsilon_o d_{ijk}(-2\omega,\omega,\omega) E_j(r,\omega) E_k(r,\omega) \tag{6.2}$$

where ϵ_o is the permittivity of free space. The above equation defines the nonlinear optical coefficients $d_{ijk}(\omega_1,\omega_2,\omega_3)$. The nonlinear tensor, d_{ijk} , is usually written in the reduced form of a single effective nonlinear coefficient, d_{eff}. The exact form of the reduction depends on the nonlinear material and the nonlinear process it is used for.

Coupled wave equations that describe second harmonic generation can be derived using Maxwell's equations and the driving polarisation for each frequency involved in the interaction. For a plane wave travelling in the z direction, assuming a lossless interaction, the coupled equations are [Byer 1977]

$$\frac{d}{dz} E(z,2\omega) = i\kappa \exp(-i\Delta k z) E^2(z,\omega) \tag{6.3}$$

and

$$\frac{d}{dz} E(z,\omega) = i\kappa \exp(-i\Delta k z) E(z,2\omega) E(z,\omega) \tag{6.4}$$

where $\kappa = \omega d_{eff}/\mathrm{nc}$, n is the index of refraction, c is the speed of light and $\Delta k = k_{2\omega} - 2k_{\omega}$, the wave vector mismatch. Arranging for $\Delta k = 0$ is known as phase matching.

Solutions of the above equations are available for low and high conversion efficiency, that is, where the fundamental field changes negligibly or not with distance during the interaction. The low conversion efficiency case is the most relevant to cw second harmonic generation. The solution is [Byer 1977],

$$I(2\omega) = I(\omega)[\Gamma \ell \sin(\Delta k \ell/2)/(\Delta k \ell/2)]^2 \tag{6.5}$$

where I(2ω) is the second harmonic intensity, I(ω) is the fundamental intensity, ℓ the interaction length and,

$$\Gamma^2 = \frac{2\omega^2 d_{eff}^2 I(\omega)}{c^3 n^3 \epsilon_o} \tag{6.6}$$

6.3 Phase matching

The efficiency of second harmonic generation is a maximum when $\Delta k = 0$. Any deviation from the phase matching condition of Δk equal to zero reduces the efficiency of the process.

Phase matching can be understood by first considering a linear and then a nonlinear material, with a propagating electric field. An incident electric wave drives oscillating dipoles which re-radiate a wave of identical frequency but different phase. The re-radiated waves from each dipole in a linear material will build up because there is a fixed phase relationship between an incident and a re-radiated wave over the interaction length. In a nonlinear material where second harmonic generation is taking place the dipoles will still re-radiate a wave with a phase that depends on the phase of the incident wave, but in this case the re-radiated wave and the incident waves may not travel at the same speed because they differ in frequency and so experience different refractive indices. If this is the case then the two waves will not maintain a fixed phase relationship and the second harmonic amplitude will not build up efficiently. For a phase matched process the two waves will maintain a fixed phase relationship and the output of second harmonic will build up.

Phase matching usually requires the refractive index at ω to equal the refractive index at 2ω. As most materials are dispersive this has to be achieved using the natural birefringence of anisotropic crystals. A birefringent material will split any ray into two orthogonally polarised components, the ordinary and extraordinary rays. The ordinary ray propagates with a refractive index which is independent of direction, while the extraordinary ray propagates with a refractive index that depends on the angle that the propagation direction makes with the optic axis.

The extraordinary index may be larger or smaller than the ordinary index, that is, a material may have positive or negative birefringence. By correctly choosing the propagation direction, it may be possible to match the indices at the fundamental and harmonic frequencies, if the two waves are not both ordinary or both extraordinary polarisations. There are two forms of index matching [Zernike and Midwinter 1973],

Type 1 where $n^e_{2\omega}(\theta) = n^o_\omega$ and,

Type 2 where $n^e_{2\omega}(\theta) = \frac{1}{2}(n^e_\omega(\theta) + n^o_\omega)$

Where this describes the situation of negative birefringence (positive birefringence requires the super scripts to be interchanged), n^o_ω, $n^e_{2\omega}$, and n^e_ω are the ordinary and extraordinary indices at ω and 2ω, and θ is the angle that the propagation direction makes with the optic axis.

6.4 Efficiency

The solution for the low conversion case of second harmonic generation shows that, when phase matched, the efficiency is proportional to the intensity of the fundamental, the interaction length squared and the effective nonlinear coefficient squared. To maximise the efficiency, each of these should be as large as possible.

The effective nonlinear coefficient is an intrinsic property of the material; it can only be maximised by choosing from the available nonlinear materials. When a material is selected the magnitude of the effective nonlinear coefficient must be weighted against other critical factors such as the ability to phase match the process and the material damage threshold. The available interaction length or crystal length is limited by the ability to produce flawless crystals of the size required. It may also be limited by the intrinsic properties of the material. For any phase matching direction other than parallel or perpendicular to the optic axis the fundamental and second harmonic beams will physically separate due to double refraction. This then limits the useful interaction length and consequently the efficiency. The simplest parameter to control is the intensity. The intensity can be improved in two ways: by focussing and by using the power build up inside

a resonant cavity.

6.5 Focussing

The efficiency can be improved if the fundamental intensity is increased by focussing using lenses or mirrors. Some care is required to find the optimum focussing efficiency. For example, if the beam focus is too small, diffraction may cause the the beam radius to change significantly over the interaction length, reducing the efficiency. A simplification by Yariv [Yariv 1975] of the work by Kleinman et al [Kleinman et al 1966] gives the optimum beam size for a given length as $W_o^2 = \ell\lambda/2\pi n$, where W_o is the gaussian beam radius, and λ the wavelength.

Equation 6.5 suggests that the efficiency is proportional to the length squared. However, if the optimum beam size (a function of length) is used the efficiency becomes proportional only to the length. This can easily be seen by substituting the above expression for W_o^2 into the efficiency equation.

6.6 Intracavity second harmonic generation

A common technique to improve the efficiency is to place the crystal inside a resonant cavity, either in the laser cavity itself or in a separate cavity pumped by the laser. This takes advantage of the higher circulating power in a high Q resonator. The resonator should ideally be a unidirectional ring to allow all the second harmonic to be collected simply. The resonant cavity technique is most important for second harmonic generation with cw lasers where the intensities are small compared to pulsed lasers.

Following a derivation by Smith [Smith 1970] for a linear intracavity doubled laser, the second harmonic power available from a unidirectional ring laser can be calculated as follows. The situation is modelled by treating the nonlinear material as a loss or as an output coupler of transmission T. T depends on intracavity power, p, such that T=qp, where q is a constant that depends on beam size and the nonlinear material used. Consider a ring laser with an intracavity nonlinear

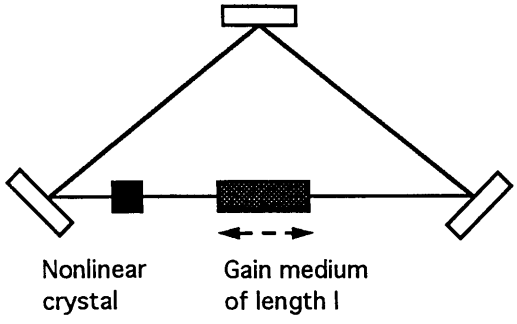

Figure 6.1: Ring laser with nonlinear loss.

crystal, as shown in figure 6.1, where the laser medium has length l and gain g, and saturates according to [Seigman 1986]

$$g = \frac{g_o}{1 + \frac{p}{p_s}} \tag{6.7}$$

where g_o is the small signal gain, and p_S the saturation intensity. The fundamental and second harmonic power can be determined from the steady state condition that the gain in a round trip must equal the loss

$$\frac{g_o l}{1 + \frac{p}{p_s}} = L + qp \tag{6.8}$$

where L is the cavity linear loss.

Equation 6.8 gives the fundamental power and second harmonic power as

$$p = \frac{p_s\left[\sqrt{(\frac{L}{g_o l} - \frac{qp_s}{g_o l})^2 + 4\frac{qp_s}{g_o l}} - (\frac{L}{g_o l} + \frac{qp_s}{g_o l})\right]}{2\frac{qp_s}{g_o l}} \tag{6.9}$$

and

$$p(2\omega) = \frac{l g_o p_s [\sqrt{(\frac{L}{g_o l} - \frac{qp_s}{g_o l})^2 + 4\frac{qp_s}{g_o l}} - (\frac{L}{g_o l} + \frac{qp_s}{g_o l})]^2}{4\frac{qp_s}{g_o l}} \tag{6.10}$$

The second harmonic power out is a maximum for $\frac{qp_s}{g_o l} = \frac{L}{g_o l}$, which gives the maximum output as $P_m(2\omega) = l g_o p_s (1 - \sqrt{\frac{L}{g_o l}})^2$ and $q = \frac{L}{p_s}$ gives the nonlinear coupling.

It is clear, from the above equations, that increasing the loss in a cavity not only reduces the quantity of second harmonic available but increases the nonlinearity required to extract it. For an intracavity process the losses associated with the crystal should be as small as possible.

It can also be shown, using the above equations, that the optimum second harmonic power that can be extracted is equal to the optimum fundamental power that can be extracted from an ordinary laser with the same losses [Smith 1970]. This is simple to see intuitively if we consider a laser with an output coupler of transmission T_1 and intracavity power P_1. Consider the case where the output coupler is replaced with a nonlinear material with coupling q, such that it has transmission T, which is equal to qP_2, where P_2 is the intracavity power in the laser. If q is increased such that qP_2 equals T_1, and (provided the losses are identical) P_2 equals P_1, then an identical quantity of power will be extracted. In this manner it can easily be seen that (for the laser described in Chapter 4) the nonlinear crystal should act as an output coupler of 8%, if all the fundamental power is to be extracted as second harmonic.

6.7 KTP

The nonlinear material chosen for our experiments was potassium titanyl phosphate, KTP, cut for type 2 phase matching. It has a large effective nonlinear coefficient and a propagation direction that is perpendicular to the optic axis (known as 90 degree phase matching), giving no walk off (KTP is a biaxial crystal but is approximated as uniaxial).

There is disagreement in the literature over the value of d_{eff} for KTP. The value measured by Zumsteg et al [Zumsteg et al 1976] and frequently referred to in many publications is more than twice as large as a more recent measurement published by Eckardt et al [Eckardt et al 1990]. The situation is not helped by the propagation through the literature of an incorrect expression for the nonlinear

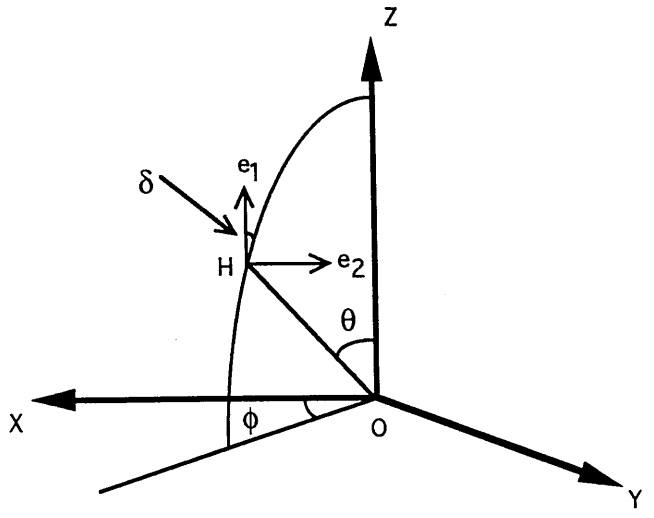

Figure 6.2: Propagation in a biaxial crystal

coefficient of crystals of the class KTP belongs to, published by Ito et al [Ito et al 1975]. A correct calculation by the author is as follows.

Figure 6.2 shows the propagation and polarisation of an optical wave in a biaxial crystal (of which KTP belongs), where OH is the propagation direction, θ is the angle OH makes with the z axis, ϕ is the angle that the projection of OH onto the x-y plane makes with the x axis, e^1 and e^2 are the allowed orthogonal polarisations and δ is the angle that e^1 makes with HZ. e^1 is the bisector of the angle formed by the optic axes and the propagation direction (this defines the allowed polarisations in the crystal [Born and Wolf 1965]). The effective nonlinear coefficient is defined as (for type 2 phase matching) [Zernike and Midwinter 1973]

$$d_{eff} = a_i d_{ijk} b_j a_k \tag{6.11}$$

where d_{ijk} is the nonlinear tensor and a_i and b_i are the direction cosines of the allowed polarisations. It is possible to reduce the nonlinear tensor to two dimensions [Zernike and Midwinter 1973]. For the class of crystals with mm2-orthorhombic

symmetry (which includes KTP) equation 11 becomes,

$$d_{eff} = d_{31}(a_1b_1a_3 + a_1b_3a_1 + a_3b_1a_1) + d_{32}(a_2b_2a_3 + a_2b_3a_2 + a_3b_2a_2) + d_{33}(a_3b_3a_3) \tag{6.12}$$

Where it is assumed [Ito et al 1975] that the tensor components $d_{31} = d_{15}$ and $d_{32} = d_{24}$. The direction cosines for b and a are, from figure 6.2, respectively

$$\begin{pmatrix} -\cos\theta\cos\phi\cos\delta - \sin\phi\sin\delta \\ -\cos\theta\sin\phi\cos\delta + \cos\phi\sin\delta \\ \sin\phi\cos\delta \end{pmatrix}$$

$$\begin{pmatrix} \cos\theta\cos\phi\sin\delta - \sin\phi\cos\delta \\ \cos\theta\sin\phi\sin\delta + \cos\phi\cos\delta \\ -\sin\theta\sin\delta \end{pmatrix}$$

Whenever these are substituted into equation 6.12 the expression for d_{eff} becomes,

$$\begin{aligned} d_{eff} &= (d_{32} - d_{31})\sin\theta\cos 2\phi\sin\delta(3\cos^2\delta - 1) \\ &+3(d_{32}\sin^2\phi + d_{31}\cos^2\phi)\sin\theta\cos^2\theta\sin^2\delta\cos\delta \\ &+(d_{31}\sin^2\phi + d_{32}\cos^2\phi)\sin\theta\cos\delta(3\cos^2\delta - 2) \\ &+d_{33}\sin^3\sin^2\delta\cos\delta \end{aligned} \tag{6.13}$$

Typically KTP is approximated to be uniaxial and in this case δ is equal to zero. This gives a simplified expression of

$$d_{eff} = (d_{31}\sin^2\phi + d_{32}\cos^2\phi)\sin\theta$$

The incorrect expression derived from [Ito et al 1975] is

$$d_{eff} = (d_{31}\sin^2\phi + d_{32}\cos^2\phi)\sin\theta + (d_{31} - d_{32})\sin 2\theta\cos 2\phi$$

The phase matching angles for type 2 KTP are $\phi = 23°$ and $\theta = 90°$. It is the phase matching condition that allowed the error to propagate in the literature, since two identical expressions are obtained with these conditions.

Initial experiments were carried out using a $5 \times 3 \times 3$ mm KTP crystal grown in China. The crystal had an anti-reflection coating for 1064 nm (the fundamental) on one face and an antireflection coating for both 1064 nm and 532 nm (the second harmonic) on the other.

6.8 Experiments using 5 mm long KTP crystals

The Nd:YAG ring laser described in Chapter 4 was capable of producing 6.5 watts of infrared light using an 8% output coupler (80 W intracavity) when in the 4 mirror cavity configuration. As discussed earlier, to obtain the full 6.5 watts of infrared light as frequency doubled visible light, the nonlinear crystal should act as an 8% output coupler. Using the Zumsteg value of d_{eff} , the laser waist of 250 μm and an intracavity power of 80 watts, the 5 mm KTP crystal acts as a 0.25% coupler. To achieve a coupling of around 8% it is necessary to use not only intracavity second harmonic generation, but also focussing. If the waist is reduced to around 40 μm, then the nonlinear material acts as coupler of around 10% . The focussing was done using intracavity lenses to form a small waist in the laser cavity.

Figure 6.3 shows the experimental arrangement used. The laser was in the form of a four mirror cavity with a figure of eight path length, the first laser configuration described in Chapter 4. To provide a small waist, two 25 mm focal length lenses were placed in the cavity as shown. This gave a beam waist, at the centre of the two lenses of approximately 40 μm. To reduce any loss and maximise the circulating fundamental power, the laser had a high reflector in place of the fundamental output coupler. Using the lenses to form a waist was a simple technique that avoided any major change to the laser cavity. However, there was a problem that the lenses, although antireflection coated, introduced loss and reduced the intracavity power by approximately 30%.

The KTP was mounted to allow orientation for phase matching. The mount had displacement in the x, y and z direction, and rotation about the x, y and z axes. When the KTP was correctly oriented at the waist in the laser formed by the two lenses, 175 mW of 532 nm light was measured.

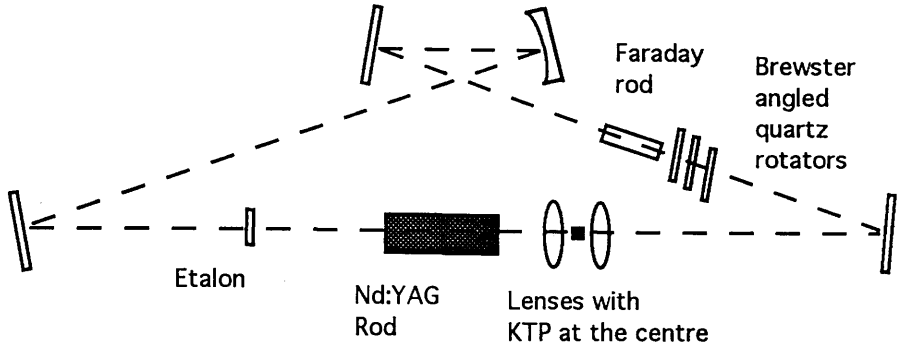

Figure 6.3: Laser arrangement used for intracavity focussed doubling.

The poor output could simply have been attributed to the cavity loss being so high (the intracavity power of only 40 W indicated that the losses were too large). However, the beam radius of 40 μm and intracavity power of 40 Watts, measured using the transmission of a high reflector, suggested that the power out should have been 2 watts, if the Zumsteg value for the nonlinear coefficient was used. This was almost an order of magnitude higher than the experimental results.

Whenever the intracavity second harmonic generation was tried without the focussing lenses, typical results were still less than expected by an order of magnitude. The table in figure 6.4 gives the results and details of the intracavity power and beam size for various doubling experiments along with the expected results calculated from data on the nonlinear coefficient from both Zumsteg and Eckardt.

There were several possible reasons contributing to the poor efficiency; uncertainty in the beam size, the intracavity power, the polarisation and the phase matching. It is unlikely that the intracavity power was incorrect as this was monitored using a power meter and the leakage light from a highly reflecting mirror. The beam size and phase matching were more likely candidates.

	Beam radius μm	Measured IR power	Measured green power	Calculated power using Zumsteg	Calculated power using Eckardt
Intracavity doubling with focussing	40	40W	175mW	2W	500mW
Intracavity doubling	350	46W	4.4mW	36mW	9mW
Intracavity doubling	350	55W	7mW	50mW	12.5mW
External doubling*	62,100	4W	4mW	24mW	6mW
External doubling**	62,100	4W	4mW	24mW	6mW
Linear cavity intracavity	40	150W	800mW	28W	7W
Linear cavity intracavity	250	80W	40mW	290mW	72.5mW

Figure 6.4: The table shows the results of several doubling experiments and the calculated values using data from both Zumsteg and Eckardt.

* ELLIPTICAL BEAM

** A DIFFERENT CRYSTAL WAS USED WITH AN ELLIPTICAL BEAM.

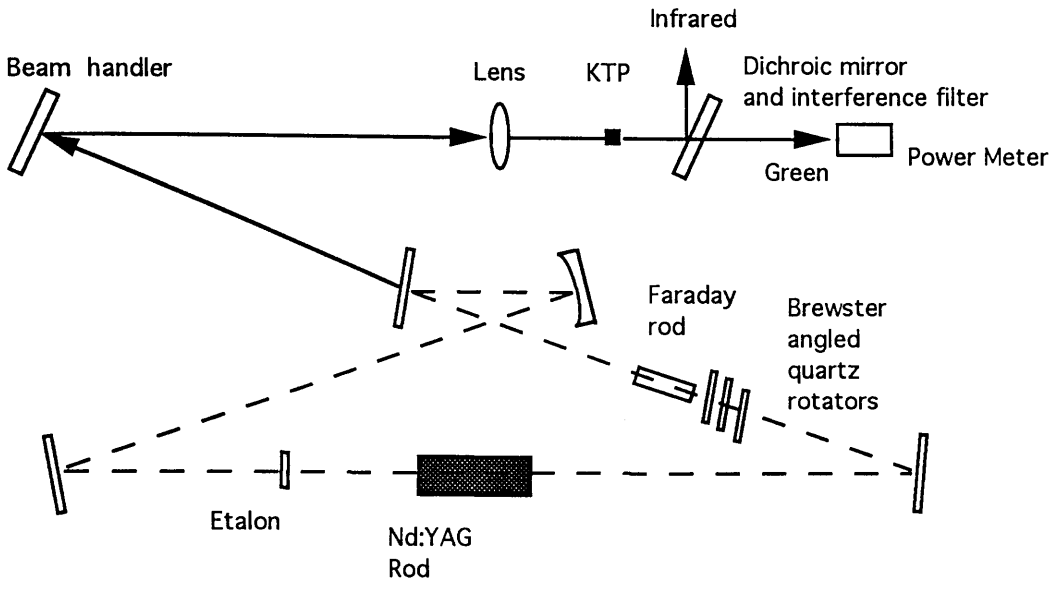

Figure 6.5: Experimental layout used for external second harmonic generation.

6.9 External second harmonic generation

To provide a more controlled experimental environment for determining the cause of the low conversion efficiency, the frequency doubling experiments were continued external to the laser cavity. In this case, because of the low conversion efficiency, focussing was required to generate a measurable quantity of second harmonic. The experimental arrangement is shown in figure 6.5.

To eliminate error in the beam size, it was measured using a pinhole and a micrometer at the point the lens was to be placed. A polarising beam splitter was used to define the polarisation and eliminate the possibility that the polarisation was not linear. A dichroic mirror and interference filter were used to separate the fundamental and the second harmonic. With a 2.5 D lens used to focus the beam the power observed was about 4 mW, while the expected power was 22 mW. Details of the beam size and the fundamental power are given in figure 6.4.

The experiment eliminated the uncertainty in fundamental power, polarisation and to a certain degree the beam size, yet there remained a significant difference in the experimental and theoretical results. There did, however, remain the possibility that the KTP itself was flawed. To check this , the experiment was repeated exactly

for two other KTP crystals. The results for these two crystals, from Germany but originating in China, were indistinguishable from the original crystal.

When the beam profile was measured in more detail it was found to be elliptical, due to the curved mirror in the ring laser cavity. Although this was taken in to account when calculating the expected power, it seemed possible that the difficulties of focussing an elliptical beam could have been responsible for the discrepancy in the results. In order to eliminate this possibility several other experiments were carried out using a linear laser cavity, see figure 6.4, but the anomaly was not eliminated.

6.10 Error in the nonlinear coefficient

The difference between the experimental and calculated results was explained by the publication of Eckardt et al [Eckardt et al1990] of precise measurements of the nonlinear coefficient of several materials including KTP. This gave a value for d_{eff} that was half the previously accepted value, which reduced the expected efficiency by a factor of four. The table, figure 6.4, shows the results of the experiments along with the predicted values calculated using both the Zumsteg et al [Zumsteg et al1976] and Eckardt et al values of d_{eff}. The results clearly indicate that the lower value of Eckardt et al is supported. The remaining differences can be explained by errors in the beamsize (possibly from the elliptical beam), fundamental power and phase matching.

6.11 Damage to KTP

During the course of the experimental investigation of KTP, several crystals were damaged. The first type of damage occurred during experiments using a focussed beam, with a typical intensity of $1\,\mathrm{kW/cm^2}$. The crystal was either completely or partially destroyed, this being due to the beam catching on the edge of the crystal or on a surface flaw. The flaw was often the result of previous damage. In these cases the damage mechanism was the absorption of too much power and the

resulting thermal expansion shattered the crystal.

The second form of damage to the KTP occurred during an intracavity focussing experiment using a linear cavity. The laser had two intracavity lenses of 25 mm focal length to form a small waist of around 80 μm diameter. The output coupler was replaced, as before, with a highly reflecting mirror to reduce the cavity losses. When the KTP was correctly aligned, 800 mW of second harmonic was produced, 400 mW in each direction. While this demonstrated the possible high power conversion, the KTP was damaged during the process. The crystal had no previous surface flaws, but was left with tracks across one surface (consistent with scanning the crystal through the beam) and 3 pits on the other (See figures 6.6 and 6.7). The damage occured at an intensity of around 3 MW/cm^2.

The damage threshold of KTP is quoted at approximately 1 GW/cm^2, but this is for a pulsed laser beam, and is likely to be lower for a cw beam because thermal effects are dominant. The coating on the crystal had a damage rating of 3 MW/cm^2, and and it appears that the coating may have disintegrated and provided a flaw for bulk damage to occur. It is clear that the intensity used should be minimised to restrict the potential for damage.

6.12 Discussion of the 5 mm KTP experiments

While high power conversion had been demonstrated (800 mW), the experiments had revealed several problems. The first was the large difference between the experimental and calculated efficiencies for second harmonic generation. This can be explained by the revised publication by Eckardt et al, while any remaining differences can be explained by errors in the beamsize, fundamental power and phase matching.

The second problem was that the efficiency was four times smaller than previously thought, calling for the decreasing of the beam size if the KTP is to act as a 10% coupler. But this contradicts the conclusion drawn from the crystal damage that a lower intensity beam should be used to avoid damage. Without focussing to a near optimum level the efficiency from a 5 mm crystal is too low for cw con-

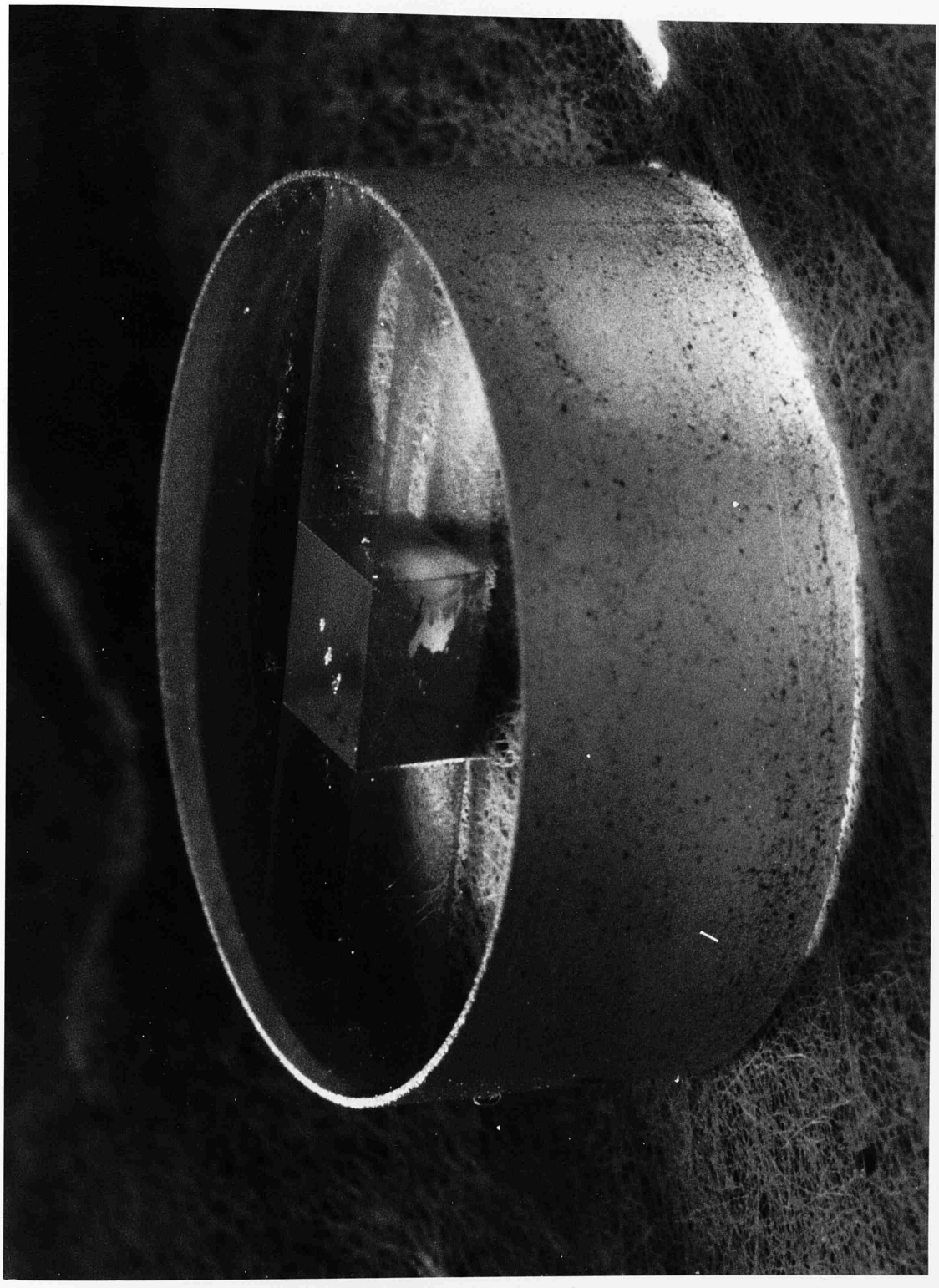

Figure 6.6: Crystal damage to KTP in a linear cavity. This side shows pits on the surface.

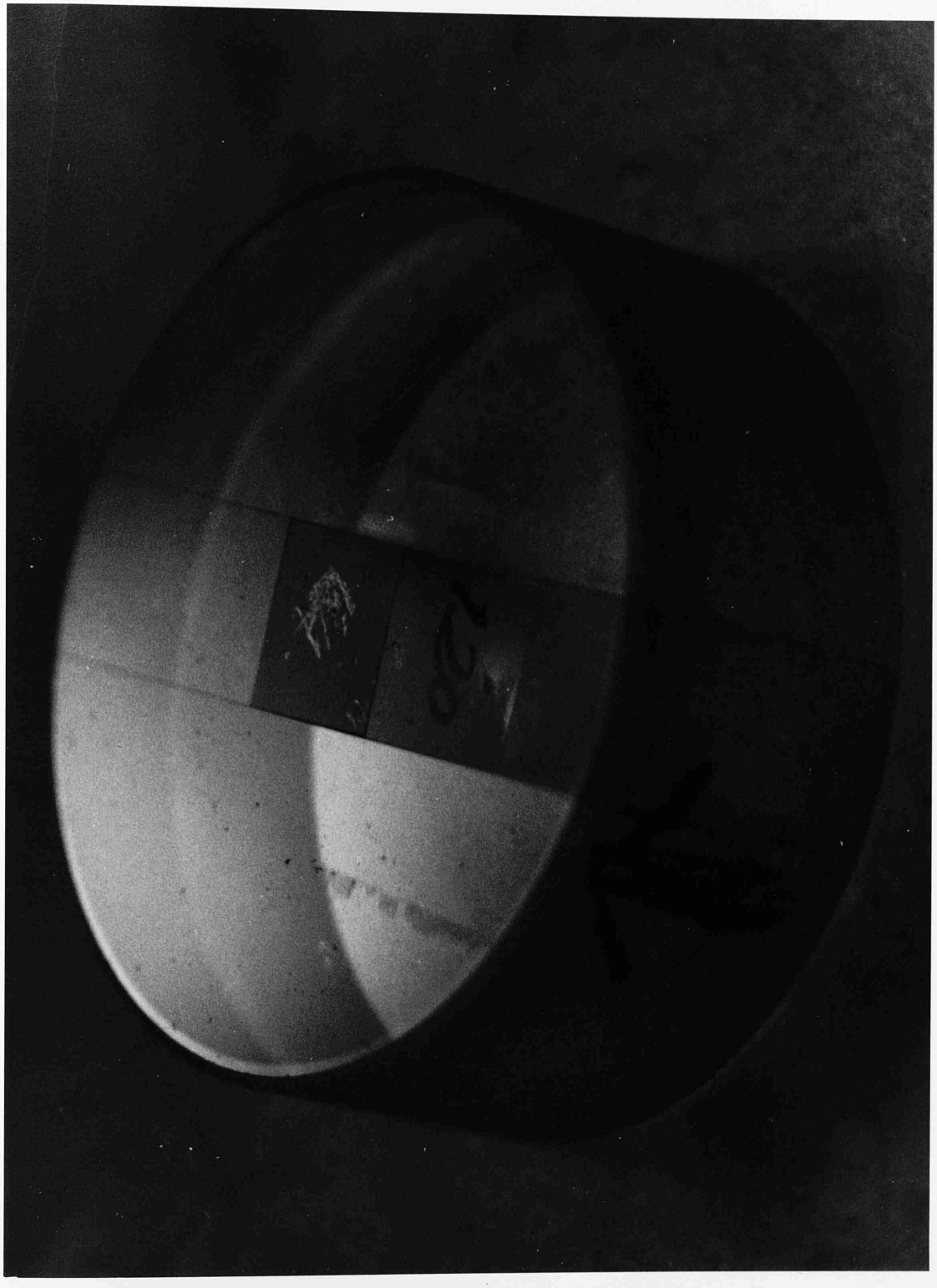

Figure 6.7: Crystal damage to KTP in a linear cavity. This side shows tracks on the surface.

version. The substitution of KTP with another crystal is not a simple solution, as KTP not only has a high nonlinear coefficient, even using the Eckardt value, but also a large damage threshold compared to other nonlinear materials.

Improvement of the efficiency to an acceptable level without focussing, and without the subsequent crystal damage, should be possible if longer crystals are used. Long crystals have a larger interaction length and so require less intensity for the same efficiency, reducing the potential for damage. The ninety degree phase matching (perpendicular to the optic axis) of KTP means that walkoff will not limit its useful length. This conclusion led to intracavity doubling using a $25 \times 3 \times 3$ mm KTP crystal, the largest available piece on the commercial market.

6.13 Experiments with a 25 mm long KTP crystal

In an initial external doubling experiment using a slowly diverging beam the relative improvement of a 25 mm crystal compared to a 5 mm crystal was measured. A half wave plate and a polarising beam splitter were used to allow power attenuation as well as allowing the polarisation to be defined. The beam diameter was about 0.6 mm and the fundamental power was 4 watts. The 25 mm crystal gave an improvement of 20 in conversion efficiency over the 5 mm crystal, a little less than the theoretical improvement of 25 for an unfocussed beam. This small discrepancy is probably due to imperfections in the 25 mm crystal.

As discussed previously, in an intracavity doubling arrangement the potential for useful conversion can be limited by the loss introduced when any nonlinear material is added. If a 25 mm cystal is to be experimentally useful then its losses should be as close to that of a 5 mm crystal as possible. It may also be critical that the absorption does not become so high that the crystal is damaged. The losses of a 5 mm and a 25 mm crystal were calculated by measuring how the finesse of a Fabry-Perot cavity changed when they were placed inside. For the 25 mm crystal the finesse dropped from 380 to 160, and for the 5 mm crystal the the finesse dropped from 380 to 240. These correspond to single pass losses of 1% and 0.5% respectively. Compared with the optimum coupling of around 8% , this loss was

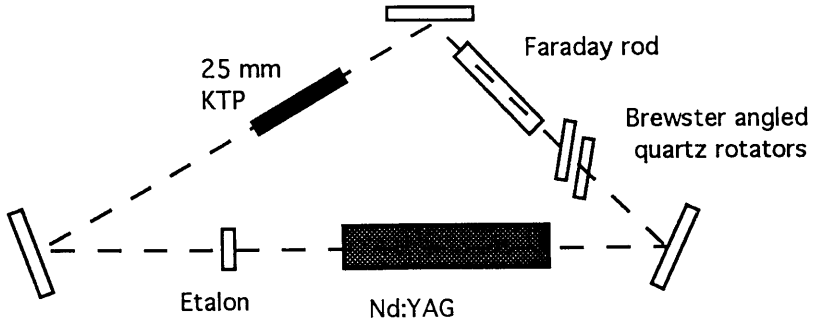

Figure 6.8: Laser arrangement for intracavity doubling using a 25 mm KTP crystal.

expected to be at an acceptable level to allow access to most of the laser output, providing of course that the efficiency was large enough and other factors did not limit it.

6.14 Intracavity doubling with a 25 mm long crystal

The doubling experiments were continued inside the laser cavity as before, but only the natural waist of the laser was used, as shown in figure 6.8. By this time the laser had been redesigned to form a three mirror ring. The cavity mirrors were all plane and were high reflectors for the fundamental wavelength, and approximately 90% transmitting for the second harmonic. The laser is fully described in Chapter 4. As before, the KTP crystal was mounted to allow correct orientation for phase matching.

With the KTP aligned and correctly oriented, 700 mW of second harmonic was measured. This was very encouraging as the measured circulating power of 180 W and beam diameter of approximately 0.6 mm gave the theoretical power as 2.1 W. Measurement of the beam gave the radius as $310\mu m \times 340\mu m$. If the laser waist could be reduced, then a higher fraction of the laser output could be obtained in the second harmonic.

A single 1 D lens was added to the cavity, as a simple demonstration; this

reduced the laser waist and improved the second harmonic output to over 1 W. (The simple lens approximation of the thermal lens breaks down here. If the two lenses are simply added as thin lenses then the cavity would be unstable.) For future work, to allow the full conversion of the available laser power, 8 W with an 8% coupler, the waist should be reduced to approximately $100\mu m$ or less to allow the KTP to act as a 8% coupler. The waist reduction should ideally be carried out using mirrors in the cavity to minimise the loss. The reduction could be achieved and still keep the intensity lower than that which caused the damage to the 5 mm KTP crystal.

6.15 Second harmonic stability

The intensity stability of the second harmonic light was poor; the highest efficiencies lasted for only a short time, usually between 30 seconds and 2 minutes. The effect was characterised by a slow decline in the second harmonic and fundamental power. The problem appeared to be due to the type 2 phase matching condition for KTP. Type 2 phase matching requires the fundamental light to be composed of 50% ordinary and 50% extraordinary polarisations in the crystal. The birefringence means that the fundamental light will not have the same polarisation when it exits unless the crystal length is able to satisfy the condition $(n^e_\omega - n^o_\omega)l = \lambda$, where l is the crystal length and λ is the wavelength.

Although the crystal may start satisfying this condition, if the path length changes, for example when the temperature of the crystal changes, the polarisation will not remain fixed. The change in polarisation causes extra loss at the Brewster plates in the cavity and consequently changes the fundamental and second harmonic power. The effect was present for both 5 and 25 mm crystals but was worse for the longer crystal. The temperature change needed to rotate the fundamental polarisation by π /4 was measured as 2 degrees centigrade for the 25 mm crystal in an external doubling experiment: the polarisation was simply measured before and after the crystal as the crystal temperature was changed. To check that the KTP interacted with the laser in the described manner, an un-

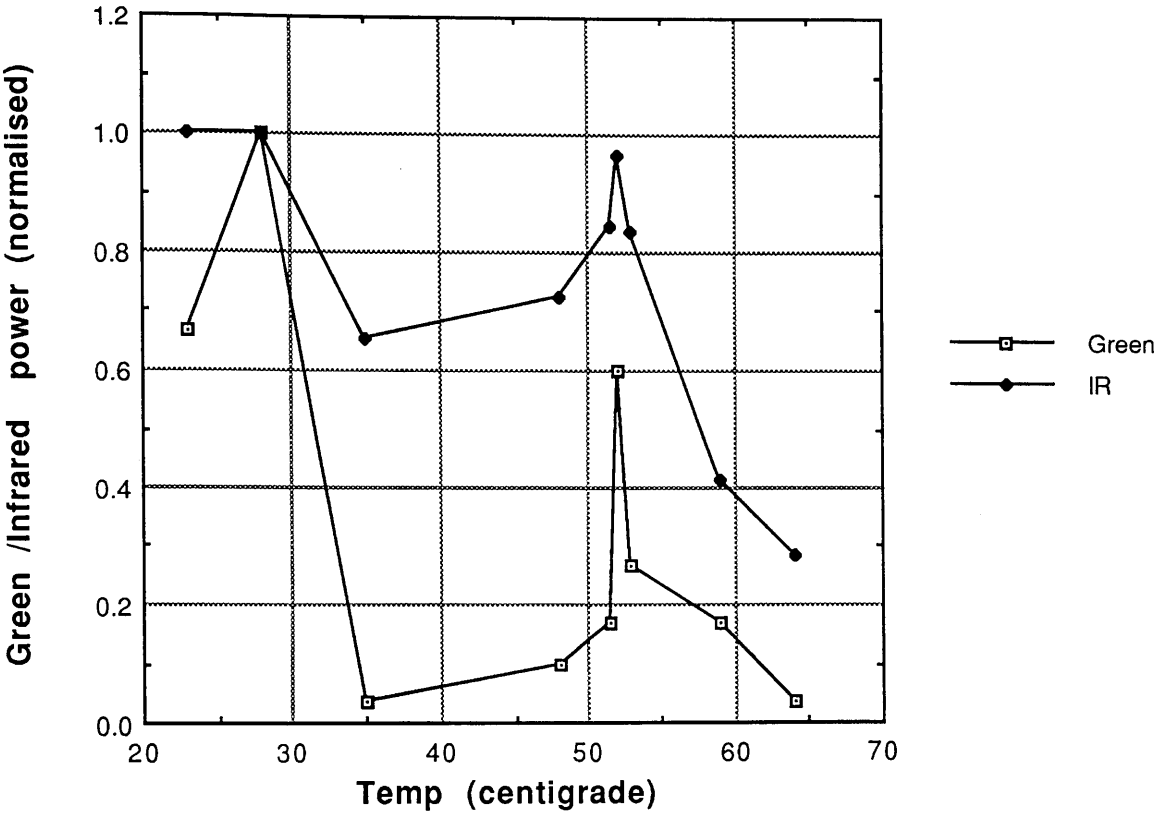

Figure 6.9: Graph of intracavity fundamental power and second harmonic output power as a function of temperature of an intracavity 5mm KTP crystal.

focussed intracavity doubling experiment was carried out using a 5 mm piece of KTP, where the KTP temperature was varied. The KTP crystal was heated using a coil wrapped around the aluminium casing of the crystal. As the temperature was increased the fundamental and second harmonic power was measured, as well as the polarisation of the fundamental.

The results of the experiment are shown in figure 6.9. The graph shows that as the temperature of the KTP is increased the intracavity fundamental power drops. The reduction in the fundamental power is accompanied by a reduction in the second harmonic output power. The changes are periodic, as the temperature continued to increase the power in the fundamental and second harmonic increased. The results are consistent with the idea that the polarisation of the fundamental

Several crystals are currently available that are suitable for second harmonic generation of the Nd:YAG fundamental. KTP was chosen because of the available crystals it had the highest non-linear coefficient. This was previously taken to be 7.3 pico metres per volt, but with the acceptance of the Eckardt value is now 3.7 pico metres per volt. Even with the Eckardt value KTP still has the highest coefficient for SHG of the Nd:YAG. KTP has the additional advantage that it uses non-critical type 2 phase matching and has a relatively high damage threshold.

Recently a suitable alternative to KTP has become available, namely, Lithium Borate (LBO). This can be non-critically phase-matched for type 1 and has a damage threshold of approximately 10 times that of KTP. In the light of the results from this thesis these properties make LBO a very promising material for further development of Nd:YAG second harmonic generation. The nonlinear coefficient is 2.5 pico metres per volt, approximately 0.7 times that of the revised value for KTP.

is rotated by the birefringence, creating additional losses; and the periodicity is a result of the crystal length once again satisfing the condition for no polarisation rotation.

To eliminate this problem requires the temperature stabilisation of the KTP. The temperature stabilisation is difficult because at high intensities heating from the laser will probably dominate, and any power fluctuation will couple into the system. It may be more effective to substitute the KTP with a nonlinear material that has type 1 phase matching. In this case the fundamental is either ordinary or extraordinary and so there is no polarisation rotation with length change.

6.16 Summary

Several intracavity and extracavity doubling experiments successfully produced green light from an infrared fundamental. The experiments demonstrated that the high intensities required for short crystals to be efficient were liable to damage the material. It was shown that a long crystal could successfully replace a shorter crystal, reducing the intensity required and consequently the potential for damage.

It is clear that for stable power output further work is required. The KTP should be temperature stabilised or replaced with a type 1 phase matched crystal, if possible. In addition the beam waist used should be reduced in an attempt to improve the efficiency: the beam waist reduction should be carried out in a way that will introduce as little additional loss as possible.

Chapter 7

Correlated Frequency Fluctuations

7.1 Introduction

The development of a high power single frequency Nd:YAG ring laser and its conversion to run in the second harmonic has been described in earlier chapters.

If such a laser is to be useful for a laser interferometric gravitational wave detector then strict demands are placed on its short term frequency stability. A stability of around $3\times10^{-8}Hz/Hz^{1/2}$ is required. The reference for the stabilisation, in current prototypes and design proposals, is an arm of the interferometer or the full path length of the interferometer [Hough et al 1989]. If the interferometer is to be operated using the second harmonic the stabilisation error signal must then be derived from the second harmonic. The error signal must then be used to control the fundamental frequency and consequently control the second harmonic. To achieve this requires the fundamental and second harmonic to have correlated frequency fluctuations.

This chapter describes the comparison of the fundamental and second harmonic frequency fluctuations and the use of the second harmonic to generate an error signal that controls the second harmonic by controlling the fundamental frequency.

7.2 Laser output

The laser was used in a similar arrangement to that described in Chapter 6. KTP was used intracavity to produce the second harmonic. The laser arrangement is

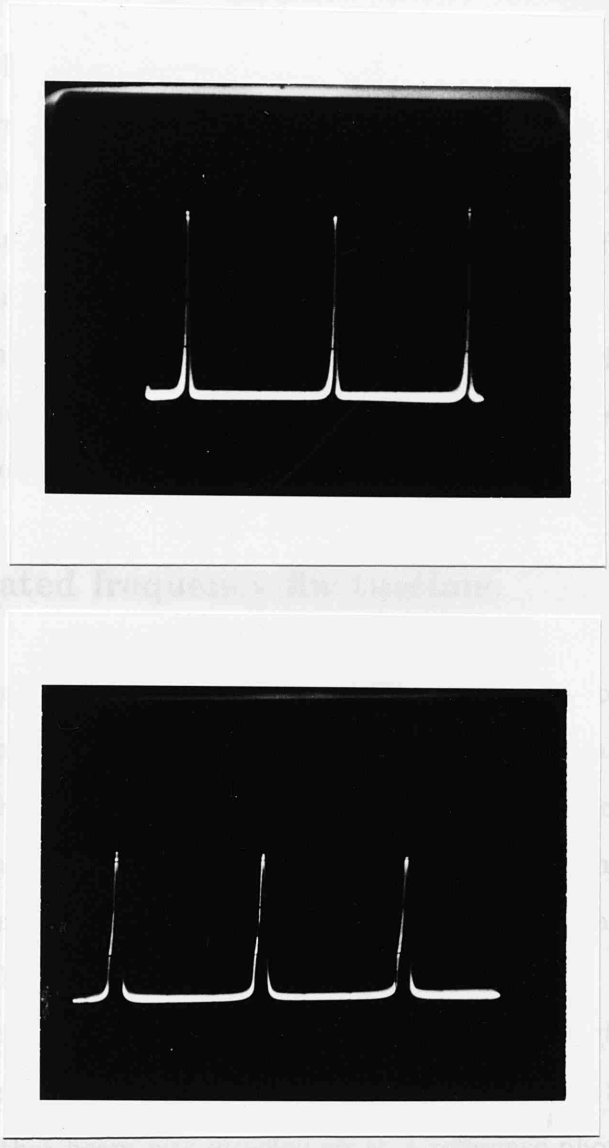

Figure 7.1: Mode structure of the fundamental (upper) and second harmonic (lower). Measured with a scanning Fabry-Perot cavity.

shown in figure 7.3.

The second harmonic output power was not at an optimum level but the laser was generating around 100 mW of second harmonic, was stable in intensity and running single mode. The single mode operation of the laser for both the fundamental and the second harmonic are shown in figure 7.1. These frequency spectra were taken using two scanning Fabry-Perot cavities. One was resonant with the fundamental and the other was resonant with the second harmonic.

The intensity fluctuations were at a 2 to 3 % level and were mostly confined to very low frequencies. Low frequency spectra of the noise for the fundamental

and the second harmonic are shown in figure 7.2. The intensity spectra show the expected correlation in intensity between the two frequencies. The intensity fluctuations, relative to the dc intensity, of the second harmonic is almost twice as large as the fluctuations of the fundamental. This is expected from a process that depends on the intensity squared.

On a long time scale intensity fluctuations were a problem. The intensity would sometimes drift to zero over 15 to 20 minutes. The cause was temperature changes of the KTP as described in Chapter 6.

7.3 Correlated frequency fluctuations

The experimental arrangement used to demonstrate correlation between the frequency fluctuations is shown in figure 7.3. Two beams were taken from the laser, one the fundamental and the other the second harmonic. Each beam was taken from a separate mirror in the three mirror laser cavity. A dichroic mirror and an interference filter were used to ensure the fundamental and the second harmonic were separated thoroughly.

To measure the frequency fluctuations, for both wavelengths, beam splitters formed two beams for each wavelength. One beam was directed in to a Fabry-Perot cavity and the other beam was directed on to a reference photodiode. A similar photodiode was placed behind the Fabry-Perot cavity to monitor the transmission. The two Fabry-Perot cavities were arranged (by means of an intracavity glass plate in one) to have the same finesse of 30. In each case the intensity of the light incident on the reference photodiode was attenuated until the photodiode signal was equal in size to half the height of a transmitted fringe. The reference signal was then subtracted from the transmitted signal using a difference amplifier giving a signal independent of any intensity fluctuations. This signal is a measure of the frequency fluctuations of the laser when the transmission of the Fabry-Perot cavity is held half way up a fringe, by means of a dc voltage applied to the PZT controlled Fabry-Perot cavity mirror.

The signal representing the fluctuations in frequency of the fundamental and

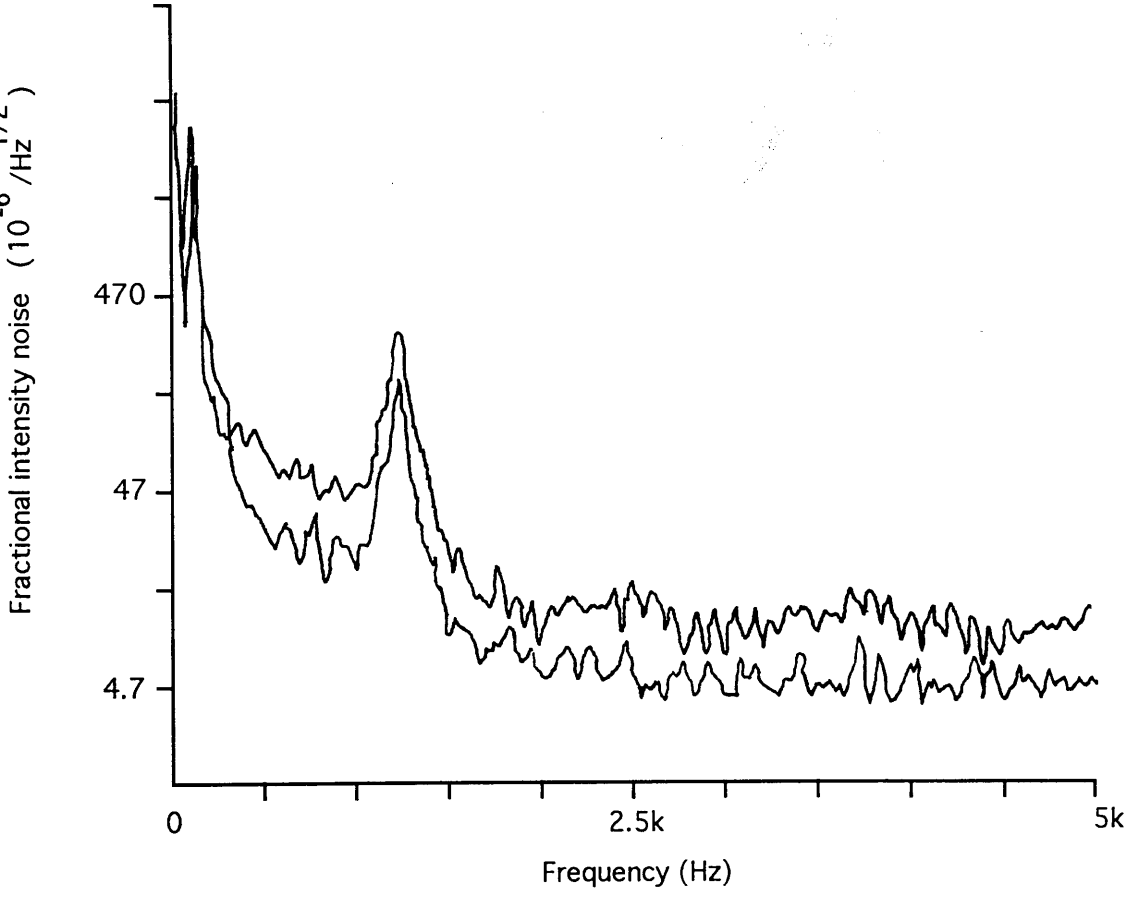

Figure 7.2: Intensity spectra of fundamental and second harmonic. The upper plot shows the second harmonic and the lower, the fundamental. In the 2-5 kHz region the relative intensity noise is $8.3 \times 10^{-6}/Hz^{1/2}$ and $4.7 \times 10^{-6}/Hz^{1/2}$ for the harmonic and fundamental respectively.

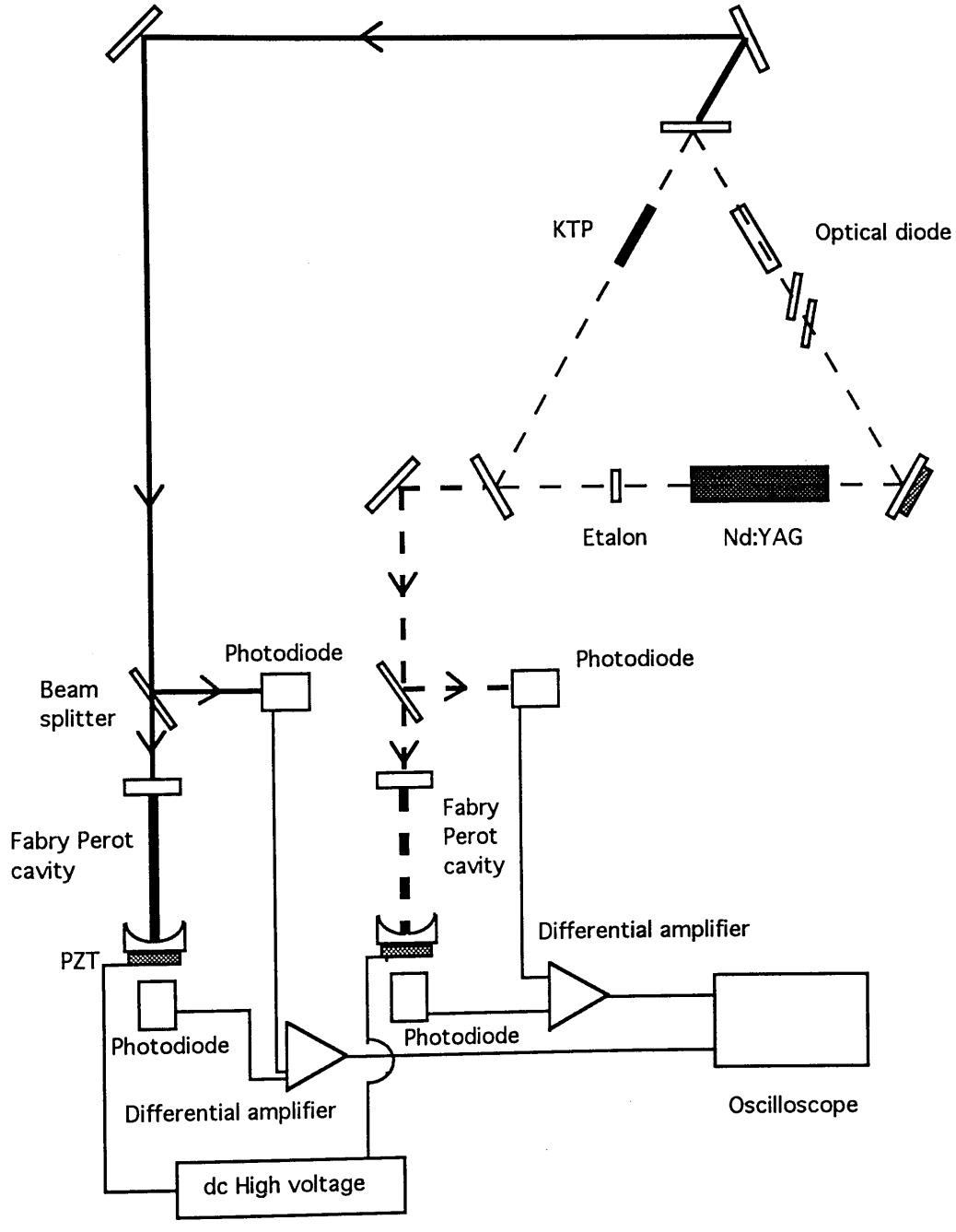

Figure 7.3: Experimental arrangement as used to demonstrate frequency noise correlation between the fundamental and second harmonic light.

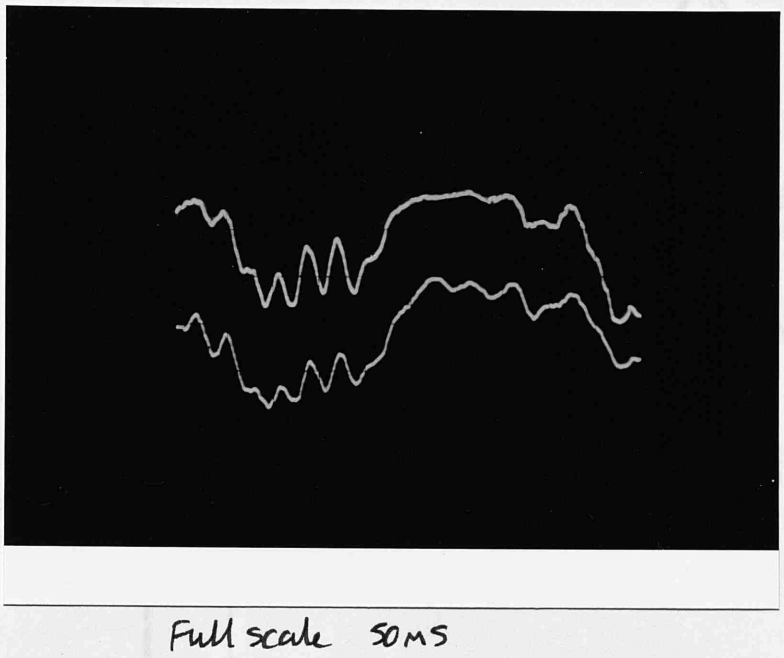

Figure 7.4: Oscilloscope picture showing the frequency fluctuations of the fundamental and the second harmonic. The upper signal is the second harmonic.

the similar signal for the second harmonic were simultaneously displayed on an oscilloscope. The oscilloscope picture in figure 7.4 shows the frequency fluctuations. The picture shows a high degree of correlation between both the low and high frequency fluctuations.

7.4 Locking the laser using the second harmonic

The laser was operated in an identical manner as used for the frequency correlation experiment. With the correlation in frequency fluctuations confirmed, the laser was then locked to a Fabry-Perot cavity resonant with the second harmonic. This is the same procedure that would be applied if the laser were to be used in a gravitational wave laser interferometer. The experimental arrangement is shown in figure 7.5.

The error signal was formed using the RF side band locking technique applied

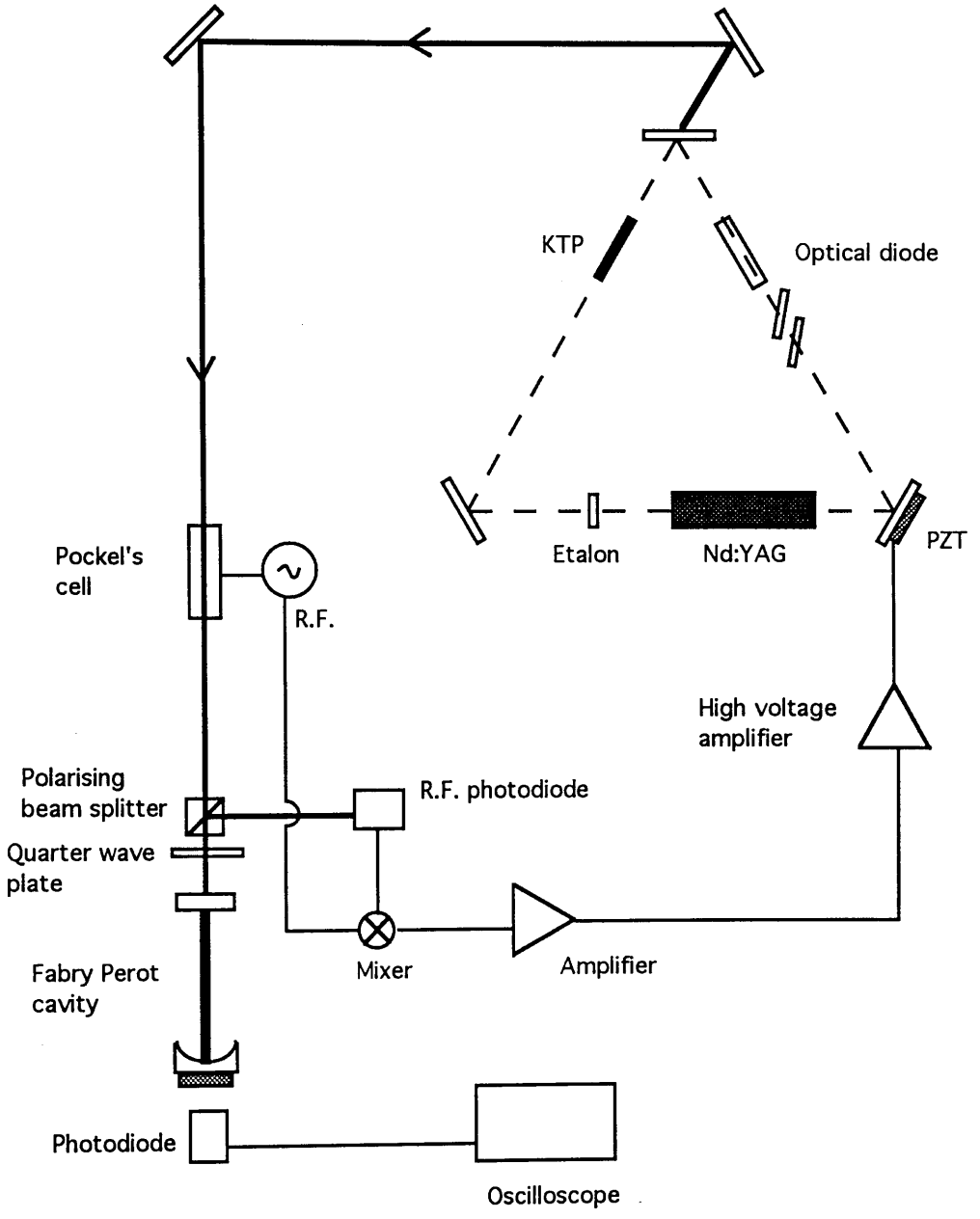

Figure 7.5: Apparatus for locking the laser using an error signal generated from the second harmonic using the RF sideband technique.

to the second harmonic. The error signal after suitable amplification was applied to a PZT controlled laser cavity mirror, which then corrected the fundamental frequency. The second harmonic was then controlled because of the correlation between the two frequencies. The servo used to lock the laser was very simple. It had one integrator at 35 Hz and a loop gain of a few hundred. The error signal while scanning the Fabry-Perot cavity is shown in figure 7.6 along with the transmission of the Fabry-Perot, and for comparison the error signal and the transmission signal are shown for the laser locked. It can clearly be seen that the laser is locking to the top of a fringe.

The spectrum of the feedback signal is shown in figure 7.7, which represents the natural frequency fluctuations of the laser. An earlier spectrum of the frequency fluctuations of the laser is shown in figure 7.8 for comparison. In this case the laser, in a similar configuration, was locked to a Fabry-Perot cavity that was resonant with the fundamental. The locking scheme was almost identical to that used for the second harmonic.

The spectra are similar but not identical as would be expected if the second harmonic process is noiseless. The difference is likely to be due to changes in environmental noise; such as increased acoustic noise. The peak in noise at 1250 Hz is found in both spectra and corresponds to a peak in the intensity noise at the same frequency. This is probably due to a mechanical resonance of the laser.

The feedback signal of the servo is a representation of the frequency noise of the fundamental as long as there is no additional noise introduced in the second harmonic process. For a direct representation of the second harmonic frequency noise the feedback would have to be to a cavity resonant with the second harmonic. It is simple to show that for a process that depends on the square of the electric field the frequency noise of the second harmonic should be double the noise of the fundamental, but the ratio of frequency fluctuations to frequency will remain the same.

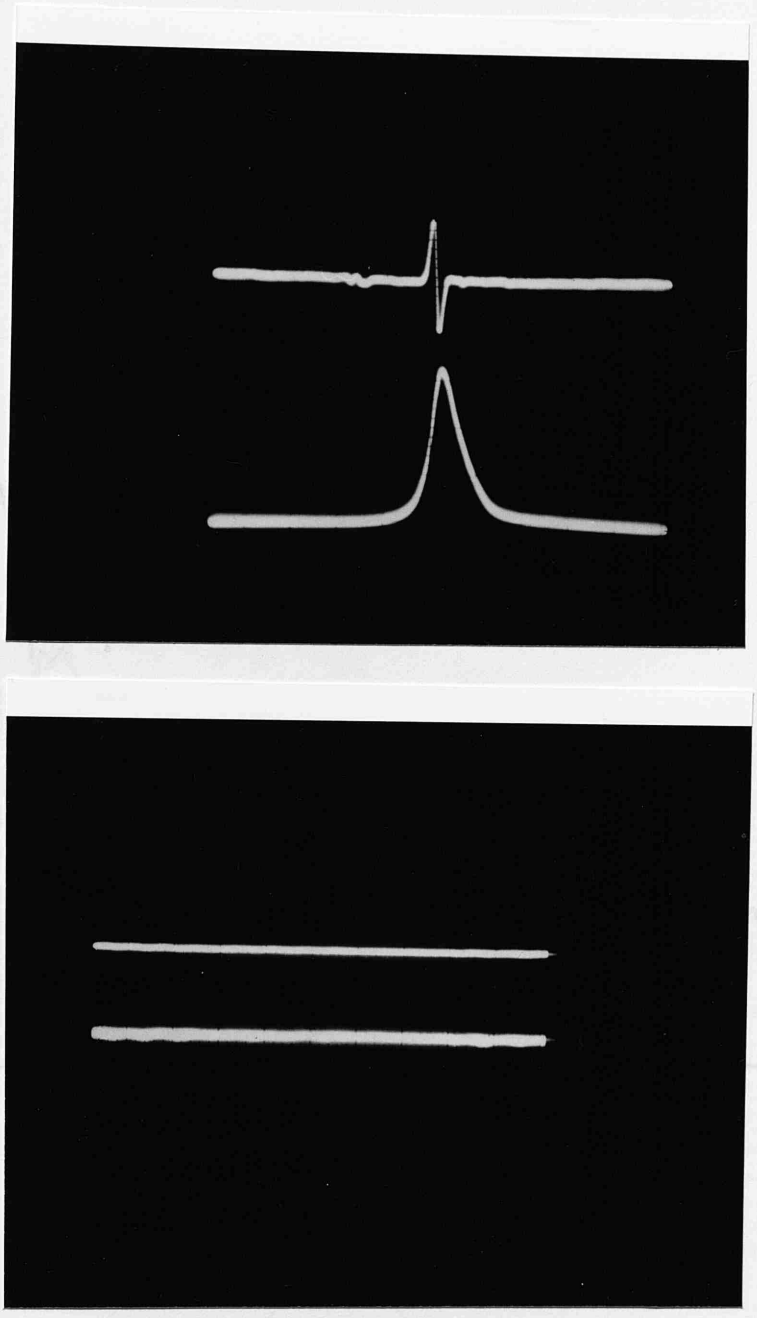

Figure 7.6: The error signal and transmission signal of the unlocked system are shown on the upper plot; the lower plot shows the same signals for the locked system.

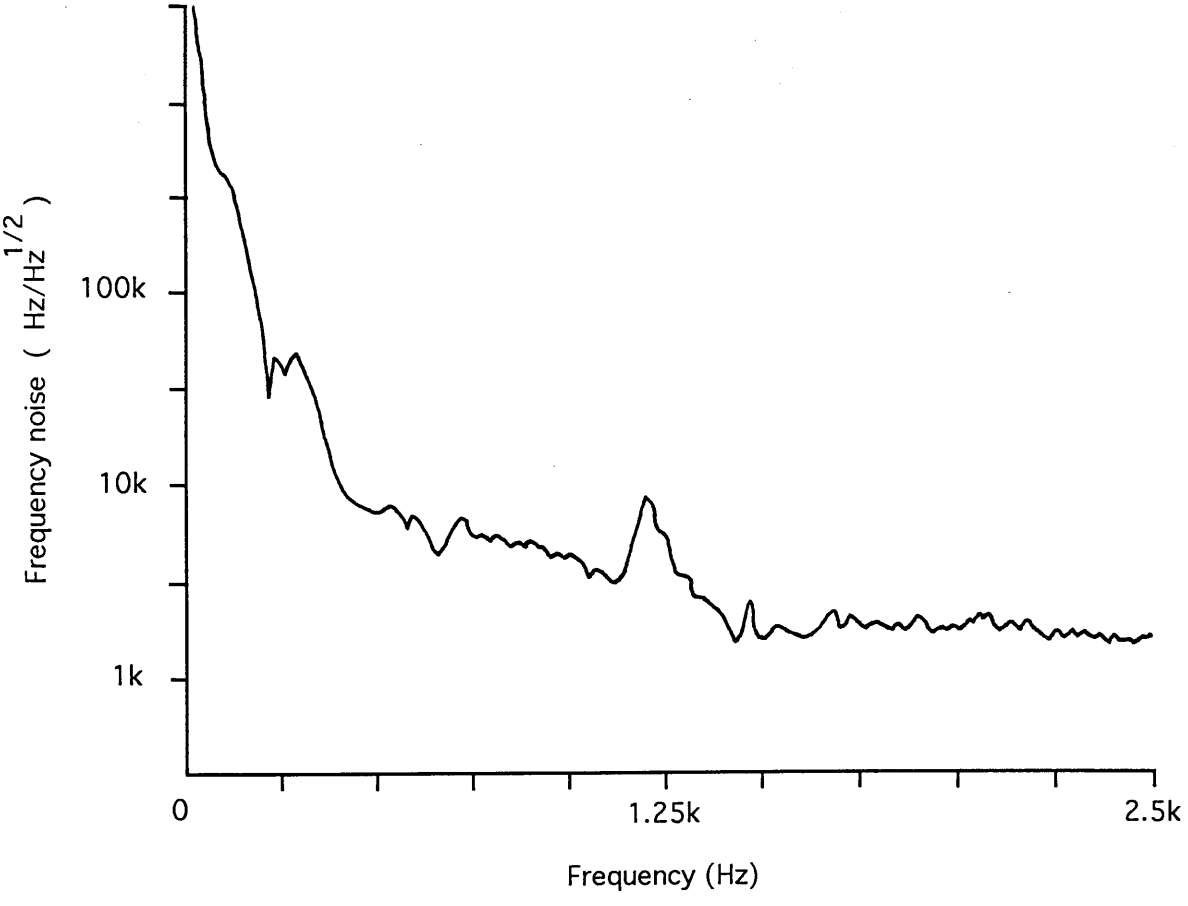

Figure 7.7: The frequency noise of the fundamental when the laser is locked using the secondharmonic.

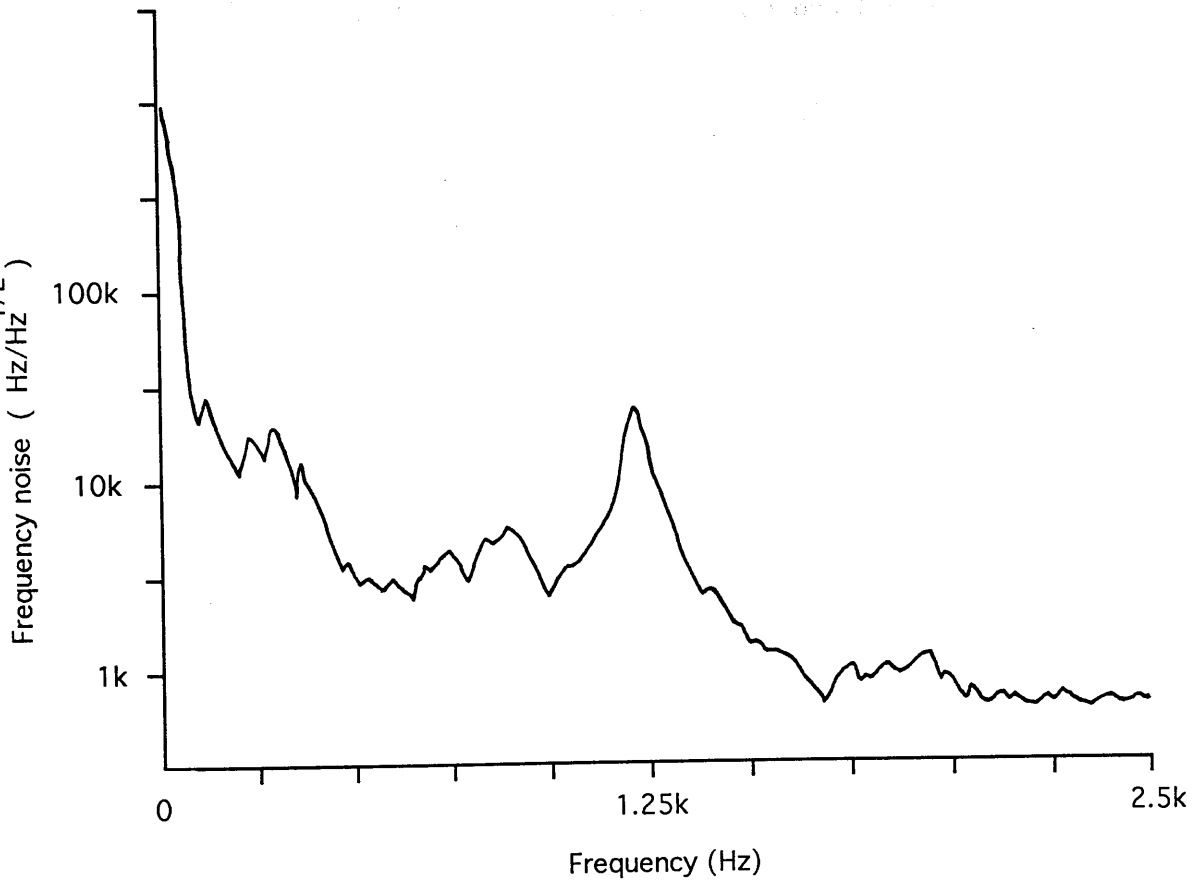

Figure 7.8: The frequency noise of the fundamental when the laser is locked using the fundamental. (WITH CRYSTAL IN PLACE)

7.5 Summary

The correlation of the frequency fluctuations of the fundamental and the second harmonic has been established. It has also been demonstrated that the laser may be locked to a cavity using an error signal derived from the second harmonic. This implies that there is potential for using a second harmonic laser in a long baseline interferometer.

Chapter 8

Conclusion

The potential of a Nd:YAG laser to be used as a substitute for a bank of Argon ion lasers in interferometric gravitational wave detectors was investigated in this thesis; both diode pumped lasers and flashlamp pumped lasers were examined.

A high level of frequency stability and efficiency from a diode pumped Nd:YAG laser was demonstrated. In addition the removal of intensity noise in the form of relaxation oscillations was demonstrated on a diode pumped Nd:YAG laser. Following this a stable high power single mode Nd:YAG ring laser pumped with a flashlamp was developed. The frequency stability was shown to be similar to that of an Argon ion laser. This is at a level suitable for further active stabilisation to the standard outlined in Chapter 1.

A low power diode pumped laser was used to injection lock the high power flashlamp pumped laser. The transfer of frequency stability from the small laser to the large laser was successful, indicating that an injection locked system may be very suitable to be developed further for use in a long base line detector.

Although a Nd:YAG laser operating at 1064 nm can be used to operate a detector, it saves on engineering if a shorter wave length laser can be used. Experiments were carried out towards the development of a high power Nd:YAG laser operating in the second harmonic. This presented problems that were overcome by the use of a 25 mm crystal of KTP, and finally allowed around 1 W of second harmonic light to be produced. The quality of the light was shown to be high by both the experimental demonstration of the correlation of frequency fluctuations, and the locking of the laser to a cavity using an error signal generated from the second har-

monic. It appears that a high power second harmonic Nd:YAG laser if developed further could make an ideal substitute for an Argon ion laser.

The criteria outlined in Chapter 1 look achievable with a Nd:YAG system; either fundamental or second harmonic. It is not clear at this time what form of laser system will be used on the two currently active long base line detector projects (LIGO in the USA and VIRGO in Europe). But it seems that a Nd:YAG laser operating at either the fundamental or second harmonic will be a strong candidate for each project.

Appendix A

Frequency noise spectra

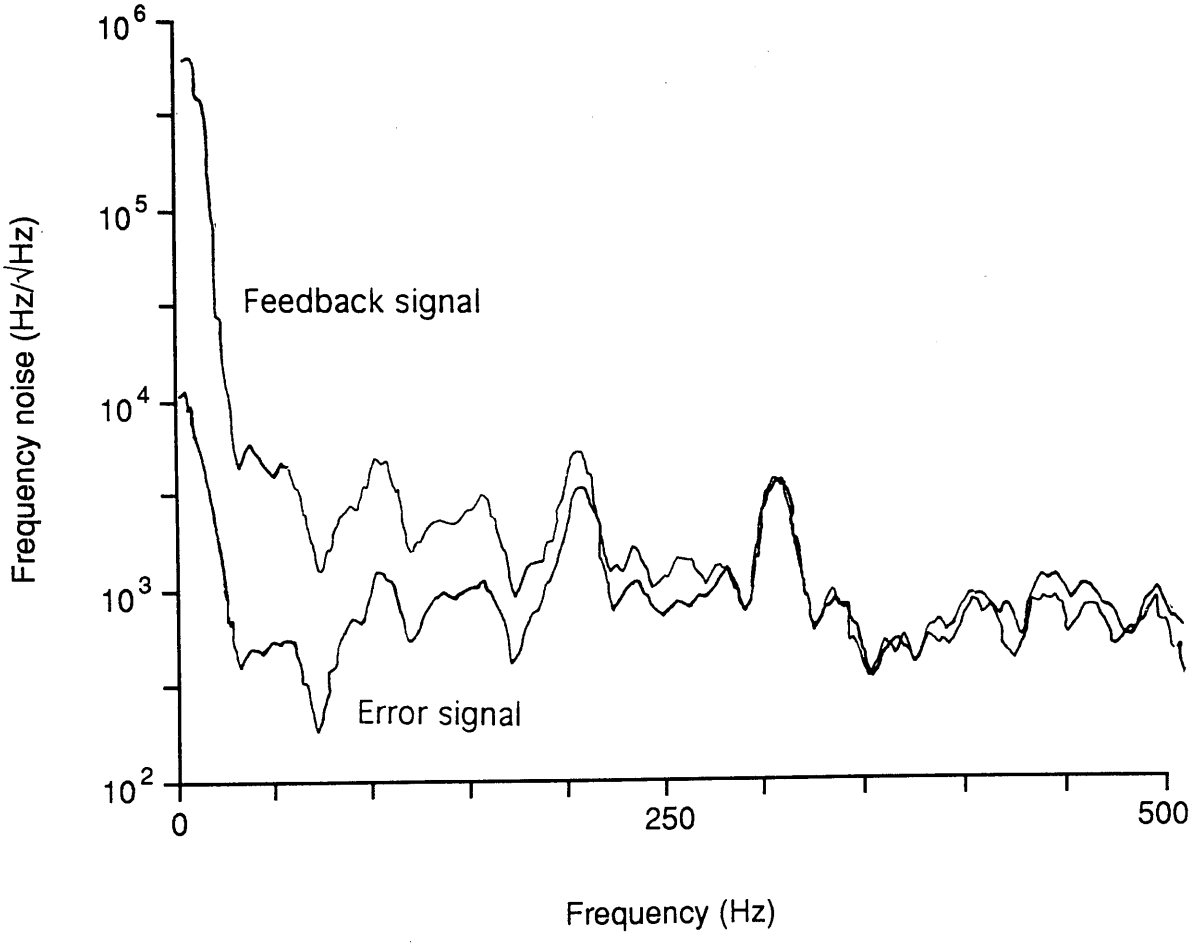

Figure A.1 Error and feedback signals for the injection locked laser (up to 500Hz).

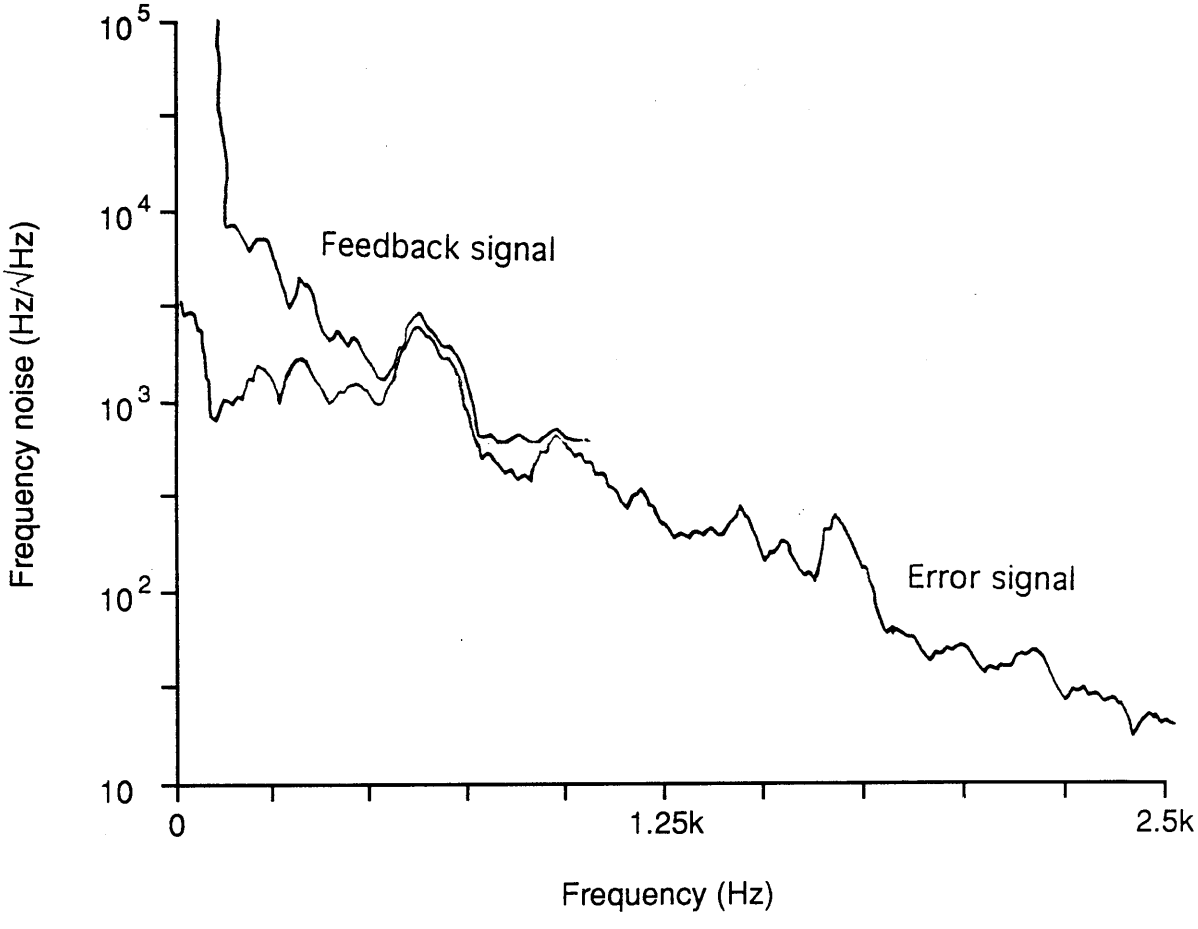

Figure A.2: Error and feedback signals for the injection locked laser.

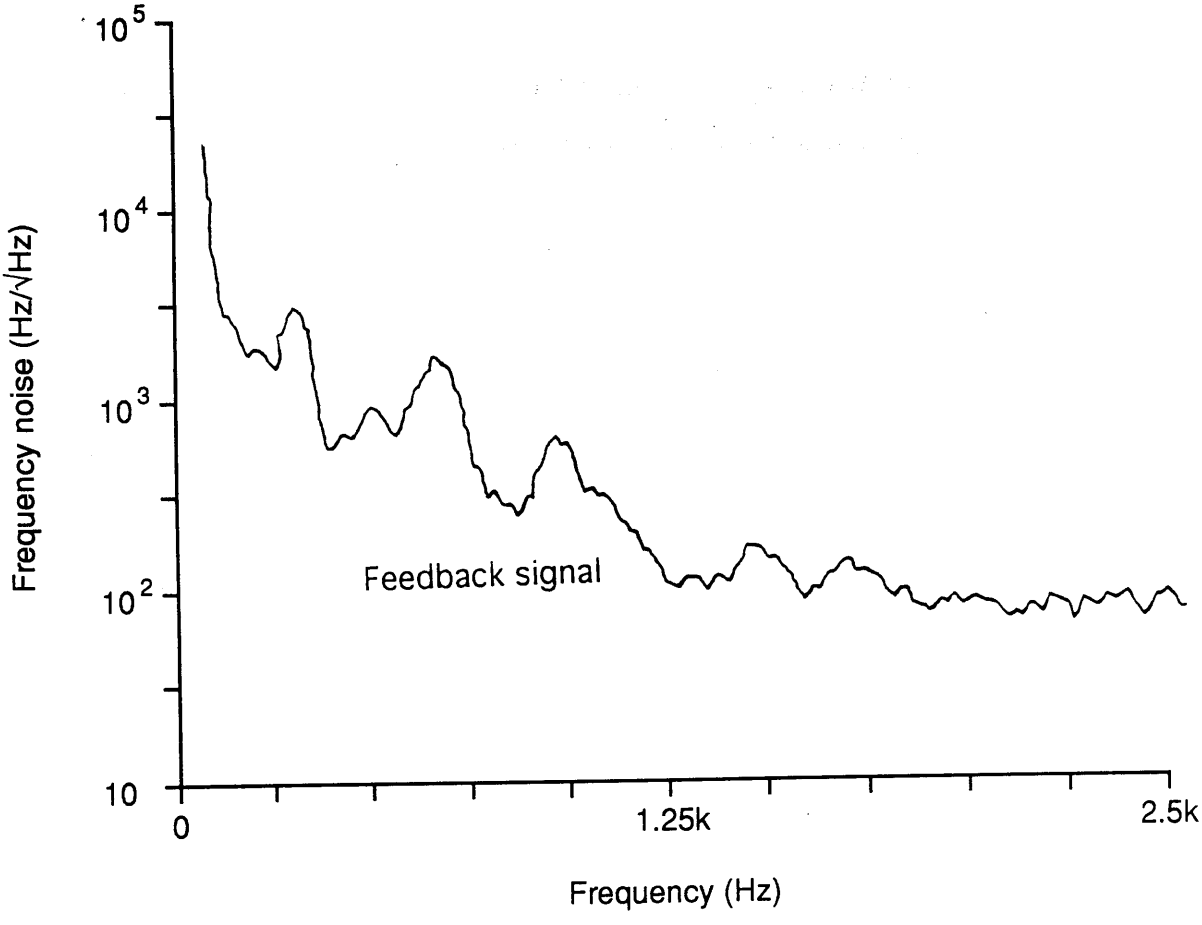

Figure A.3: Feedback signal for the Miser (limited by measurement noise above 1kHz).

Bibliography

[Blair 1991] D. Blair in *The Detection of Gravitational Radiation.* D. Blair, editor. Cambridge University Press, Cambridge, England, 1991.

[Burnham and Hays 1989] Burnham and Hays. *Optics Letters*, **14**, 27, 1989.

[Blair et al 1989] D. Blair, J. Ferreirinho, P. Veitch, R.J. Sandeman, H.A. Bachor, D. McClelland and A. Wrightson. *Proposal for the Australian International Gravitational Observatory*, 1989.

[Born and Wolf 1965] M. Born and E. Wolf. *Principles of Optics*, Pergamon Press, Oxford, 1965.

[Braginsky 1977] V.B. Braginsky. In *8th International Conference on General Relativity and Gravitation*, August 7-12, 1977. Waterloo, Ontario, Canada.

[Byer 1977] R.L. Byer. In *Nonlinear Optics.*, Proceedings of 16th Scottish Universities summer school in physics 1975, Academic Press, London, 1977.

[Campbell 1991] A.Campbell. Private communication 1991.

[Caves 1980] C.M. Caves. *Physical Review Letters*, **45**, 75, 1980.

[Caves 1981] C.M. Caves. *Physical Review D*, **23**, 8, 1981.

[Caves et al 1980] C.M. Caves, K.S. Thorne, R.W.P. Drever, V.D. Sandberg and M. Zimmerman. *Reviews of Modern*

Physics, **52**, 341, 1980.

[Chow 1982] W.W. Chow. *Optics Letters*, **7**, 417, 1982.

[Cregut et al. 1989] O. Cregut, C.N. Man, D. Shoemaker, A Brillet, A. Menhert, P. Peuser, N.P. Schmitt, P. Zeller and K. Wallermoth. *Physics Letters A*, **140**, 294, 1989.

[Drever 1983] R.W.P. Drever. In *Gravitational Radiation,* eds. N. Deruelle and T. Piran, editors, North Holland press: Amsterdam, The Netherlands, 1983.

[Drever et al 1983] R.W.P. Drever, J.L. Hall, F.V. Kowalski, J. Hough, G.M. Ford, A.J Munley and H. Ward. *Applied Physics B*, **31**, 97, 1983.

[Eckardt et al. 1990] R.C. Eckardt, H. Masuda, Yuan Xuan Fan and R.L. Byer. *IEEE Journal of Quantum Electronics*, **26**, 922, 1990.

[Einstein 1916] A. Einstein. *Sitzunger Preuss. Akad. Wiss.*, 688, 1916.

[Freitag 1990] I. Freitag. Diploma thesis, Institute for Quantum Optics, University of Hanover, Germany, 1990.

[Giazotto et al] A. Giazotto, A. Brillet and colleagues. The VIRGO Project report, 1989.

[Hanover 1990] Unpublished report, Institute for Quantum Optics, University of Hanover, Germany, 1990.

[Hanover 1990 b] I. Schutz, Private communication.

[Hough et al 1989] J. Hough, B.J. Meers, G.P. Newton, N.A. Robertson, H. Ward, G. Leuchs, T.M. Niebauer, A. Rudiger, R. Schilling, L. Schnupp, H. Walther, W. Winkler, B.F.

Schutz, J. Ehlers, P. Kafka, G. Schafer, M.W. Hamilton, I. Schutz, H. Welling, J.R.J. Bennett, I.F. Corbett, B.H.W. Edwards, R.J.S. Greenhalgh and V. Kose. *Proposal for a Joint German-British Interferometric Gravitational Wave Detector.* Technical Report MPQ 147 and GWD/137/JH(89), September 1989.

[Ito et al 1975] H.Ito, H.Naito and H. Inaba. *Journal of Applied Physics*, **46**, 3392, 1975.

[Johnson and Proffitt 1980] J.F. Johnson and W. Proffitt. *IEEE Journal of Quantum Electronics*, **16**, 483, 1980.

[Kafka 1988] P. Kafka. *Physics and Astrophysics of Gravitational waves.* Space Science and Fundamental physics, proceedings of Alpbach summer school, Austria 1987. ESA SP-283, May 1988.

[Kane 1990] T.J. Kane. *IEEE Photonics Technology Letters,* **2**, 244, 1990.

[Kane and Byer 1985] T. Kane and R.L. Byer. *Optics Letters*, **10**, 65, 1985.

[Kazovsky and Atlas 1990] L.G. Kazovsky, D.A. Atlas. *Journal of Light Wave Technology*, **8**, 294, 1990.

[Kerr 1986] G.A. Kerr. PhD Thesis, University of Glasgow, 1986.

[Kerr and Hough 1989] G.A. Kerr and J. Hough. *Applied Physics B*, **49**, 491, 1989.

[Kleinman et al. 1966] D.A. Kleinman, A. Ashkin and G.D. Boyd. *Phys Rev*, **145**, 338, 1966.

[Koechner 1970] W. Koechner. *Applied Optics*, **9**, 2548, 1970.

[Koechner 1972] W. Koechner. *IEEE Journal of Quantum Electronics*, **8**, 656, 1972.

[Kogelnik and Li 1966] H. Kogelnik and T. Li. *Proc IEEE*, **54**, 1312, 1966.

[Mackenzie 1989] N. L. Mackenzie. PhD thesis, Glasgow University, Glasgow, September 1989.

[Mangan 1988] J.B. Mangan. PhD thesis, University of Glasgow, Glasgow, 1988.

[Meers 1988] B.J. Meers. *Physical Review D*, **38**, 2317, 1988.

[Morrison et al 1991] E. Morrison, G.P. Newton, H. Ward, J. Hough, D.I. Robertson and B.J. Meers. In *6th Marcel Grossman meeting on General Relativity*, June, 1991, Kyoto, Japan.

[Nabors et al 1989] C.D. Nabors, A.D. Farinas, T. Day, S.T. Yang, E.K. Gustafson and R.L. Byer. *Optics Letters*, **14**, 1189, 1989.

[Robertson 1990] D.I. Robertson. PhD thesis, Glasgow University, Glasgow, 1990.

[Schilling et al. 1981] R. Schilling, L. Schnupp, W. Winkler, H. Billing, K. Maischberger and A. Rudiger. *Journal of Physics E: Scientific Instruments*, **14**, 65, 1981.

[Shoemaker et al 1988] D. Shoemaker, R. Schilling, L. Schnupp, W. Winkler, K. Maischberger and A. Rudiger. *Physical Review D*, **38**, 423, 1988.

[Schutz 1988] B.F. Schutz, editor.*Gravitational Wave Data Analysis*, B.F. Schutz,editor. NATO ASI series C: Mathematical and Physical Sciences **253**. Kluwer Academic Publishers, Dordrecht, The Netherlands, 1988.

[Siegman 1986] A.E. Siegman. *Lasers*, Oxford University Press, Oxford, England 1986.

[Smith 1970] R.G. Smith. *IEEE Journal of Quantum Electronics*, **6**, 215, 1970.

[Spectron 1991] Spectron Lasers, Private communication, 1991.

[Taylor and Weisberg 1982] J.H. Taylor and J.M. Weisberg. *The Astrophysical Journal*, **253**, 908, 1982.

[Thorne 1987] K. Thorne. In S.W. Hawking and W. Israel, editors *300 Years of Gravitation*. Cambridge University Press, England 1987.

[Veitch1991] P. Veitch. *The Detection of Gravitational Radiation*. D. Blair, editor. Cambridge University Press, Cambridge, England, 1991.

[Vogt et al 1989] R.E. Vogt, R.W.P. Drever, K.S. Thorne, F.J. Raab and R. Weiss. *A Laser Interferometric Gravitational Wave Observatory*. California Institute of Technology and Massachusetts Institute of Technology, 1989.

[Weber 1969] J. Weber, *Physical Review letters*, 22,1302

[Weiss 1972] R. Weiss. Electromagnetically coupled broadband gravitational antenna. *Quarterly Progress Report, Research Laboratory of electronics, MIT*, **105**, 54, 1972.

[Yang et al 1991] S.T. Yang, C.G. Pohalski, E.K. Gustafson, R.L. Byer, R.S. Feigelson, R.J. Raymakers and R.K. Route. *Optics Letters*, **16**, 1493, 1991.

[Yariv 1975] A. Yariv. *Quantum Electronics 2nd Edition*, J. Wiley and Sons, London, 1975.

[Zernike and Midwinter 1973] F. Zernike and J.E. Midwinter. *Applied Nonlinear Optics*, Wiley, New York, USA, 1973.

[Zuc er et al 1991] M. Zucker et al. As reported at the *6th Marcel Grossman meeting on General Relativity*, June, 1991, Kyoto, Japan.

[Zumsteg et al 1976] F.C. Zumsteg, J.D. Bierlein and T.E. Gier. *Journal of Applied Physics*, **47**, 4980, 1976.